PB 295786

REPORT NO. DOT-TSC-RSPA-79-10

INVESTIGATION OF THE DYNAMICS OF A MAGLEV VEHICLE TRAVERSING A FLEXIBLE GUIDEWAY: THEORY AND EXPERIMENT

Roger M. Katz
THE MITRE CORPORATION
1820 Dolly Madison Blvd.
McLean VA 22102

APRIL 1979
FINAL REPORT

Prepared for

U.S. DEPARTMENT OF TRANSPORTATION
RESEARCH AND SPECIAL PROGRAMS ADMINISTRATION
Office of Transportation Programs Bureau
Washington DC 20590

Technical Report Documentation Page

1. Report No.	2. Government Accession No.	3. Recipient's Catalog No.
DOT-TSC-RSPA-79-10		PB295786

4. Title and Subtitle	5. Report Date
INVESTIGATION OF THE DYNAMICS OF A MAGLEV VEHICLE TRAVERSING A FLEXIBLE GUIDEWAY: THEORY AND EXPERIMENT	APRIL 1979
	6. Performing Organization Code

7. Author(s)	8. Performing Organization Report No.
Roger M. Katz	DOT-TSC-RSPA-79-10

9. Performing Organization Name and Address	10. Work Unit No. (TRAIS)
The MITRE Corporation* 1820 Dolly Madision Blvd. McLean VA 22102	RS906/R9505
	11. Contract or Grant No. DOT-TSC-1263

12. Sponsoring Agency Name and Address	13. Type of Report and Period Covered
U.S. Department of Transportation Research and Special Programs Administration Office of Transportation Programs Bureau Washington DC 20590	Final Report July 1976 - June 1978
	14. Sponsoring Agency Code DOT/TSC

15. Supplementary Notes

*Under contract to: U.S. Department of Transportation
Research and Special Programs Administration
Transportation Systems Center
Cambridge MA 02142

16. Abstract

This report presents the results of a research program conducted jointly by the United States Department of Transportation and the Federal Republic of Germany Ministry for Research and Technology. The object of this program was to study the dynamics of a maglev vehicle traversing a flexible guideway. Work in the U.S. was carried out at MITRE/Metrek in McLean, Virginia; work in the FRG was carried out at Transrapid-EMS in Munich.

Two types of experiments were conducted using the full-scale KOMET test track in Manching, Germany. In the first, sinusoidal guideway deviations were deliberately introduced, and the KOMET vehicle was run over these at various speeds up to 324 KM/HR. The second type of test involved removing pier supports from the test track in order to make it more flexible. Theoretical predictions of the dynamic motions from a MITRE computer program are compared to the experimental results.

17. Key Words	18. Distribution Statement
High Speed Ground Transportation, Maglev, Magnetic Suspension Vehicle/Guideway Dynamics	DOCUMENT IS AVAILABLE TO THE PUBLIC THROUGH THE NATIONAL TECHNICAL INFORMATION SERVICE, SPRINGFIELD, VIRGINIA 22161

19. Security Classif. (of this report)	20. Security Classif. (of this page)	21. No. of Pages	22. Price
Unclassified	Unclassified	136	A07-A01

Form DOT F 1700.7 (8-72) Reproduction of completed page authorized

PREFACE

On June 12, 1973, after preliminary negotiations by the Federal Railroad Administration (FRA) and the Office of the Secretary (OST) with the German Ministry of Research and Technology (MORT) and the German Ministry of Transport (MOT), DOT Secretary Brinegar signed an agreement providing for cooperation between the U.S. and Federal Republic of Germany in the area of advanced systems technology, and in particular, magnetic levitation (MAGLEV). A working group meeting was held between U.S. and German principals from FRA, OST, MORT, and MITRE on October 28 and 29, 1975, for the purpose of identifying specific project areas for cooperation. An agreement was initiated for a joint vehicle/guideway test program, the purpose of which is to validate U.S. (FRA/MITRE) developed MAGLEV/guideway simulations and to use these simulations to determine guideway roughness and flexibility limits for an attraction MAGLEV system. The tests, using the German KOMET vehicle and test facilities at Manching, were conducted in October 1976. This report deals with the results of those tests.

By mutual agreement with FRA, the initiative for Non-Contact Suspension/Propulsion Technology resides with the Transportation Advanced Research Projects (TARP) program, which is currently being conducted by the Research and Special Projects Administration (RSPA).

Several individuals made significant contributions to this work. Mr. John Anderes participated in the design of the test plan, execution of the experiments, coordination of data transfer, calculation of guideway deflections, and development of a coupled vehicle/guideway model. In addition, he provided helpful comments concerning guideway dynamics and design. Mr. Alan Robbins was extremely helpful in optimizing both staff and computer execution time with original and efficient approaches towards narrowly targeted computer programming problems.

METRIC CONVERSION FACTORS

Approximate Conversions to Metric Measures

Symbol	When You Know	Multiply by	To Find	Symbol
		LENGTH		
in	inches	2.5	centimeters	cm
ft	feet	30	centimeters	cm
yd	yards	0.9	meters	m
mi	miles	1.6	kilometers	km
		AREA		
in^2	square inches	6.5	square centimeters	cm^2
ft^2	square feet	0.09	square meters	m^2
yd^2	square yards	0.8	square meters	m^2
mi^2	square miles	2.6	square kilometers	km^2
	acres	0.4	hectares	ha
		MASS (weight)		
oz	ounces	28	grams	g
lb	pounds	0.45	kilograms	kg
	short tons (2000 lb)	0.9	tonnes	t
		VOLUME		
tsp	teaspoons	5	milliliters	ml
Tbsp	tablespoons	15	milliliters	ml
fl oz	fluid ounces	30	milliliters	ml
c	cups	0.24	liters	l
pt	pints	0.47	liters	l
qt	quarts	0.96	liters	l
gal	gallons	3.8	liters	l
ft^3	cubic feet	0.03	cubic meters	m^3
yd^3	cubic yards	0.76	cubic meters	m^3
		TEMPERATURE (exact)		
°F	Fahrenheit temperature	5/9 (after subtracting 32)	Celsius temperature	°C

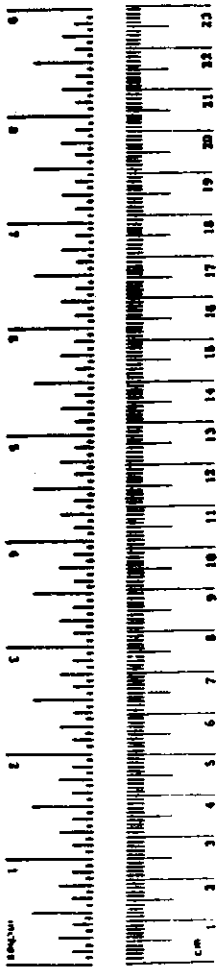

Approximate Conversions from Metric Measures

Symbol	When You Know	Multiply by	To Find	Symbol
		LENGTH		
mm	millimeters	0.04	inches	in
cm	centimeters	0.4	inches	in
m	meters	3.3	feet	ft
m	meters	1.1	yards	yd
km	kilometers	0.6	miles	mi
		AREA		
cm^2	square centimeters	0.16	square inches	in^2
m^2	square meters	1.2	square yards	yd^2
km^2	square kilometers	0.4	square miles	mi^2
ha	hectares (10,000 m^2)	2.5	acres	
		MASS (weight)		
g	grams	0.035	ounces	oz
kg	kilograms	2.2	pounds	lb
t	tonnes (1000 kg)	1.1	short tons	
		VOLUME		
ml	milliliters	0.03	fluid ounces	fl oz
l	liters	2.1	pints	pt
l	liters	1.06	quarts	qt
l	liters	0.26	gallons	gal
m^3	cubic meters	35	cubic feet	ft^3
m^3	cubic meters	1.3	cubic yards	yd^3
		TEMPERATURE (exact)		
°C	Celsius temperature	9/5 (then add 32)	Fahrenheit temperature	°F

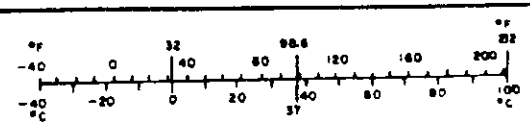

TABLE OF CONTENTS

TABLE OF CONTENTS
(continued)

LIST OF ILLUSTRATIONS

LIST OF TABLES

1. INTRODUCTION

The object of this research project was to study the dynamics of a magnetically levitated (maglev) vehicle traversing a flexible guideway. Guideways of increased flexibility are of interest because of their potential to reduce guideway construction costs, and understanding the nature of the vehicle/guideway dynamics is necessary to evaluate the limitations on tracking ability they impose.

Experimental verification of the analytical models used to simulate a maglev vehicle and guideway was obtained by use of data from the KOMET, a maglev test carrier at the LHP facility in Manching, FRG. This facility is operated by the Transrapid-EMS group in the Federal Republic of Germany (FRG).

The mechanically simple guideway structure for the KOMET, consisting of iron beams (of an inverted-T cross section) supported by iron piers, allowed structural modifications to be made relatively easily. Two types of guideway modifications were made: 1) the introduction of a rigid, sinusoidal disturbance by means of adjustment of the support height at the piers, and 2) an increase in the guideway flexibility by removing the support at some of the piers. Both the vehicle and guideway were instrumented to provide data for vehicle motion and guideway deflection.

Section 2 of this report discusses the experimental procedure. Section 3 describes the control system strategy used on the KOMET. Section 4 discusses the response to the sinusoidal guideway, including examples of comparisons of theoretical and experimental time histories. Section 5 presents the results for the flexible guideway. Section 6 describes a general parameter study to identify the range for system

parameters which are likely to present vehicle guideway interactions. This generalizes the results beyond the limitations of the specific control scheme and guideway used for the tests. Section 7 gives a summary and recommendations for future work.

2. EXPERIMENTAL PROCEDURE

The KOMET is an unmanned, magnetically levitated test carrier developed by Transrapid-EMS. It is accelerated to the desired test speed by a hot water rocket pusher, the DANIEL. At the end of this acceleration the pusher falls behind allowing the KOMET to coast alone through a 48 meter long test section. Braking is initiated by a trip wire, and the KOMET decelerates on the remaining length of track. The LHP guideway is depicted in Figure 1. The guideway cross section is shown in Figure 1a, the acceleration, coasting and braking sections are shown in Figure 1b. Four sections, identified as sections # 43 through 46, were modified for this experiment. Two types of modifications were involved, 1) the introduction of a rigid, sinusoidal disturbance, and 2) an increase in the beam flexibility. Beams on both sides of the guideway in each section were modified in order to avoid roll excitation to the KOMET.

The LHP test facility was not originally designed with such studies in mind, and the achievable modifications were somewhat constrained. The MITRE Corporation and Transrapid-EMS jointly worked on the details of a test plan for this experiment.

2.1 Sinusoidal Guideway Modifications

Figure 2a depicts the sinusoidal modifications made to the guideway. Four 12 m beams (sections #43 through #46) on each side of the guideway were adjusted at the pier supports to approximate a rigid sinusoidal disturbance with a 12 m wavelength and 2 mm amplitude. The adjustments were made at the bolts attaching the beam support arm to the pier. The location of these bolts is indicated in Figure 1a.

2.2 Flexible Guideway Modifications

Piers for the beams on each side of the guideway in sections #43 through #46 were effectively removed to increase the guideway flexibility. This was accomplished by removing the beam support arm

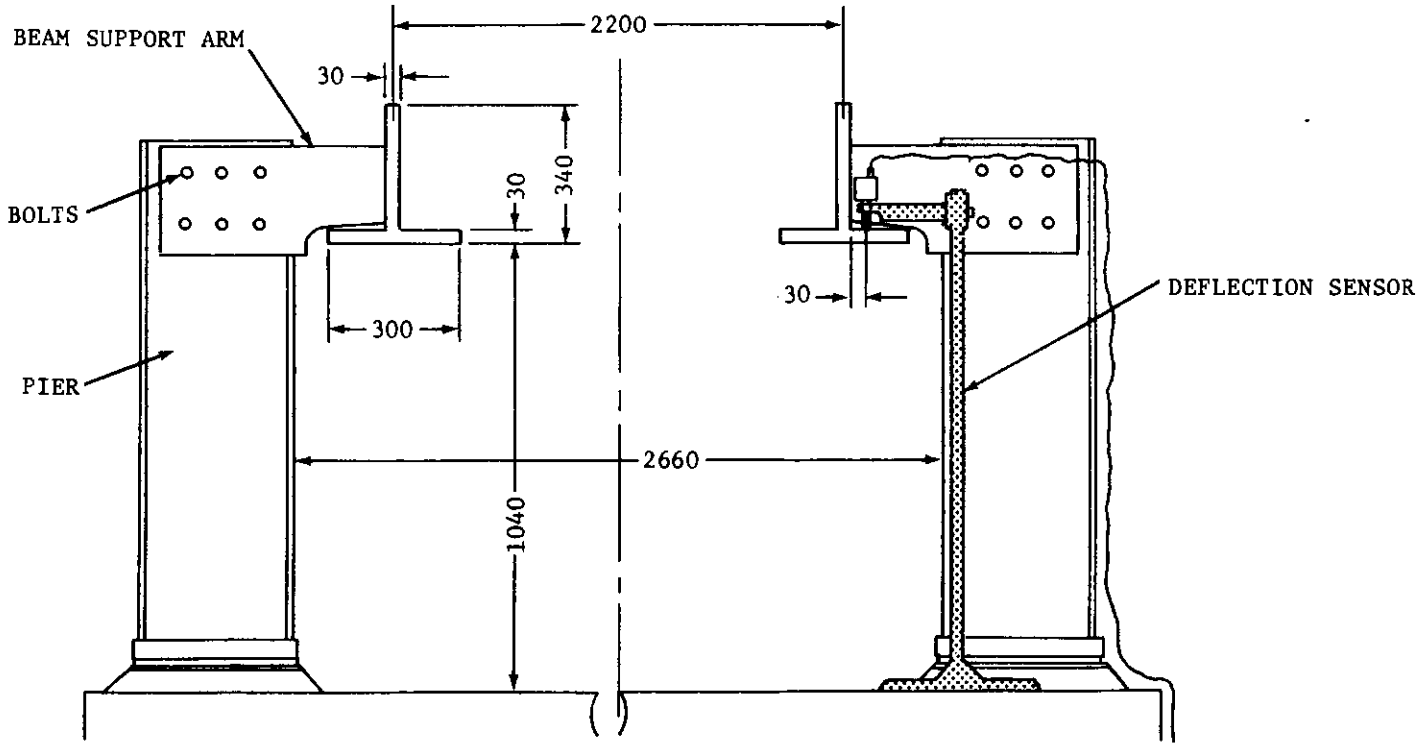

DIMENSIONS IN MILLIMETERS

1a

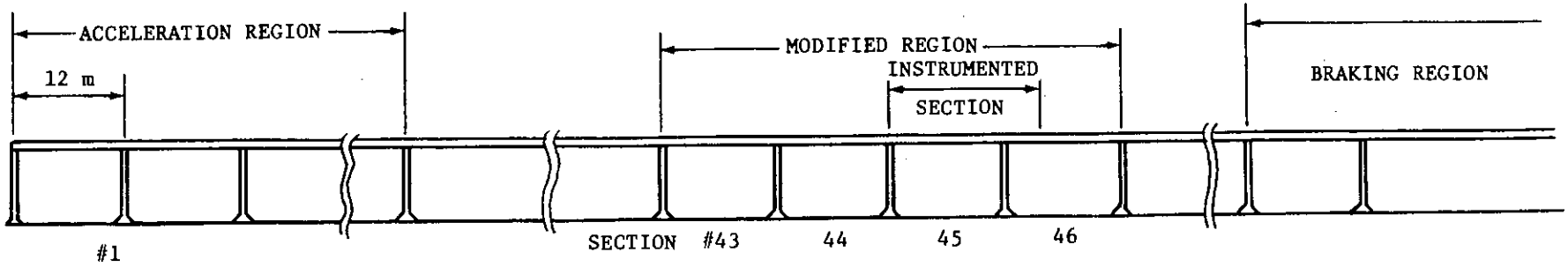

1b

FIGURE 1
LHP TEST TRACK

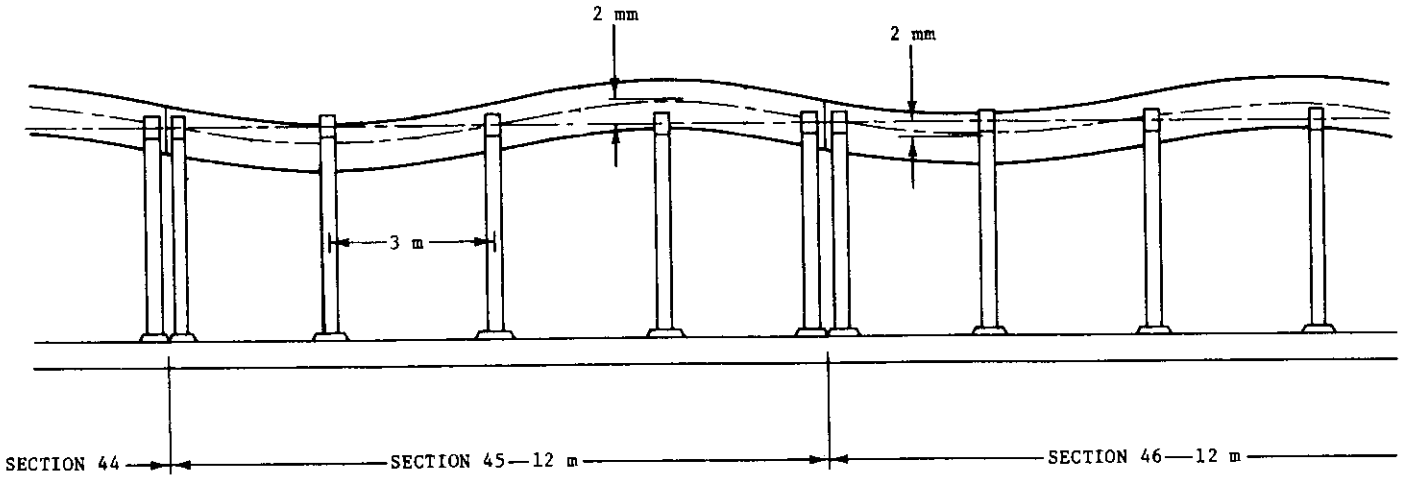

2a.

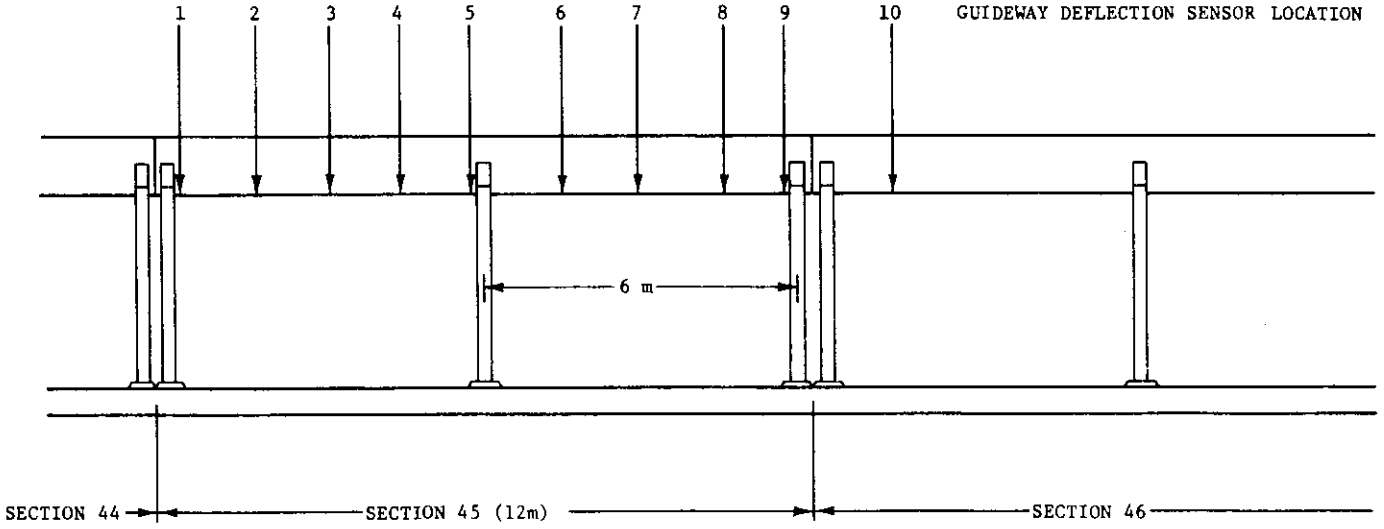

2b.

FIGURE 2
GUIDEWAY MODIFICATIONS

attaching bolts, allowing freedom in the vertical direction. This provided a two span flexible beam, 12 m long, depicted in Figure 2b. Although the piers were not physically removed, they are not shown in the figure.

2.3 Guideway Instrumentation

The 3rd and 4th beams in the test section were instrumented to measure the vertical guideway deflections, as illustrated in Figure 2b. Ten displacement sensors, spaced approximately 1.5 m apart, were used to measure the vertical guideway deflections as the KOMET traversed the guideway. The displacement sensor fixture is depicted in Figure 1a.

2.4 Instrumentation on the KOMET

The KOMET is depicted in Figure 3. Note the locations of the vertical gap sensors and accelerometers at the front and rear of the vehicle, and the five magnets along each side used for lift. These sensors and magnets are used to control the heave and pitch modes of the KOMET, which are the only motions of interest for this experiment.

In addition, three vertical gap sensors and a slot detector, not shown in the figure, were onboard. These gap sensors were used only for data acquisition, not for the control system. They were placed at the vehicle center of gravity as well as 3.7 m in front and 3.6 m behind it.

The slot detector, placed 2.5 m aft of the vehicle C.G., detected passage across guideway piers. This provided a vehicle/guideway synchronization signal for the purpose of locating the vehicle position as it traversed the guideway.

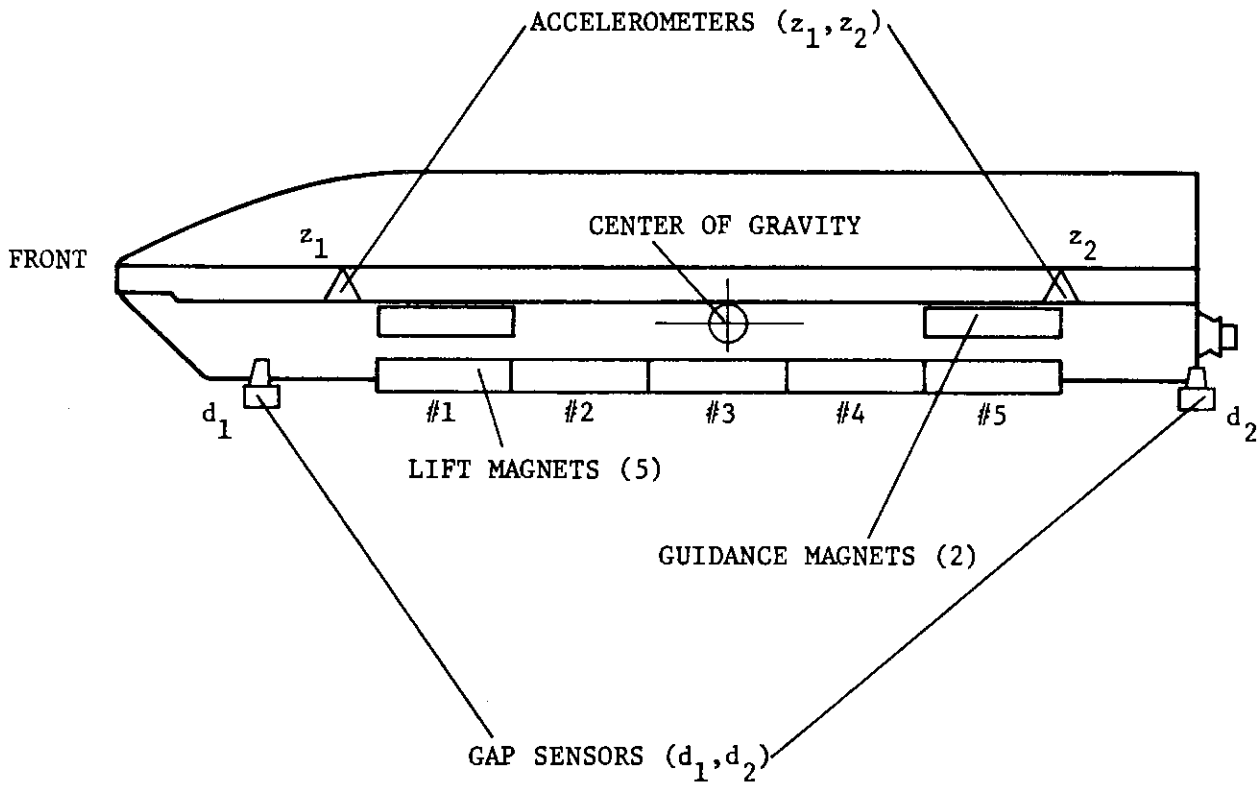

FIGURE 3
KOMET

MITRE was not originally aware that separate gap sensors were used for data acquisition, and had assumed that the front and rear gap sensor data obtained from Transrapid-EMS came from the control system gap sensors (located 3.81 m fore and aft of the vehicle C.G.) at the time of our analysis. Hence calculated gaps at $\pm$ 3.81 m from the vehicle C.G. are compared with measured gaps 3.7 m in front and 3.6 m behind the C.G. throughout this report.

In addition, the location of the slot detector was not correctly known by MITRE at the time of analysis, and it was assumed to be 2.31 m aft of the C.G., rather than 2.5 m. Hence the synchronization between calculated and measured time histories presented in this report are slightly in error (no more than 2 ms). The calculations should actually be advanced in time slightly from those presented.

These corrections do not materially affect the results presented herein.

2.5 Tests Conducted/Data Collected

Transrapid-EMS supplied test data to MITRE in two forms, 1) strip chart recordings in a data report [1], and 2) an FM analog tape. MITRE subcontracted to Underwater Systems, Inc. to digitize the data from the tape. The digitized data is used throughout this report for comparisons of calculations with data.

A total of eight tests were conducted in October and November of 1976, four tests with sinusoidal, four with flexible guideway modifications. Table I lists these tests with a reference number used throughout this report. The corresponding Transrapid-EMS reference number is given. (As test #8 was aborted, only seven tests produced data.)

The control system parameter ω (given in Section 3.0) was normally 10 rps, but was increased to 15 rps for Test 4. It is not clear

TABLE 1
LIST OF TESTS CONDUCTED

TEST		DATE	VELOCITY	GUIDEWAY MODIFICATIONS	COMMENTS
MITRE REFERENCE NO.	TRANSRAPID EMS REFERENCE NO.		KM/HR		
1	LHP-5-82	10/12/76	188	elastic	synchronization off by 20 ms. (see Sec. 4.1.2)
2	LHP-5-83	10/14/76	261	elastic	
3	LHP-5-84	10/15/76	331	elastic	
4	LHP-5-85	10/19/76	328	elastic	ω=15 rps
5	LHP-5-86	10/26/76	129	sinusoidal	
6	LHP-5-87	10/28/76	258	sinusoidal	synchronization off by 22 ms. (see Sec. 4.1.1)
7	LHP-5-89	11/04/76	324	sinusoidal	ω=15 rps? (see Section 2.5.1)
8	LHP-5-88	?	321	sinusoidal	aborted test

whether ω = 15 rps for Test 7, as will be discussed in the next section.

Unresolved Questions Concerning the Data

There are several outstanding questions regarding the data. The most significant are as follows:

o MITRE had requested that the control system be altered to obtain higher vehicle accelerations during a few tests. This was attempted by increasing the control system parameter, ω (presented in Section 3.0), from 10 rps to 15 rps. Two questions regarding this change are unresolved:

a. While the data report [1] specifically states that only Test 4 used ω = 15 rps, the final report [2] states that Tests 4 and 7 had ω = 15 rps.

b. The final report [2] indicates that ω = 15 rps only for the heave channel, while verbal information [3] indicated that both heave and pitch used ω = 15 rps.

In light of these uncertainties, MITRE did not model the ω = 15 rps cases. In addition, we assumed that Test 7 was conducted with ω = 10 rps, as the data book states. In Section 4, these uncertainties will be shown to leave unclear whether discrepancies between the theory and calculations are due to incorrect control system assumptions or a failure of the model for the "high speed" region of motion.

o There are discrepancies between the scale factors for some of the data channels. In particular, a variation in excess of 20% was found for data from one guideway deflection sensor when the strip charts in the data book [1] were compared to the same data on the digital tape.

o The front and rear gap sensor signals appear to have the wrong sign. This was determined in two ways, 1) comparison of the phase of the accelerometer signals and control voltages with gap signals for consistency, and 2) comparison of guideway deflections with the measured gaps.

MITRE reversed the sign of all front and rear gap sensor data obtained from Transrapid to account for this. (As the strip chart recordings in the data book [1] and the digitized data agree in sign, we rule out errors during the digitization.)

o The synchronization signals for Test 1 and Test 6 appear to be in error by about 20 ms, as discussed in Sections 4.1.1 and 4.1.2.

3. CONTROL SYSTEM DESCRIPTION

The control system for the KOMET has been documented elsewhere by Transrapid-EMS [4] and it will only be briefly summarized here. Details regarding the control system were supplied to MITRE by Transrapid-EMS.

For the purpose of this experiment, only pitch and heave modes were considered in the model. The other rigid body modes, however, were controlled in an analogous manner.

Figure 4 depicts the control strategy for the pitch and heave modes of the KOMET. The information collected by the gap sensors (d_1 and d_2) and the accelerometers (Z_1 and Z_2) is transformed into heave and pitch signals. These signals are deviations from the nominal, or bias, levels. For the heave channel,

$$d_h = 1/2(d_1 + d_2)$$

$$Z_h = 1/2(Z_1 + Z_2),$$

while for the pitch channel,

$$d_p = 1/2(d_1 - d_2)$$

$$Z_p = 1/2(Z_1 - Z_2)$$

where d_h and d_p are the heave and pitch "gaps," and Z_h and Z_p are the heave and pitch "accelerations", respectively. These signals are processed by digital heave and pitch observer-controllers where they are transformed into heave and pitch mode control voltages. Figure 5 depicts an analog equivalent to the digital observer-controllers. The heave and pitch mode control voltages, U_h and U_p respectively, are transformed into the magnet voltages U_1 through U_5, as follows:

$$U_1 = U_2 = U_h + U_p$$

$$U_3 = U_h$$

$$U_4 = U_5 = U_h - U_p$$

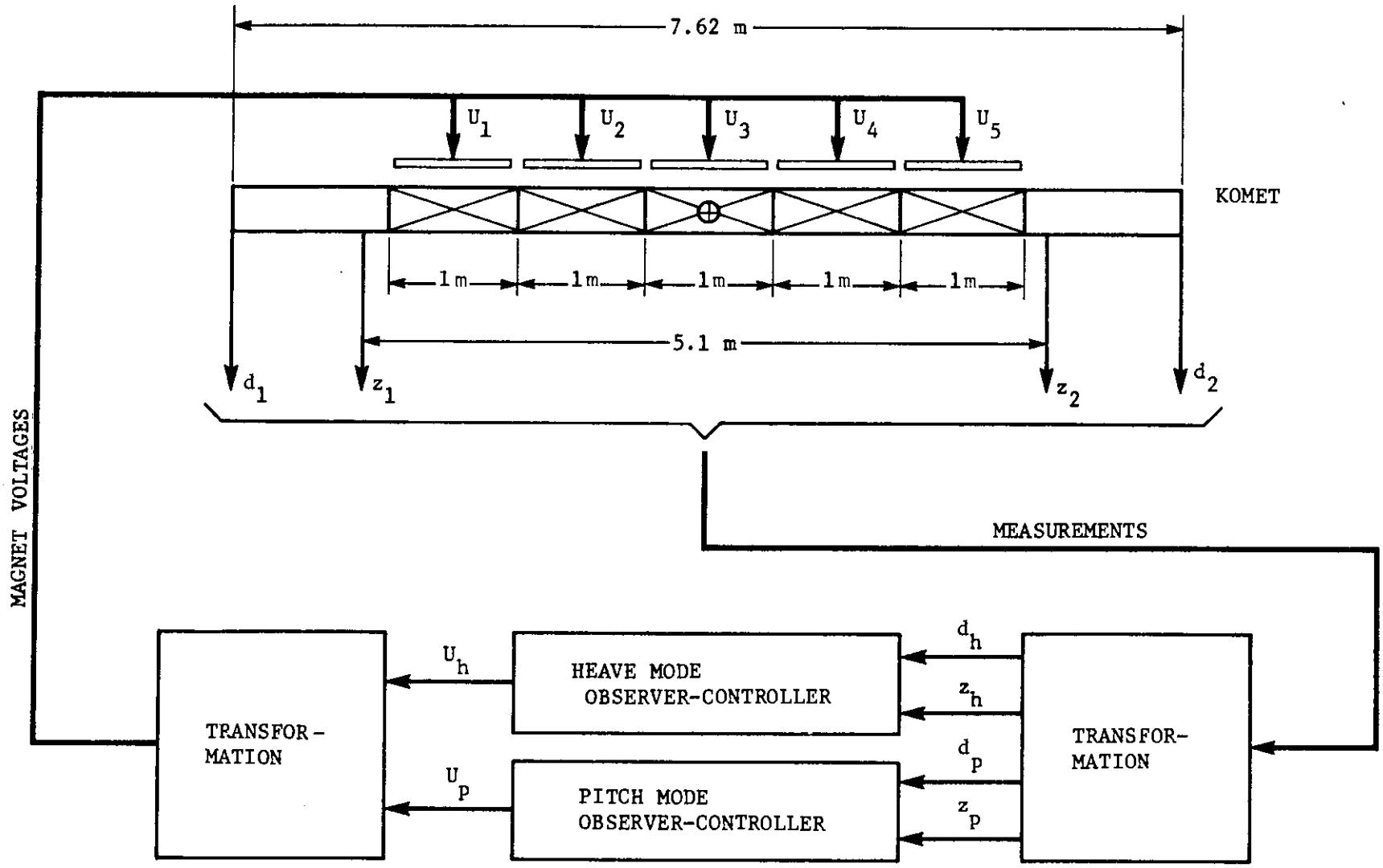

FIGURE 4
BLOCK DIAGRAM OF THE CONTROL SYSTEM

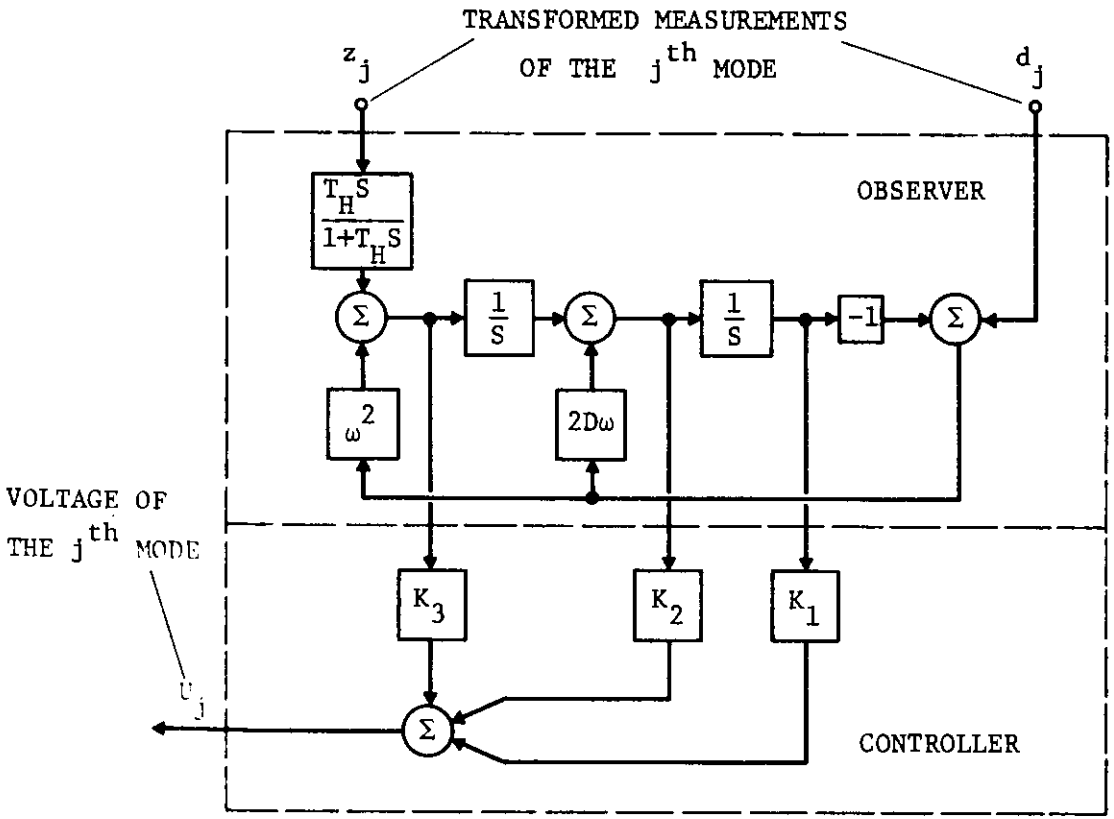

FIGURE 5
BLOCK DIAGRAM OF THE OBSERVER-CONTROLLER

where the subscripts 1 through 5 correspond to the magnet locations given in Figure 3.

For the purpose of modeling the vehicle, magnets #1 and #2 are taken to act at a single point 1.5 m in front of the center of gravity (CG), magnet #3 at the CG, and magnets #4 and #5 are taken to act at a single point 1.5 meters behind the CG.

Linearized expressions of the magnet force laws were used to model the magnets. The incremental magnet force of the j^{th} magnet, F_j, was taken as a function of the incremental current I_j, and the incremental magnet pole face to guideway gap g_j, as follows:

$$F_j = C_1 I_j - C_2 g_j$$

where C_1 and C_2 are constants of the magnet. The current I_j was computed as a function of the magnet voltage from the following equation:

$$U_j = C_3 \dot{I}_j - C_4 \dot{g}_j + R \cdot I_j$$

where R is the magnet electrical resistance, and C_3 and C_4 are constants. Details regarding these constants were supplied to MITRE by Transrapid-EMS [5].

4. RESPONSE TO SINUSOIDAL GUIDEWAY

The calculated steady state response of the KOMET to the sinusoidal disturbance depicted in Figure 2a is given in Figure 6, which depicts the position of the front and rear gap sensors in an inertial reference frame. This figure illustrates the nature of the vehicle response. Note, in contrast to low speeds, for speeds above 200 km/hr the motion of the front gap sensor is small compared to both the 2 mm amplitude of the disturbance and the amplitude of the motion of the rear gap sensor. Hence, for the higher speeds the motion can be roughly described as though the front of the vehicle glides in an inertial path while the rear of the vehicle oscillates vertically. Thus there are both "low speed" and "high speed" regions of vehicle motions of interest for the tests. The actual velocities of the tests are indicated in Figure 6. Note that Test 5 corresponds to a "low speed" region while Tests 6 and 7 correspond to a "high speed" region. This type of motion is not optimal for tracking the guideway disturbance given, but optimal tracking was not the object of the experiment, since the KOMET control system was designed to other criteria. The object of this experiment, to verify analytical models, was constrained to using the control scheme of the KOMET which existed at the time of the tests.

Figures 7 through 9 display the response of the KOMET to the 2 mm amplitude sinusoidal disturbance depicted in Figure 2b. For the purpose of summarizing the results of the tests, measured values are also indicated in these figures. The amplitudes of the measured values were visually estimated from the time histories, since the waveforms were not pure sinusoids. (The actual time histories are compared in Section 4.1.)

Figure 7 displays the calculated gaps at the front, center and rear gap sensors, and the measured gaps at the front and rear gap

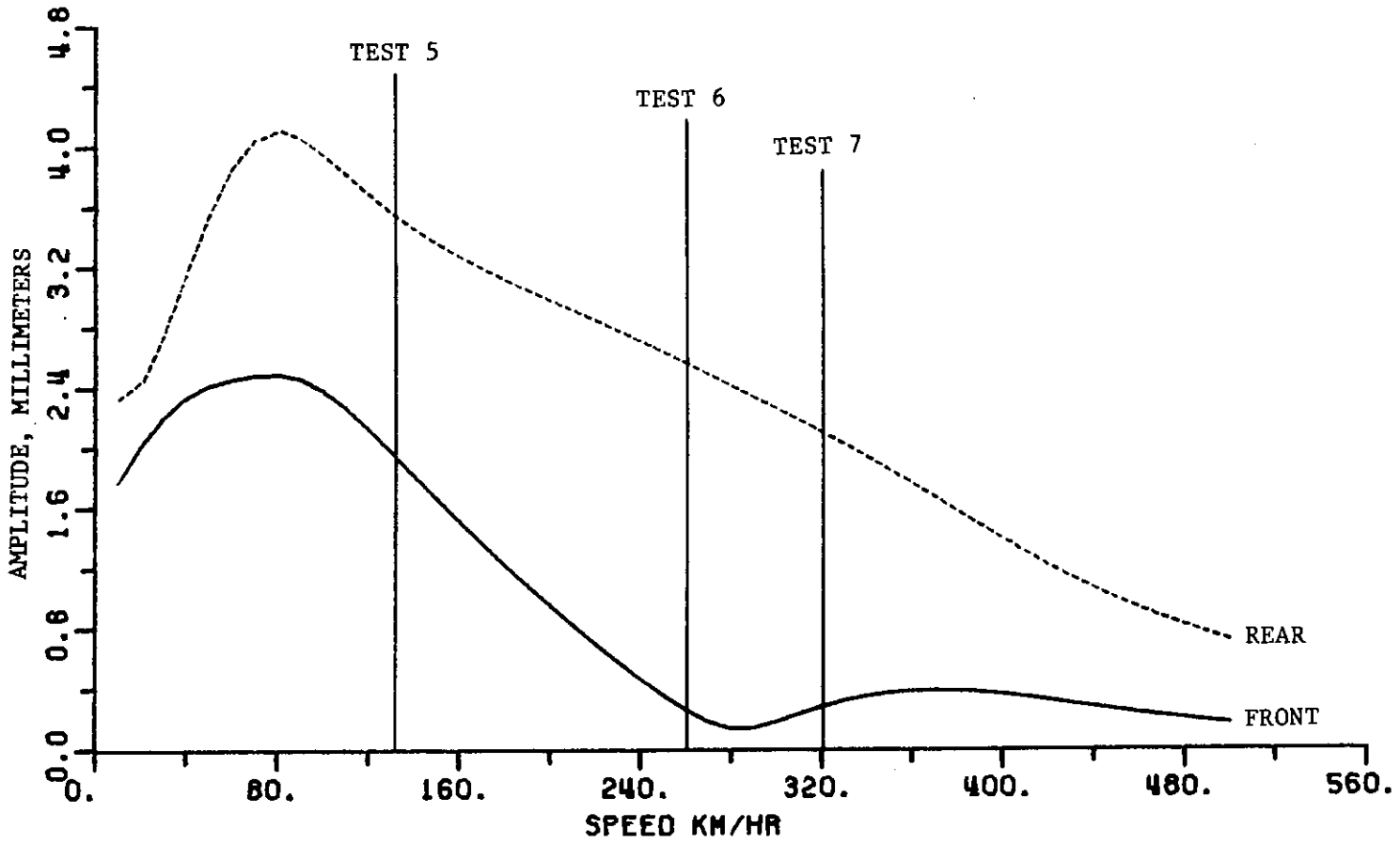

FIGURE 6
POSITION OF FRONT AND REAR GAP SENSORS IN AN INERTIAL REFERENCE FRAME

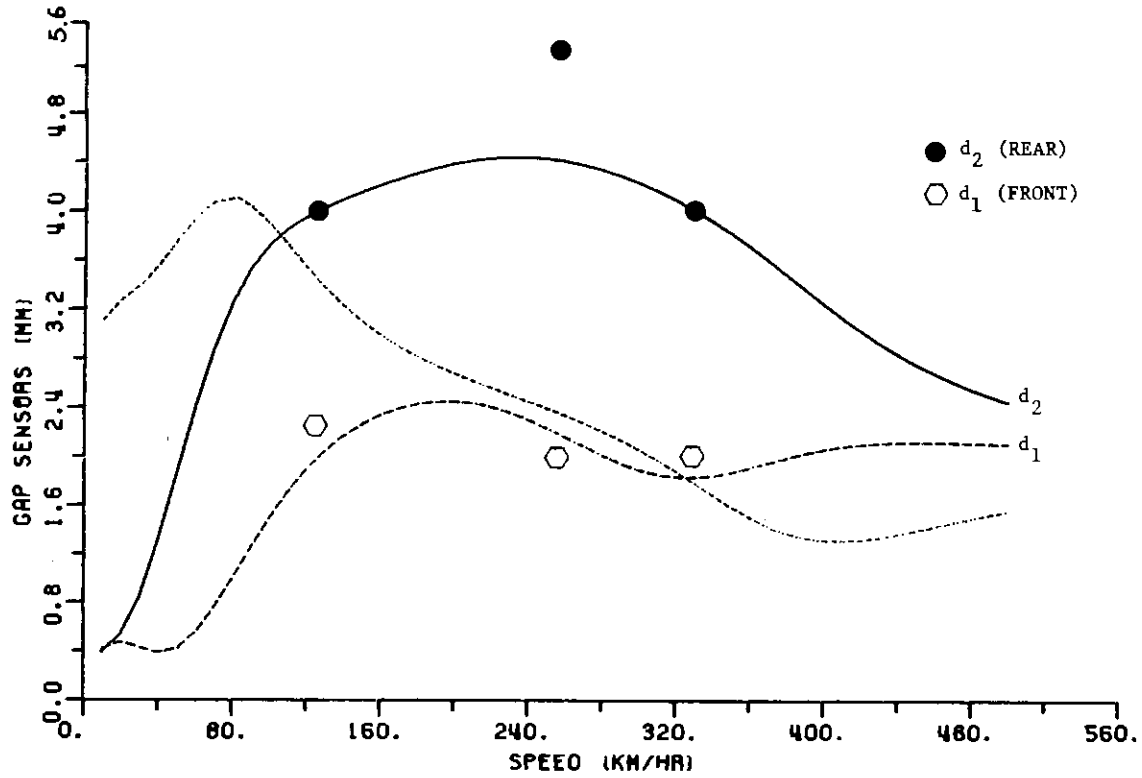

FIGURE 7
VEHICLE/GUIDEWAY GAPS

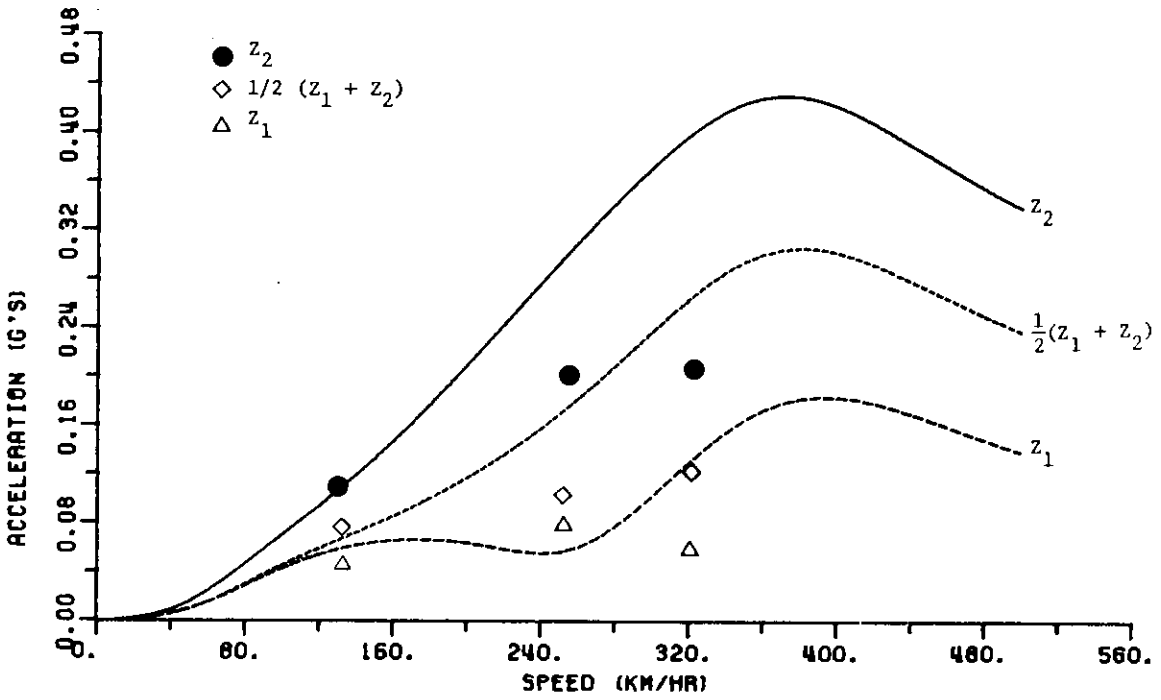

FIGURE 8
ACCELERATIONS

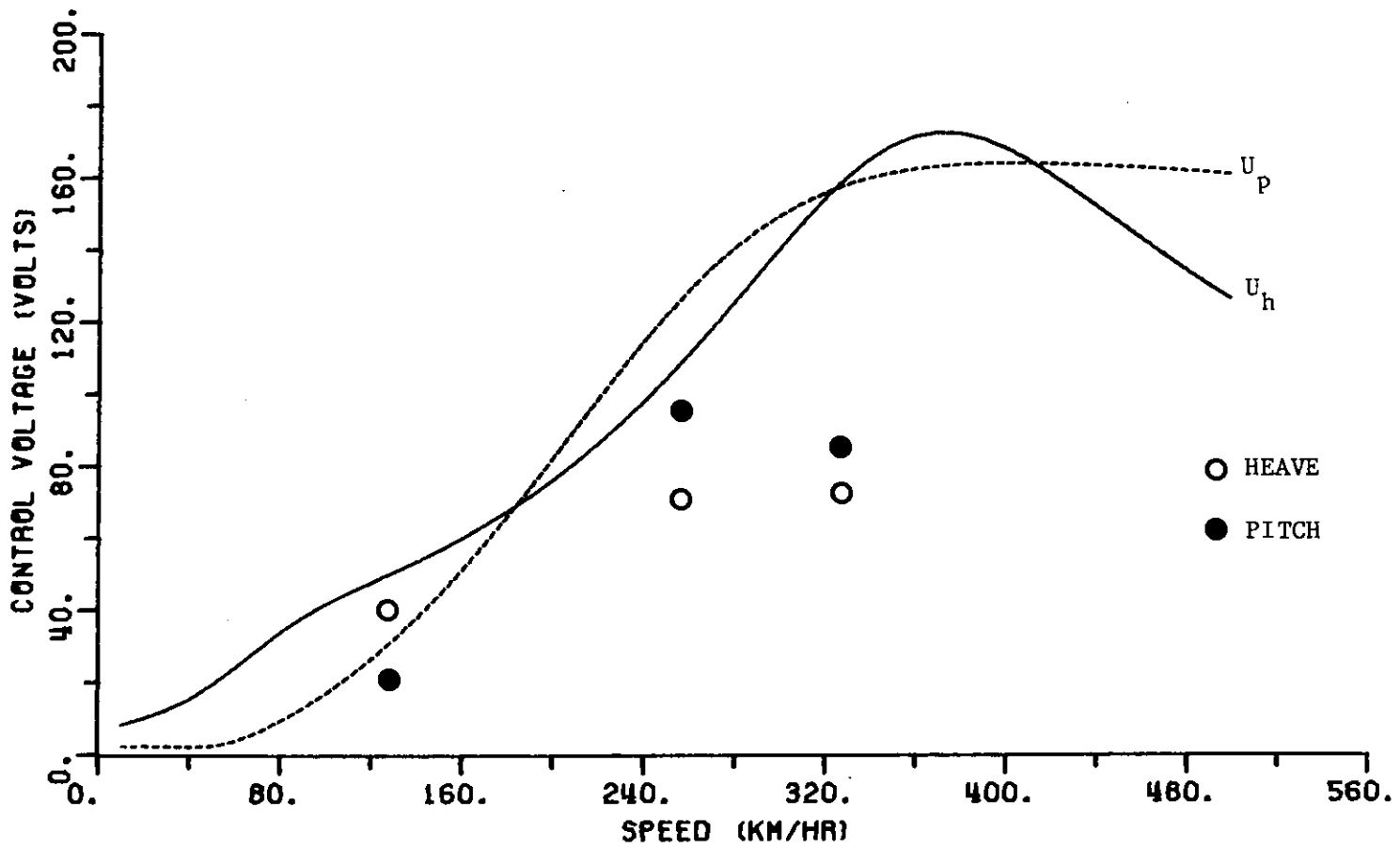

FIGURE 9
HEAVE AND PITCH MODE CONTROL VOLTAGES

sensors. Figure 8 gives the calculated acceleration at the front and rear accelerometers as well as at the center of gravity. Also shown are the measured accelerations at the front and rear accelerometer. Figure 9 gives the calculated and measured heave and pitch mode control voltages.

Note that good agreement between theory and experiment exists for the gaps for all the tests, except for the rear gap in Test 6.

With respect to the accelerations and voltages, the calculations and measurements are in fair agreement for Tests 5 and 6. The calculations of the accelerations and voltages are significantly higher than the measured values for Test 7, the highest speed test.

These results can be assessed with regard to the "low" and "high" speed regions of vehicle tracking. Since the low speed region corresponds to those cases where the vehicle is actively tracking the guideway at a reasonable excitation frequency (3Hz), this case is the most significant one for validating the model. The good agreement for this case can be considered to validate the model for the "low speed" region.

The guideway excitation frequencies were considerably higher for Tests 6 and 7, 6.0 Hz and 7.5 Hz respectively. These tests, which correspond to the "high speed" region, are important for assessing the transient response as well as the stability of the control system. Although the poorer correlation between theory and experiment for the "high speed" region could be due to various physical phenomena, we cannot be sure of the extent of the uncertainties in the data obtained, as discussed in Section 2.5.1.

Examples of unmodeled physical causes for discrepancies between theory and experiment for the high speed region are:

- o magnet force law nonlinearity
- o track and magnet armature eddy currents

There is insufficient data to identify specific physical causes in light of the overall uncertainties in the data.

In general, the following points should be noted:

1. The model may only be valid for small values of vehicle accelerations, since good agreement between theory and experiment was only obtained for Test 5, the low speed test, where vehicle accelerations were below .1g. This would imply that a nonlinear model may be more appropriate at higher accelerations. Note that calculations for Tests 6 and 7 predicted accelerations over .3g for the rear accelerometer.

2. In the high speed region of motion there is reasonably good agreement for the rear gaps, but not for the rear accelerations. This is apparently an inconsistency in the data, since good agreement for the rear gap would imply good agreement for the rear accelerations (considering the large motion at the rear of the vehicle).

(Poor agreement for the front acceleration and good agreement for the front gap is not necessarily inconsistent, since the front of the vehicle moves essentially in an inertial plane of flight with low acceleration. The front gap is primarily determined by the guideway modifications, not the vehicle acceleration, therefore large errors in the front acceleration would be necessary to cause noticeable errors in the measured gaps for the high speed region.)

It is difficult to draw specific conclusions in light of the uncertainties in the data (Section 2.5.1) and the apparent contradictions inherent in the data (discussed above). However, the following points can be made.

- o The gap is the most significant parameter, since the physical phenomena of interest is avoiding contact.
- o The gap sensors tend to read the "cleanest" signals, since accelerometers tend to be quite noisy. This is typical of such instruments in this application, since even very small displacements at high frequencies give rise to large acceleration signals. As the mode control voltages utilize signals from the accelerometers, they too tend to be noisy. Hence the most reliable measure of vehicle motion is the gap sensor.
- o For large motions in inertial space, as are exhibited by the rear of the vehicle for the high speed tests, one would expect the magnet accelerations and voltages to be in reasonable agreement since the gaps were in agreement.

For tracking in the "low speed" region, the region of most significant interest, the model is reasonably well validated. This is substantiated by the good agreement of theory and experiment for the gaps and reasonable agreement for the accelerations and voltages.

Although motion in the "high speed" region does not appear to have fully validated the model, there are sufficient uncertainties in the data to allow the possibility that better agreement does actually exist than was found.

Comparisons of the Time Histories

The previous section compared estimated amplitudes of the measured vehicle motion with calculated values. In addition to amplitude, the phase should be considered, and comparisons of theory and experiment

for the actual time histories were made. These comparisons included the following parameters

- o front and rear gap sensors
- o front and rear accelerometers
- o heave and pitch mode control voltages
- o heave and pitch accelerations (these were calculated from the data by appropriately combining the data for the front and rear accelerometers).

Typical examples will be presented in this section, and for completeness, additional time histories are presented in the appendices. Section 4.1.1 presents results for Test 5, a "low speed" region test, and Section 4.1.2 presents results for Test 7, a "high speed" region test.

4.1.1 Low Speed Region (Test 5)

Figures 10 through 15 present comparisons of the measured and calculated time histories for Test 5 (V = 129 km/hr). This test characterizes the "low speed" region of motion.

The bias levels in the figures, characteristic of the instrumentation used, have not been calibrated as they are not of interest. The average value of each calculated curve was equated to that of the corresponding experimental curve for the purpose of the graphical comparisons shown. The broken lines give the calculated results. Alignment of the calculated curve along the time axis was achieved by utilizing the synchronization signal obtained from the slot detector mentioned in Section 2.4. The guideway section locations under the front gap sensor, as determined from the synchronization signals, are indicated in Figure 10. The time at which the front sensor enters and leaves a section is marked on each side of the section number with a vertical line.

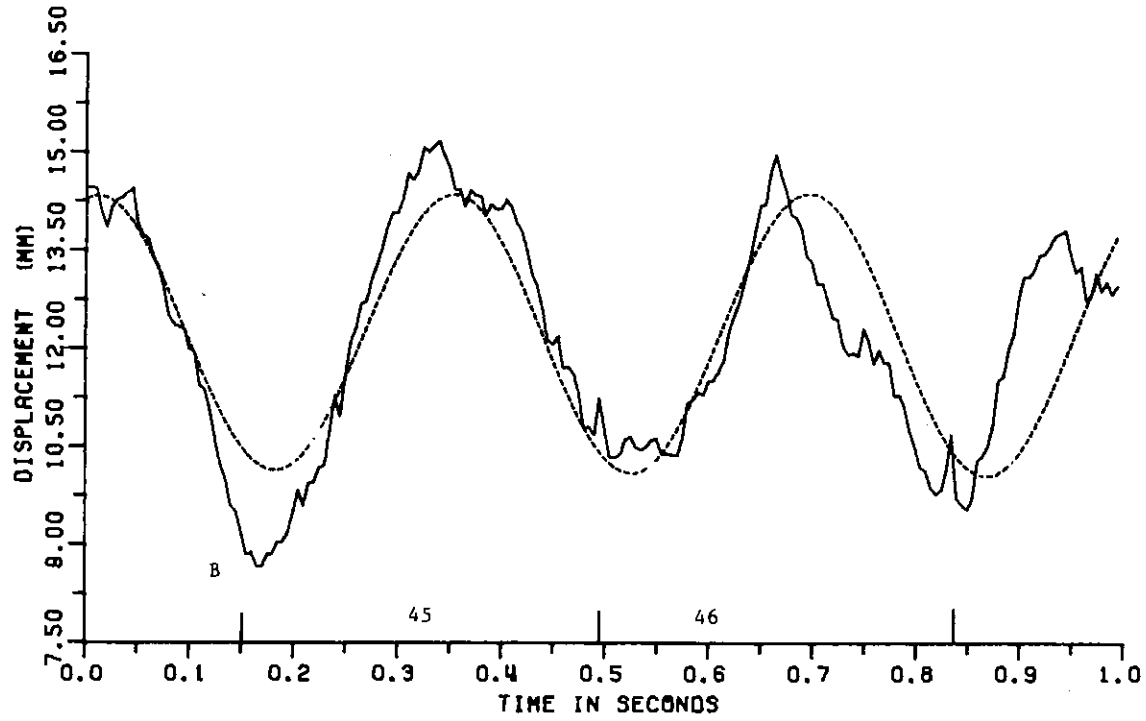

FIGURE 10
FRONT GAP SENSOR

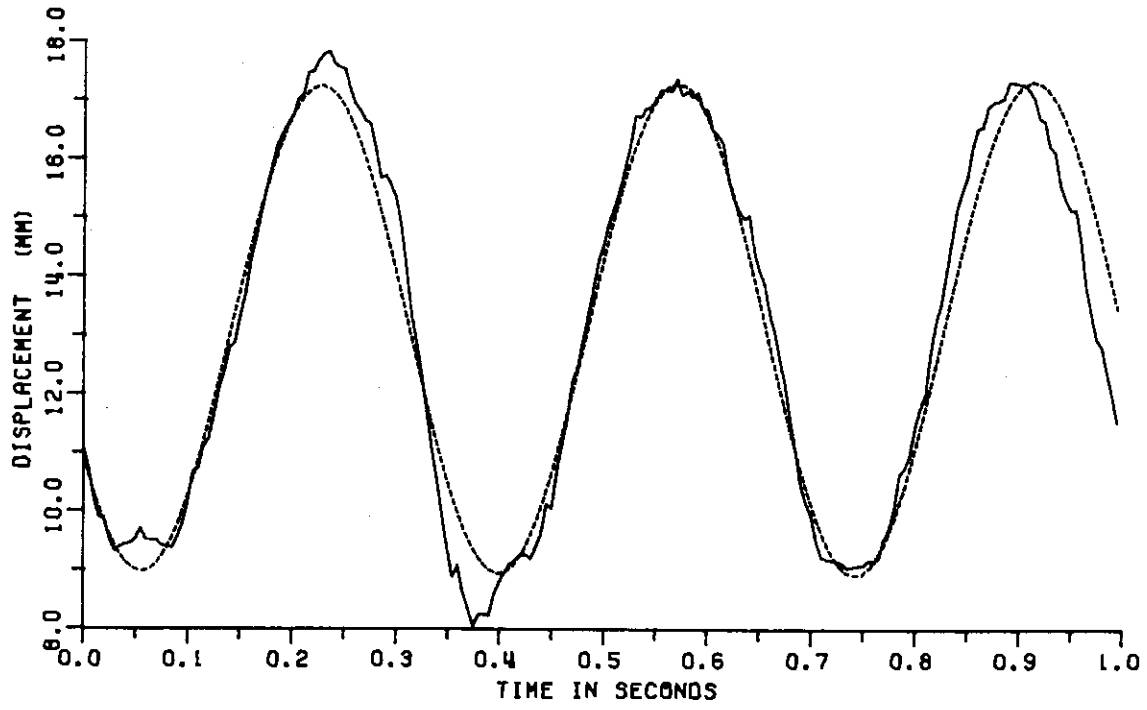

FIGURE 11
REAR GAP SENSOR

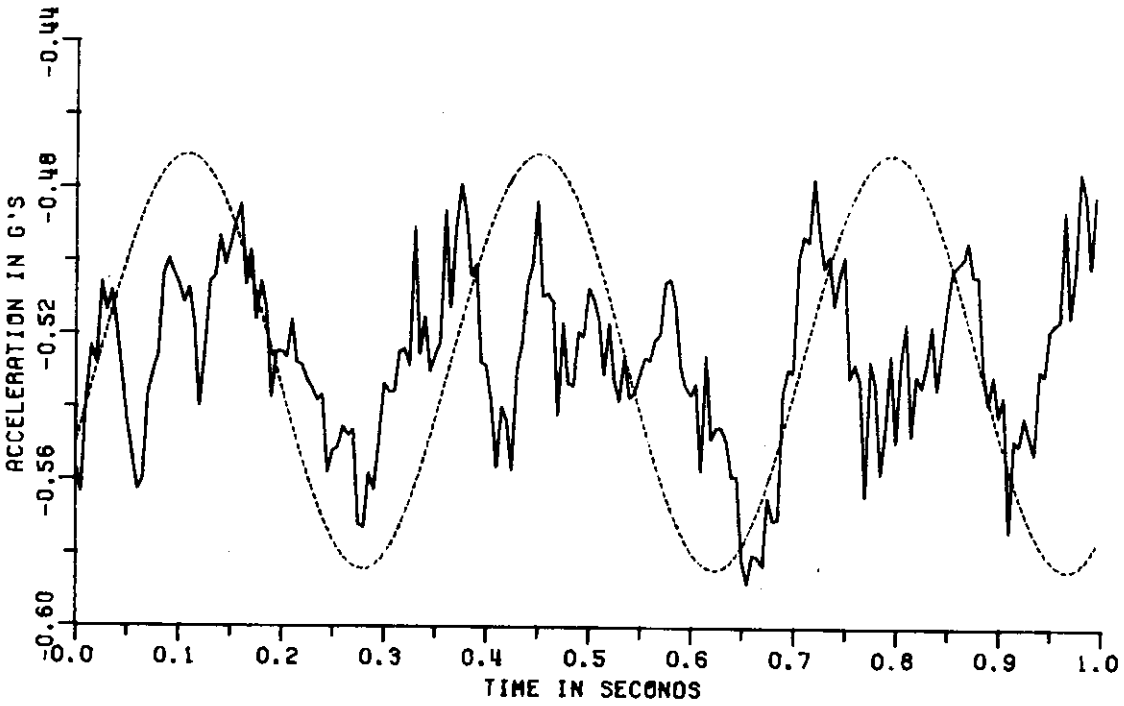

FIGURE 12
FRONT ACCELEROMETER

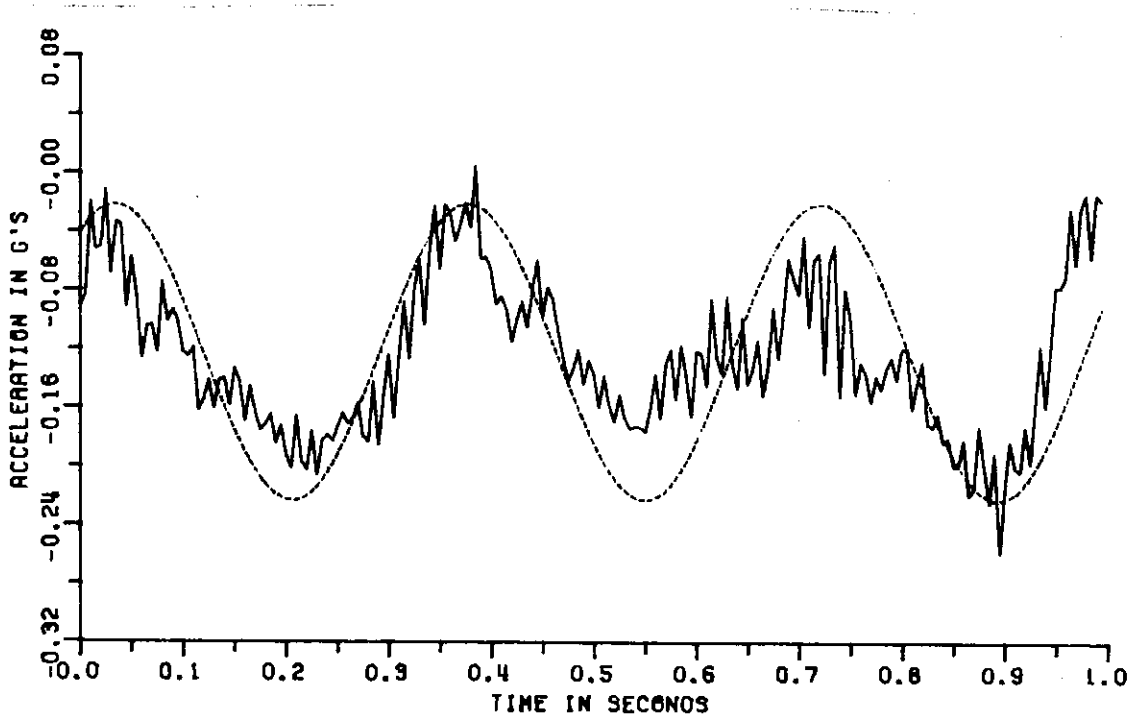

FIGURE 13
REAR ACCELEROMETER

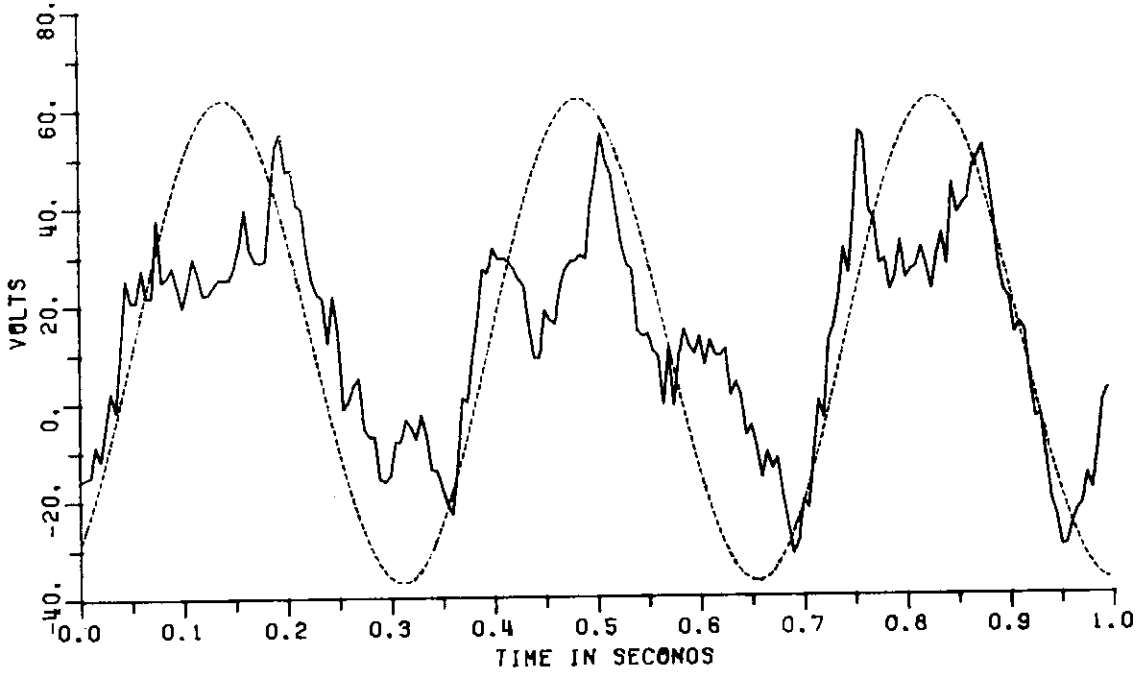

FIGURE 14
HEAVE MODE CONTROL VOLTAGE

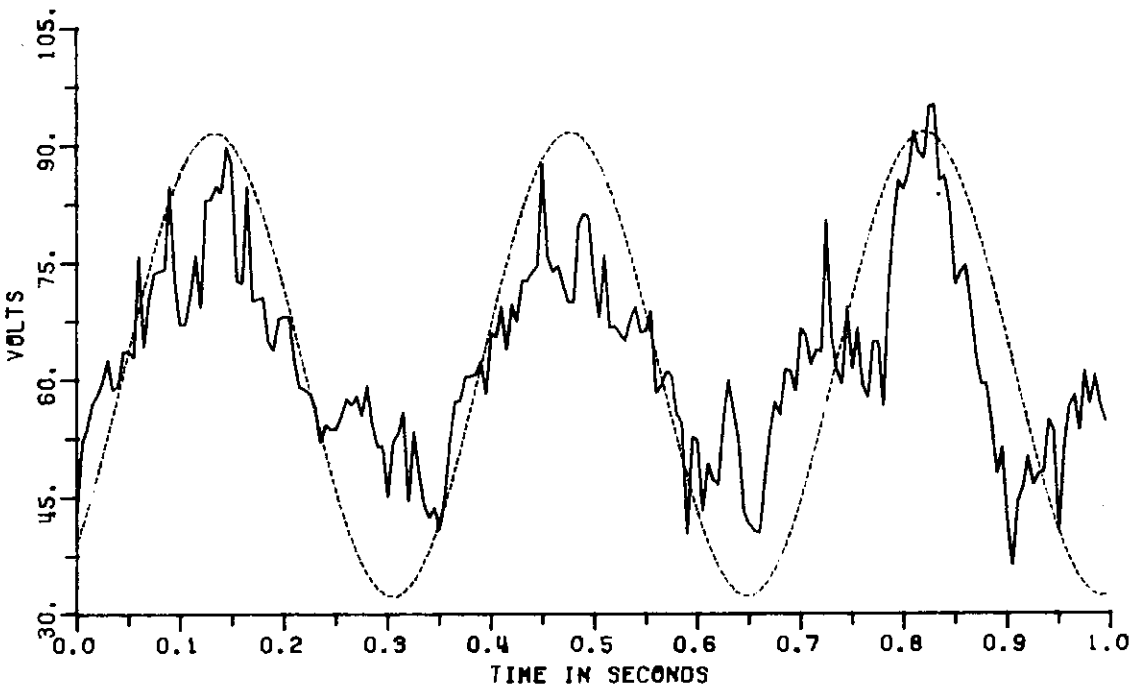

FIGURE 15
PITCH MODE CONTROL VOLTAGE

Figures 10 and 11 display the front and rear gap sensors. Figures 12 and 13 display the front and rear accelerometers. Figure 14 and 15 display the heave and pitch mode control voltages. The heave and pitch acceleration time histories are given in Appendix A. Agreement between the experiment and the calculations is excellent for the gap sensors considering the simplifications made in the simulation. The correlations of accelerations is not as good, but the comparison of accelerations is of less significance than that of the gap sensors. The signals from the accelerometers are noisy, as is typical of such instruments in this application. The mode control voltages utilize the signals from the accelerometers, hence they too are noisy.

4.1.2 High Speed Region (Tests 6 and 7)

Figures 16 and 17 give the gaps at the front and rear gap sensors for Test 7* (324 km/hr). Time histories for the accelerations and voltages are given in Appendix B. The bias values and time synchronization were handled in the manner discussed in Section 4.1.1. The front sensor does not enter the test section until .4 seconds have elapsed, after which the calculated motion for the steady state is approached (see Figure 17). The figures show the agreement between the experiment and the calculations for the gaps are also good for this higher speed test.

Note that the measurements show larger and smaller gaps than predicted at the points designated A and B in Figures 10 and 16. These discrepancies appeared at the same locations for all the tests - both for sinusoidal and flexible guideway test cases. It is likely that these discrepancies are due to a guideway misalignment.

Similar agreement was obtained for Test 6 (258 km/hr), given in Appendix C. For an unknown reason, the calculated and measured time

*Assuming ω = 10 rps, as discussed in section 2.5.1

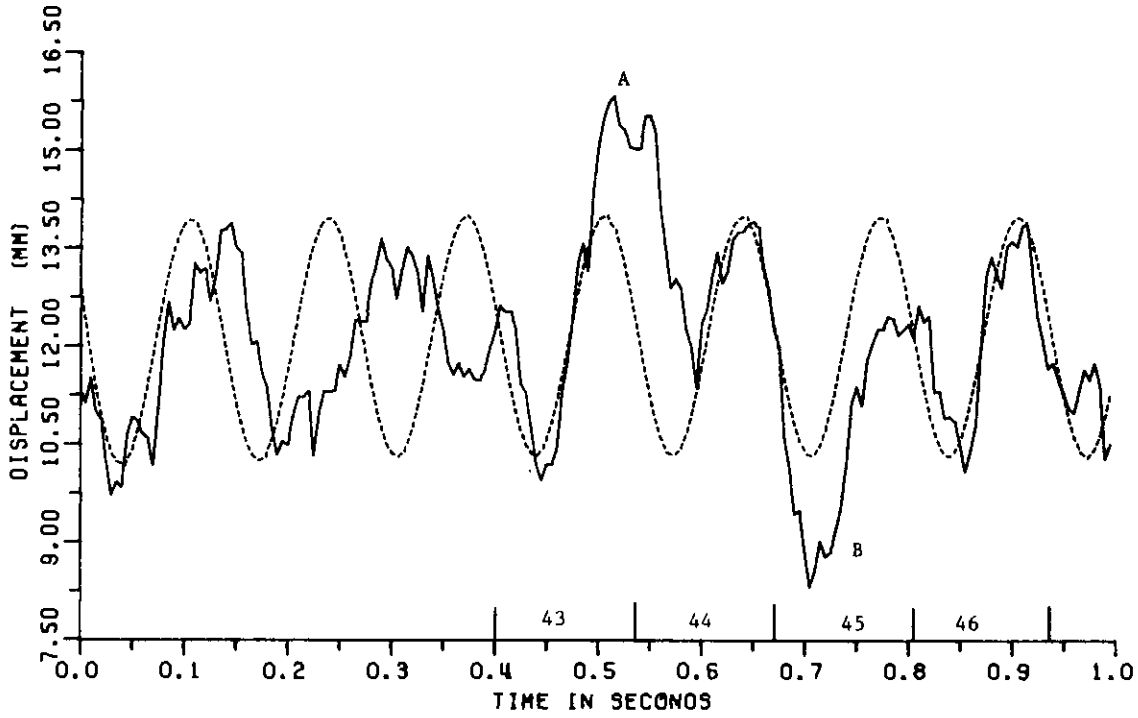

FIGURE 16
FRONT GAP SENSOR

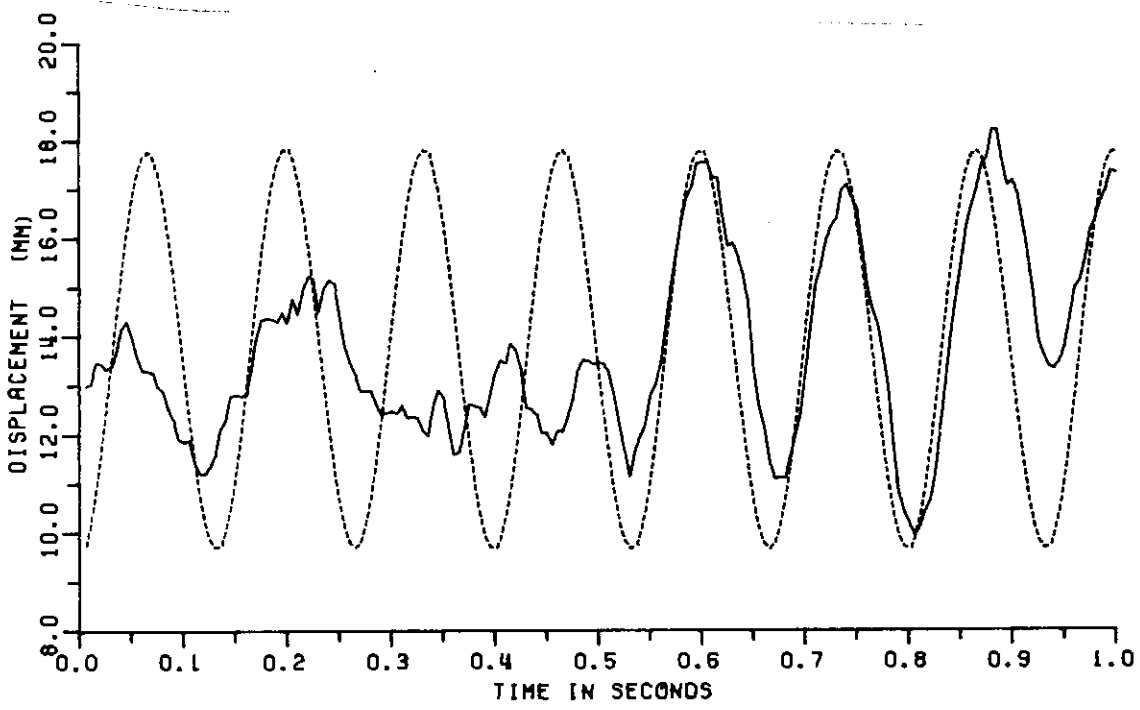

FIGURE 17
REAR GAP SENSOR

histories for Test 6 agreed in phase significantly better if an additional time shift of 22 ms (corresponding to a 1.6 m displacement) was invoked. The results for Test 6 with a 22 ms time shift are given in Appendix D.

As is seen in Appendices B, C and D, the correlations of accelerations and voltages for the high speed tests are even poorer than for the low speed test.

5. RESPONSE TO FLEXIBLE GUIDEWAY

As discussed in Section 2.0, the range of modification of parameters for the LHP test facility was limited to the cases given in Figure 2. For the flexible guideway given in Figure 2b, the test was not expected to induce a significant dynamic interaction between the vehicle and the flexible guideway. It did allow, however, checking the analytical model in the degenerate case for the following two limits:

1) there is no significant dynamic amplification of the guideway deflections, as the crossing frequency ratio is well below the critical value of 2, for a 2-span beam. This dimensionless ratio, given by the vehicle velocity divided by the pier span length and the beam fundamental frequency, is only .69 at 354 km/hr.

2) the vehicle and guideway are uncoupled, as the dynamic tracking forces were relatively small. The guideway, therefore, sees essentially a moving, constant force load.

5.1 Guideway Deflections

Figure 18 shows a comparison of the calculated and measured time histories for Test 1 (188 km/hr). The case shown is that for the sensor indicated as number 2 in Figure 2b. The guideway deflection was calculated for the case of a constant force load (uniformly distributed over a 5 m length) traversing the guideway. As this model has been documented elsewhere it will not be discussed here[6]. For the KOMET tests, the guideway parameters used are as follows: span length ℓ = 6 m, moment of inertia I = 41792 cm^4, weight per unit length ω = 2884 N/m, and cross section area A = 374 cm^2.

As is seen from Figure 18, the calculated and measured deflections agree very well. This was found to be the case for all the elastic guideway tests. The results for several deflection sensors along the instrumented sections for Test 3 are given in Appendix E.

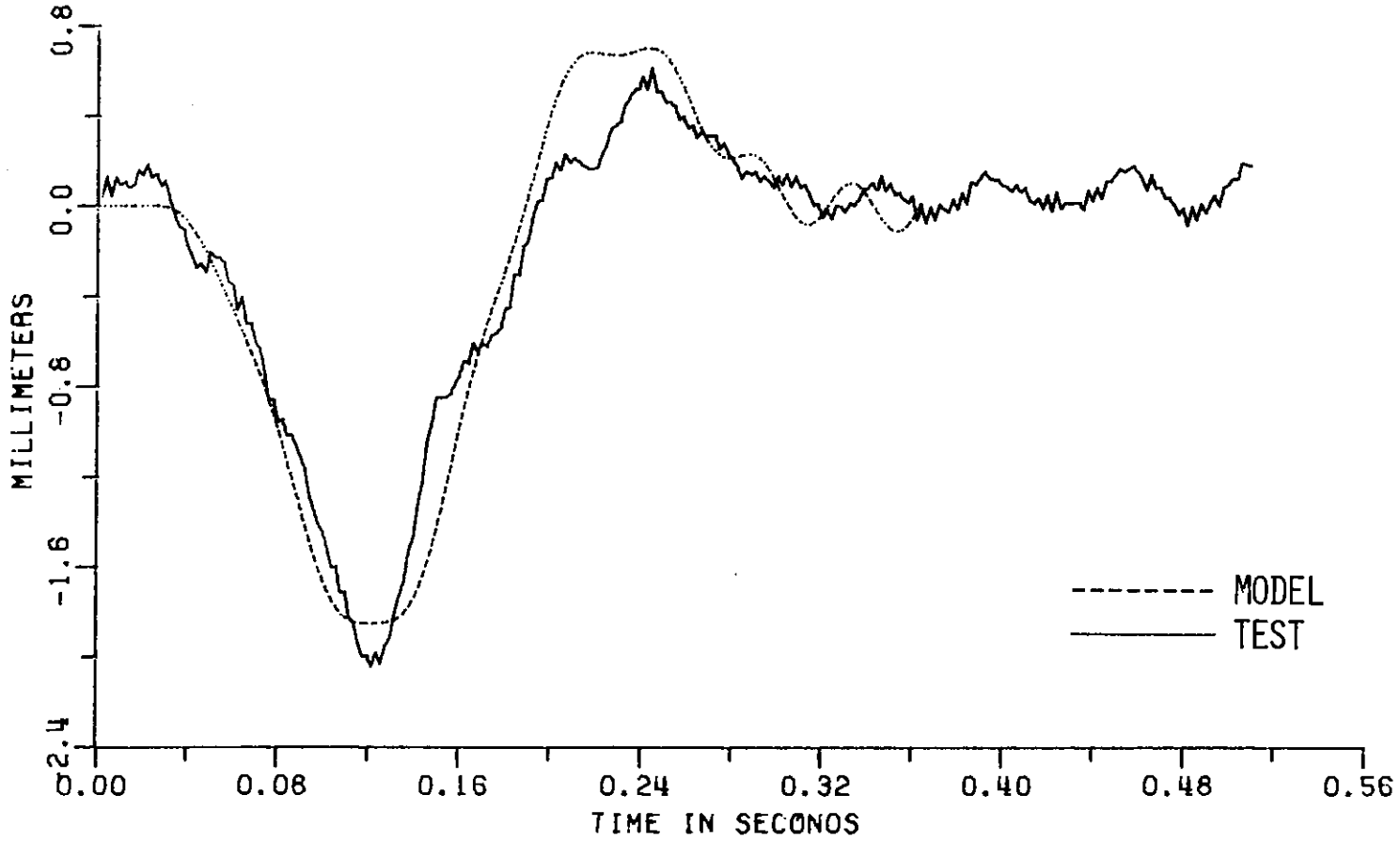

FIGURE 18
FLEXIBLE GUIDEWAY DEFLECTION

Figure 19 gives the maximum deflections, calculated as well as measured, for Test 1 at six of the points measured along the 2 span beam. As expected, no significant dynamic amplification or vehicle/guideway coupling was noted. This is borne out by the good agreement of the measured deflections and those calculated from the moving constant force, distributed load case.

5.2 Vehicle Motion

The guideway deflections calculated from the moving, constant force load were used as a forcing function for an uncoupled vehicle model. This approximation applies to the tests conducted, as discussed in Section 5.0.

Figures 20 through 22 compare the calculated and measured time histories for the front and rear gap sensors and the heave mode control voltage for Test 3 (331 km/hr). The bias levels and phase of the calculated curves were adjusted in the manner described in Section 4.1.1. The agreement between the calculated and measured values is reasonable.

As can be seen in Figure 20, the guideway roughness outside the test sections (#43 to 46) is comparable to the guideway deflections, so that the vehicle response is only partly determined by the guideway flexibility. In addition, since the guideway deflection under the sensor is quite small for one span of the two span beam, the dominant excitation wavelength is actually on the order of 6 m, too short for the vehicle to track. For these reasons, the flexible guideway tests do not provide a thorough check of the model. The discrepancies at points A and B in Figure 20, apparently due to a guideway misalignment, were discussed in Section 4.1.2. In addition, the discrepancy noted as point C was found to occur for all the flexible guidway tests, and is also thought to be a guideway misalignment.

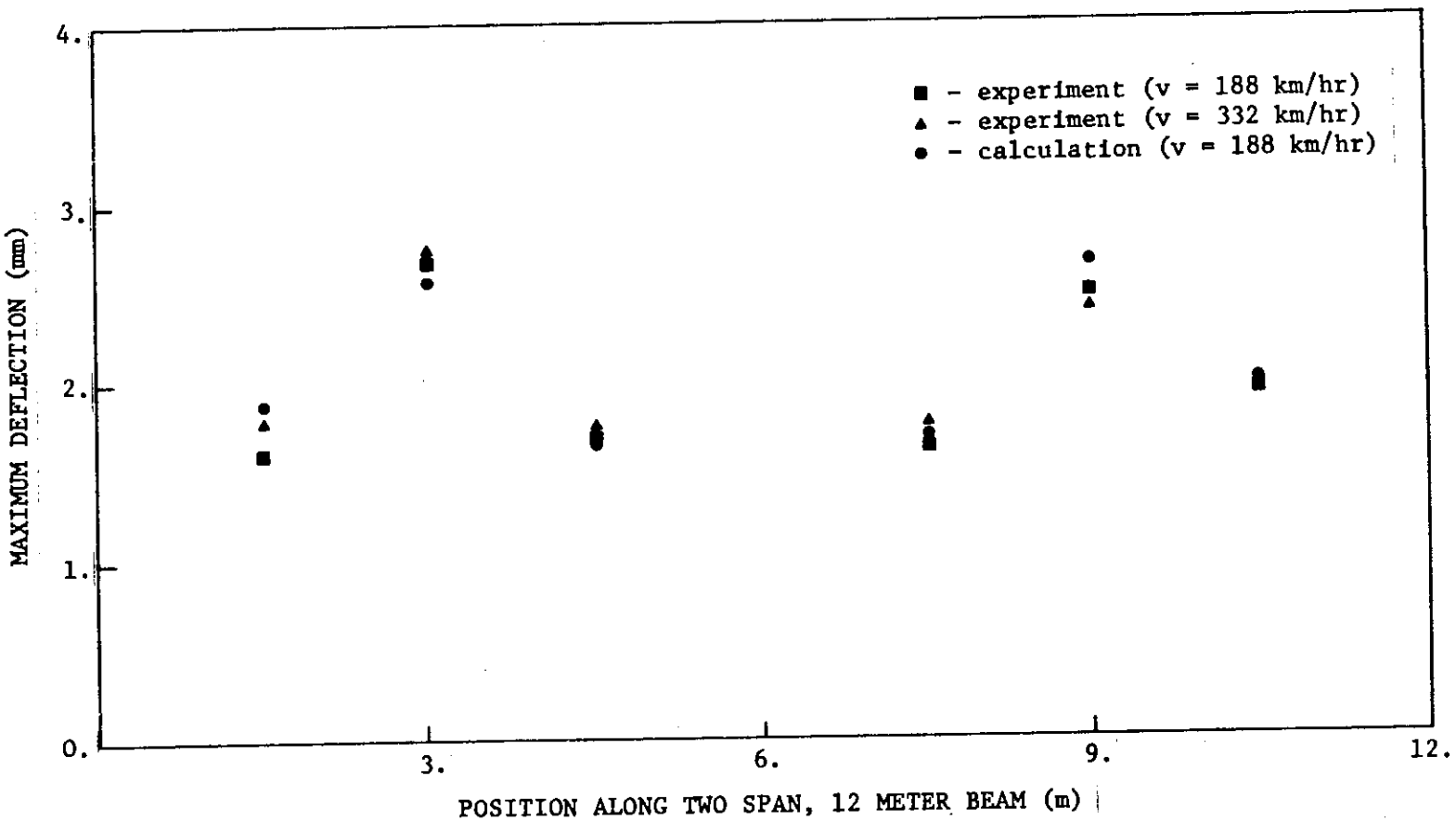

FIGURE 19
MAXIMUM DEFLECTION VS. POSITION

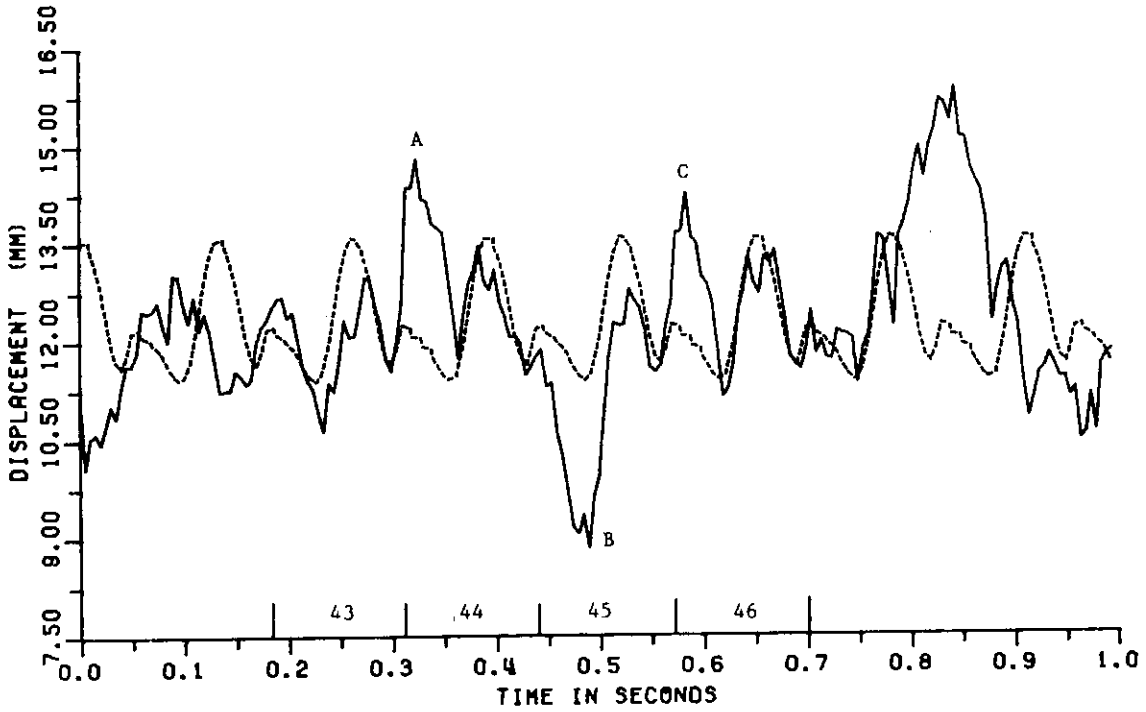

FIGURE 20
FRONT GAP SENSOR

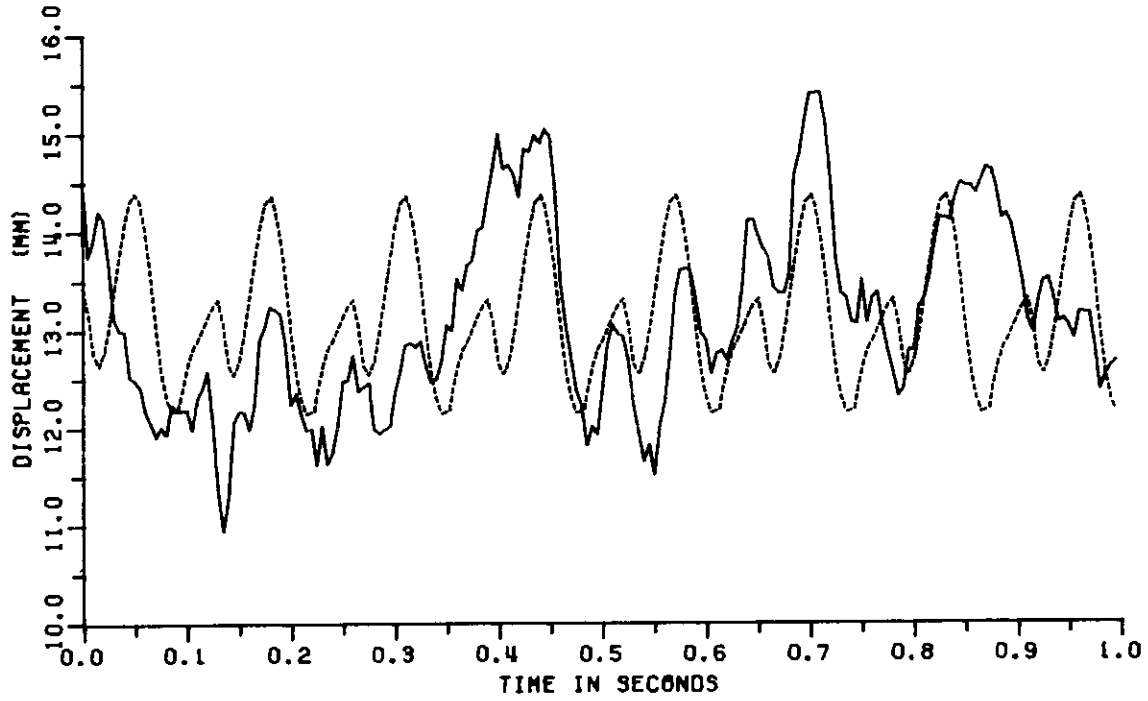

FIGURE 21
REAR GAP SENSOR

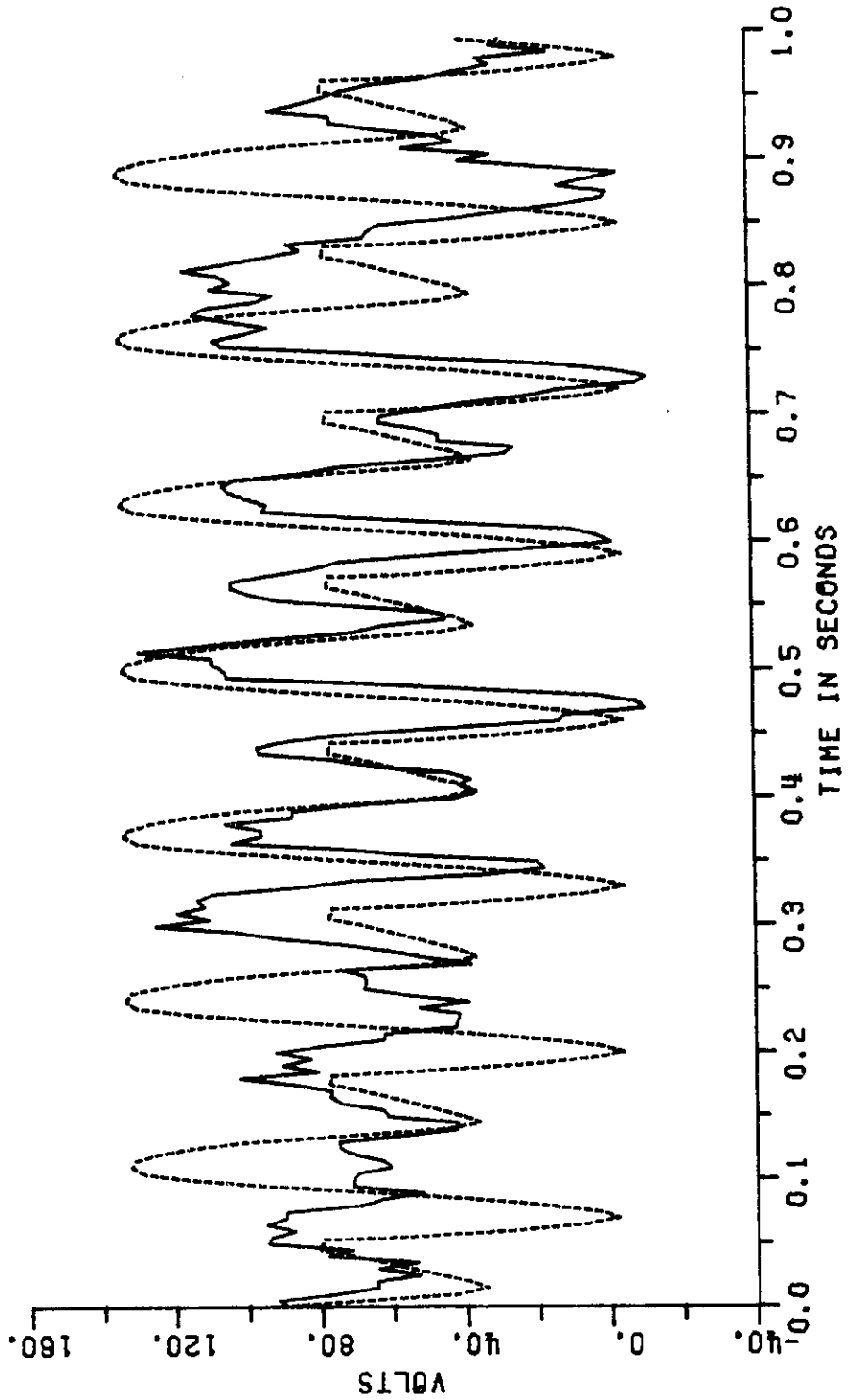

FIGURE 22
HEAVE MODE CONTROL VOLTAGE

The other time histories for this test are given in Appendix F. The time histories for Tests 1 and 2 are given in Appendices G and H. For an unknown reason, the calculated and measured time histories for Test 1 agreed in phase significantly better if an additional time shift of 20 ms is used. The results for this case are given in Appendix I.

6. PARAMETER STUDY

The previous sections of this report dealt with the verification of a specific analytical model, control system, vehicle and guideway. As was discussed in Section 2.0 the control scheme utilized on the KOMET had been designed to criteria other than optimal tracking of flexible guideways. In addition, the achievable guideway modifications were limited by the existing test track. In order to deal with the general problem of vehicle/guideway interactions it is necessary to take a broader approach to control system and guideway design. Reasonable verification of the type of analytical models used for a maglev vehicle was shown in the previous sections.

The detailed problem of a maglev vehicle traversing a flexible guideway will be treated in a general manner. Section 6.1 will discuss the general physical constraints on any maglev vehicle which affect the extent of vehicle/guideway interactions, while Section 6.2 will identify the general conditions which must exist for interactions to be expected.

6.1 Maximum Allowable Guideway Deflection

6.1.1 Acceleration Limit

The maximum guideway deflection that can be negotiated is limited by the lift/weight ratio (L/W) of the magnet bogie. Since a DC magnet cannot repel the guideway, it cannot fall faster than it would when the magnet current drops to zero. If it is assumed that the roughest guideway shape to be tracked is symmetric (it has an equal requirement for upward and downward accelerations), the roughest guideway that can be followed tightly will be limited by this effect. This is termed the "acceleration limit". It has been shown [7] that the peak magnet acceleration $\ddot{X}_{max}$ for this case is limited by the lift to magnet weight ratio, L/W, and the gravity acceleration g, or

$$\ddot{X}_{max} = \frac{L}{W}g \qquad (6.1)$$

Figure 23 defines the coordinate system for the suspension system. The magnet bogie position is X(t), the guideway position under the magnet is $X_g(t)$ and X_o is the bias gap. The gap error $X_e(t)$ is defined as

$$X_e(t) \triangleq X(t) - X_g(t) - X_o \qquad (6.2)$$

For a perfect tracker, the magnitudes of accelerations $\ddot{X}$ and $\ddot{X}_g$ are

$$\left|\frac{d^2}{dt^2} X(t)\right| = \ddot{X} = \left|\frac{d^2}{dt^2} X_g(t)\right| = \ddot{X}_g \qquad (6.3a)$$

and

$$X_e = 0 \qquad (6.3b)$$

If the guideway is sinusoidal in shape, $\ddot{X}_g = A\omega^2$ where A is the amplitude and ω is the frequency of the guideway excitation. The maximum sinusoidal guideway amplitude A_o that can be followed is given by

$$A_o = \ddot{X}_{max}/\omega^2 \text{ (acceleration limit)} \qquad (6.4)$$

The control system is not, however, required to provide perfect tracking. Some gap error is allowed, and A can be increased above the acceleration limit A_o by loosening the tracking; e.g., allowing some gap error. The next section discusses the limit to A imposed on a general control system by the acceleration limit.

6.1.2 Control System Limit

The limit to the tracking ability of a generalized maglev suspension requires treatment by a nonlinear model due to the square law nature of the magnet force law. For the present purpose, a quasi-linear approximation will serve to estimate this limit.

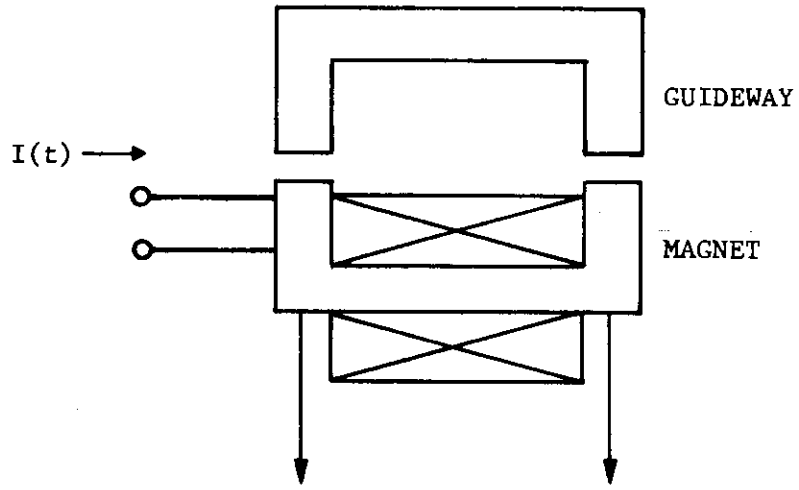

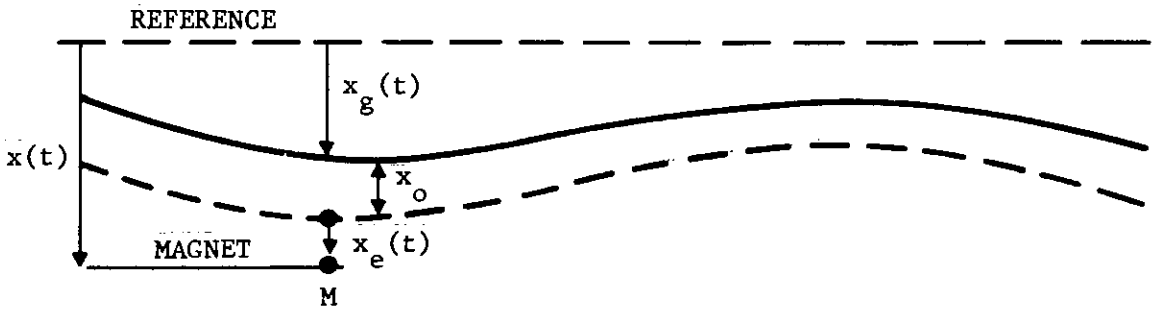

FIGURE 23
COORDINATE SYSTEM FOR MAGNET AND GUIDEWAY

If iron saturation is neglected, the magnet force law is of the form

$$F = F_o \left[\frac{I_o + I(t)}{I_o}\right]^2 \left[\frac{X_o}{X_o + X_e(t)}\right]^2 = F_o + \Delta F(t) \qquad (6.5)$$

where ΔF is the incremental attractive force, F_o is the bias force, I_o is the bias current, X_o the bias gap, $I(t)$ the incremental control current and $X_e(t)$ is the gap error. The deviation from the bias value of F_o is $\Delta F(t)$.

This force law can be linearized to give the LaPlace transform:

$$\Delta F(s) = 2 F_o \left[\frac{I(s)}{I_o} - \frac{X_e(s)}{X_o}\right] \qquad (6.6)$$

Summing forces on the magnet bogie,

$$-\Delta F(s) = Ms^2 X(s) + \Delta F_2(s) \qquad (6.7)$$

where M is the magnet mass and $\Delta F_2(s)$ is the incremental force due to the motion of the secondary suspension. We can take $\Delta F_2(s) = 0$ since ride comfort dictates a soft secondary suspension, hence

$$-\Delta F(s) = s^2 MX(s) \qquad (6.8)$$

Equations 6.6, 6.7 and 6.8 give

$$-s^2 MX(s) = 2F_o \cdot \left[\frac{I(s)}{I_o} - \frac{X_e(s)}{X_o}\right] \qquad (6.9)$$

The fractional control current $\alpha(s) = I(s)/I_o$ is defined by

$$\alpha(s) \triangleq \frac{I(s)}{I_o} = \frac{\ddot{X}_e(s)}{X_o} - \frac{\ddot{X}(s)}{g_o} \qquad (6.10)$$

where $g_o \triangleq \frac{2F_o}{M} = 2(L/W)g$

Without loss of generality, we can assume the suspension transfer function $X(s)/X_g(s)$ is $H(s)$, or

$$H(s) = \frac{X(s)}{X_g(s)} \tag{6.11}$$

the gap error $X_e(s)$ is then given by

$$X_e(s) = X(s) - X_g(s) = \left[H(s)-1\right] X_g(s) \tag{6.12}$$

We evaluate $H(s)$ at the guideway frequency, ω,

$$H(j\omega) = H_r(\omega) + jH_i(\omega) \tag{6.13}$$

where H_r and H_i are the real and imaginary parts of the transfer function. The magnitude of the vehicle acceleration, $\ddot{X}$, and gap error, X_e, are given by

$$\ddot{X} = \left[H_r^{\,2}(\omega) + H_i^{\,2}(\omega)\right]^{\frac{1}{2}} \cdot A\omega^2 \tag{6.14}$$

$$X_e = \left[H_r^{\,2} + 1 - 2H_r + H_i^{\,2}\right]^{\frac{1}{2}} \cdot A \tag{6.15}$$

where A is the amplitude of the frequency of the guideway waveform.

Equations 6.14 and 6.15 are general for a linearized system. They can be solved for $H_r(\omega)$ and $H_i(\omega)$ to give

$$H_r(\omega) = \tfrac{1}{2}\left[\frac{1-\gamma^2}{\beta^2} + 1\right] \tag{6.16}$$

and

$$H_i^{\,2}(\omega) = \frac{1}{\beta^2} - H_r^{\,2}(\omega) \tag{6.17}$$

where the real, positive dimensionless parameters β and γ are defined as

$$\beta \triangleq \frac{A\omega^2}{\ddot{X}} \tag{6.18}$$

and

$$\gamma \quad \Delta \frac{X_e \omega^2}{\ddot{X}} \tag{6.19}$$

The maximum permissible value for γ occurs for $X_e = X_o$, to prevent collisions. Note that solutions do not exist for $H_i^2(j\omega)<0$, which places the following limits on β,

$$\beta_{min} = 1-\gamma \tag{6.20}$$

and

$$\beta_{max} = 1+\gamma \tag{6.21}$$

This limitation simply represents the fact that there must be a minimum gap error, represented parametrically by γ, if the magnet acceleration does not equal the input acceleration; e.g., $\beta \neq 1$.

This result can be used to solve for the maximum guideway amplitude that can be followed, A_{max}, regardless of the control scheme utilized. Substitution of Equation 6.21 into Equation 6.18 gives

$$A_{max} = \frac{\ddot{X}_{max}}{\omega^2} + X_o = A_o + X_o \tag{6.22}$$

when $X_e = X_o$ and $\ddot{X} = \ddot{X}_{max}$. This simple yet important result states that the maximum value for the guideway amplitude that can be followed can be no more than the bias gap X_o plus the acceleration limit A_o which characterizes the perfect tracker, regardless of the control scheme utilized. This is termed the "control system limit".

6.1.3 Consideration of Force Law Nonlinearity

A magnet control system operating about a bias force requires the force to decrease with decreasing current. Equation 6.5 shows that negative currents increase the attractive force rather than decrease it, hence negative currents are not useful for control purposes and are to be avoided. For this reason, the prediction of

negative currents by a linearized model should be interpreted as indicating that the model's range of validity is exceeded. To insure that extreme current excursions are avoided, we impose the condition

$$\alpha \triangleq \left|\frac{I(j\omega)}{I_o}\right| \leq \tfrac{1}{2} \tag{6.23}$$

where $\frac{1}{2}$, chosen in consideration of the square law nature of the force law, helps prevent the force from becoming negative in the linearized model of Equation 6.6.

From Equation 6.10

$$\frac{I(j\omega)}{I_o} = \frac{\omega^2 X(j\omega)}{g_o} + \frac{X_e(j\omega)}{X_o} \tag{6.24}$$

Substituting Equations 6.14 and 6.15 into 6.24, it can be shown that the magnitude α of the current ratio $\alpha(j\omega)$ is given by

$$\alpha = |\alpha(j\omega)| = \left\{\left(\frac{\ddot{X}}{g_o}\right)^2 \left[1 - \frac{(\beta^2-1)}{\Delta\varepsilon}\right] + \left(\frac{X_e}{X_o}\right)^2 \cdot \varepsilon\right\}^{\frac{1}{2}} \tag{6.25}$$

where the parameters

$$\Delta\varepsilon \triangleq \frac{\omega^2 X_o}{g_o} \tag{6.26}$$

and

$$\varepsilon \triangleq 1 + \Delta\varepsilon \tag{6.27}$$

characterize a general system.

Equations 6.14, 6.15 and 6.25 are not specific to any control scheme, and they represent basic physical constraints which cannot be exceeded by any control system design. They define requirements for gain and phase of the control system at a specific excitation frequency ω for a guideway with amplitude A if the vehicle parameters are X_o (the bias gap) and g_o (defined by the lift/weight ratio of the bogie). They can be used to predict the control system parameters β and γ which are necessary for vehicle guideway interactions to be likely.

Figure 24 gives an example for parameter variations of β and γ for a given $\Delta\varepsilon$. The case shown is for ω = 20 rps, X_o = 15 mm, g_o = 10g and $\ddot{X} = \ddot{X}_{max} = .5g_o$. This figure gives α vs. A for various values of gap error. The range of A for which solutions exist for α is limited by Equations 6.20 and 6.21 for β_{min} and β_{max}. Note that larger values of gap error allow wider ranges for α than exist in the figure. A control system can be designed for any β and γ which result in reasonable control currents and gap errors, or $\alpha \leq \frac{1}{2}$ and $X_e \leq X_o$. The perfect tracker can have $\ddot{X} = \frac{1}{2}g_o$ only at $A = A_o = .1225$ m, while several combinations of β and γ will give $\ddot{X} = \frac{1}{2}g_o$ if the gap error is allowed to vary. For example, gap errors between 5 mm and 10 mm will give $\alpha \leq \frac{1}{2}$ if A=.129 m, as can be seen in the figure.

6.1.4 A Specific Control System

The previous results are general. For a specific control system, the choice of β and γ will not be independent.

As an example, we take a control system with gap error and absolute velocity feedback, or

$$\frac{I(t)}{I_o} = K_o X_e(t) + K_1 \dot{X}(t) \tag{6.28}$$

where

$$\dot{X}(t) = \frac{d}{dt} X(t) \tag{6.29}$$

and K_o and K_1 are constants. It has been shown [7] that this yields a magnet suspension with natural frequency ω_n and damping ξ. Solving for β and γ, we obtain

$$\beta = \left[\left(\frac{\omega}{\omega_n}\right)^4 + (4\xi^2-1)\left(\frac{\omega}{\omega_n}\right)^2 + 1\right]^{\frac{1}{2}} \tag{6.30}$$

and

$$\gamma = \left[\left(\frac{\omega}{\omega_n}\right)^4 + 4\xi^2\left(\frac{\omega}{\omega_n}\right)^2\right]^{\frac{1}{2}} \tag{6.31}$$

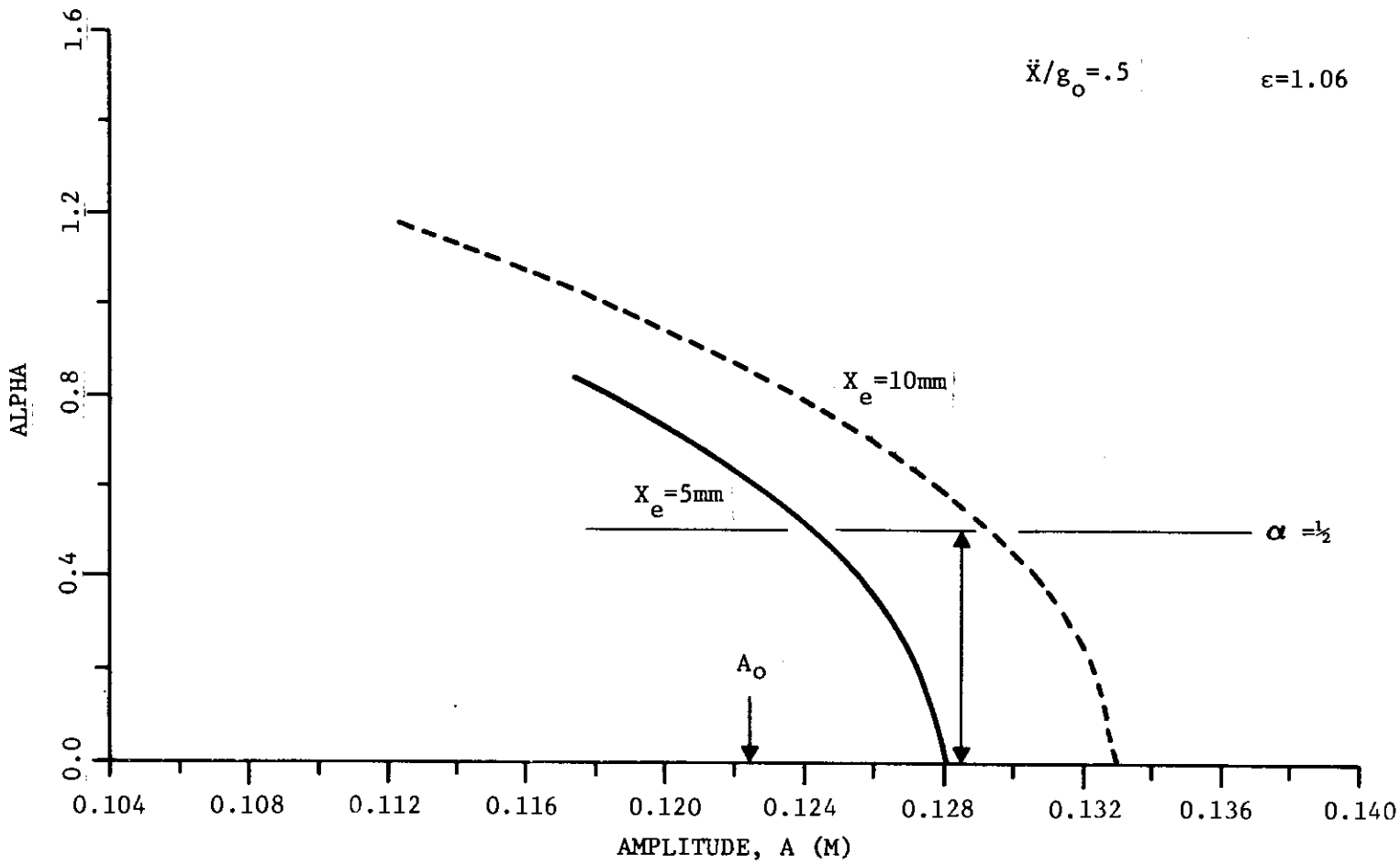

FIGURE 24
PARAMETER STUDY

The choice of control system parameters ω_n and ξ set β and γ. As an example, the case $\xi = \sqrt{2}/2$ is discussed next.

From Equations 6.30 and 6.31, if $\xi = \sqrt{2}/2$,

$$\beta = \left[\left(\frac{\omega}{\omega_n}\right)^4 + 1\right]^{\frac{1}{2}} \tag{6.32}$$

and

$$\gamma = \left(\frac{\omega}{\omega_n}\right)\left[\left(\frac{\omega}{\omega_n}\right)^2 + 2\right]^{\frac{1}{2}} \tag{6.33}$$

The relationships between system parameters have now been established in general, as well as for a specific example. The next section examines the conditions of these parameters which are necessary for vehicle/guideway interactions to exist.

6.2 Conditions for Vehicle/Guideway Interactions

If there is to be an interaction, the magnet acceleration $\ddot{X}$ must be comparable to $\ddot{X}_{max}$. Otherwise, the vehicle could be approximated by a moving constant force distributed load equal to the bias value of the lift, which is not considered an "interaction" in this report. The conditions for developing such accelerations are discussed next.

Figure 25 depicts a vehicle with N independently sprung primary suspensions traversing at velocity V a guideway with pier spacing L_p. The unloaded beam deflection is d_{beam}, the maximum deflection as the vehicle traverses a beam is d_{max}.

Note that the "full wave rectified sinusoidal" shape of the guideway is given by its Fourier series,

$$X_g(t) = d_{max}\,[1 + 2/3 \cos \omega t - 2/15 \cos 2\,\omega t + \cdots]\cdot \frac{2}{\pi} \tag{6.34}$$

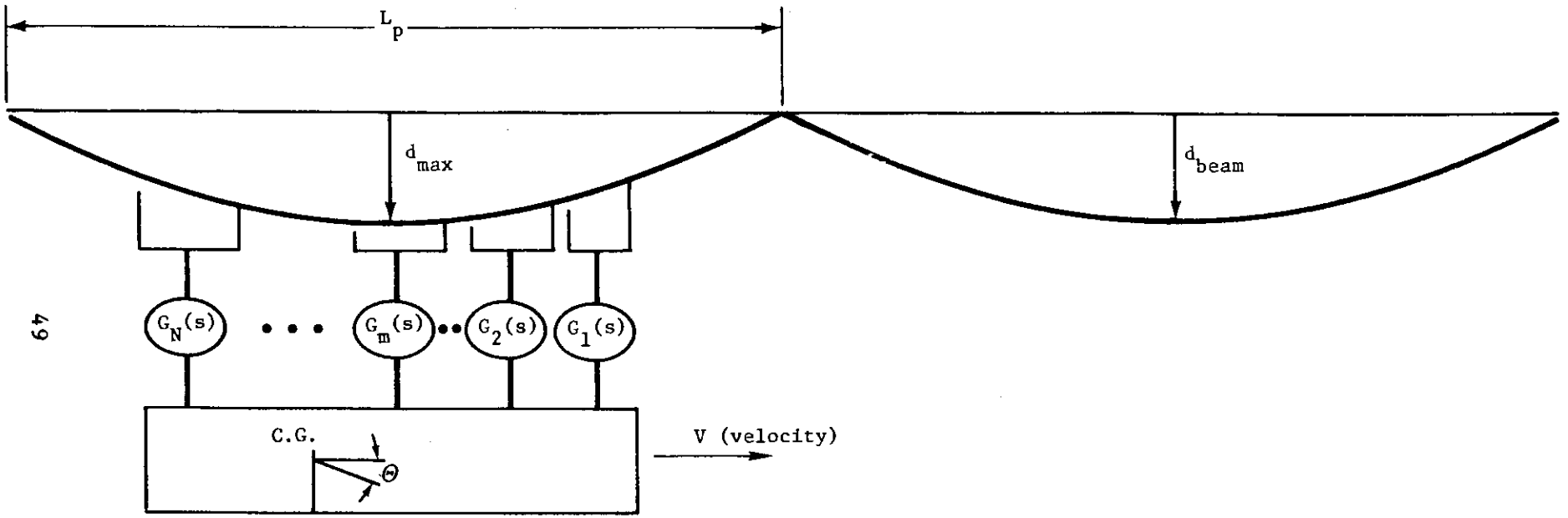

FIGURE 25
VEHICLE AND GUIDEWAY

where $\omega = 2\pi V/L_p$. The pier spacing is L_p and ω is the fundamental frequency of the guideway waveform. The acceleration of the guideway, $\ddot{X}_g(t)$ is then given by

$$\ddot{X}_g(t) = -\frac{2}{\pi}\omega^2 d_{max}\left[\frac{2}{3}\cos\omega t - \frac{8}{15}\cos(2\omega t) + \cdots\right] \qquad (6.35)$$

which is the acceleration a "perfect tracker" would develop. Since the object of the suspension is to avoid collisions, and the first two guideway harmonics account for most of the midspan guideway deflection, it is not necessary, normally, to track the higher harmonics to avoid collisions. The effect of the higher harmonics, which are necessary to define the cusp in the guideway shape near the piers, is primarily to cause short duration gap increases and force "spikes" as the magnet crosses the pier supports. Close tracking of these cusps is not important, as they cause sudden gap increases, not contact. Assuming that the "full wave rectified" guideway is described by only the first two harmonics, Equation 6.35 gives the peak acceleration of the magnet, $\ddot{X}$, as

$$\ddot{X} = .75\omega^2 d_{max} \text{ (first and second harmonics)} \qquad (6.36)$$

which occurs at the pier support. The acceleration due to the first harmonic alone is 55% of that given in Equation 6.36, therefore only 55% of $\ddot{X}_{max}$ can be utilized for tracking the fundamental, the remaining available acceleration is developed by tracking the second harmonic. The acceleration limit to the amplitude of the first harmonic A_o can be expressed in terms of the fundamental frequency ω, as

$$A_o = .55\ddot{X}_{max}/\omega^2 \qquad (6.37)$$

which gives an approximation for the acceleration limit for the case of the "full wave rectified" guideway shape.

The maximum guideway deflection allowed is found by equating the amplitude of the first harmonic in Equation 6.34 to A_{max} which gives

$$d_{max} = 2.4A_{max} \tag{6.38}$$

Invoking Equation 6.22 for A_{max}, but using Equation 6.37 for A_o

$$d_{max} = 2.4\left[.55\ddot{X}_{max}/\omega^2 + X_o\right] \tag{6.39}$$

is the midspan guideway deflection that will cause $\ddot{X} \cong \ddot{X}_{max}$, or interactions to be likely, for the guideway shown in Figure 25.

Figure 26 gives d_{max} vs. L_p for magnet accelerations from .5 to 10 g for the case X_o = 15mm, and Equation 6.39 is used for d_{max}. Since deflections less than the magnet bias gap need not be followed (they do not cause contact), d_{max} becomes constant as ω increases, as indicated in the figure. These curves bound d_{max}, because an unsprung magnet (L/W = 1) will be likely to cause interactions if $.5g<\ddot{X}<1g$, while a magnet sprung with an L/W of 10 (a practical maximum) will be likely to cause interactions if $5g<\ddot{X}<10g$.

The maximum guideway deflection due to vehicle motion must be significant compared to the unloaded beam deflection, or

$$\frac{d_{max}}{d_{beam}} > 1 \tag{6.40}$$

since unless the dynamic deflections are significant they do not affect the tracking ability of the suspension.

Therefore, for interactions to be possible, the beam must be prestressed if d_{beam} (the beam sag without prestressing) is comparable to the values of d_{max} given in Figure 26. Since $d_{max} \propto L_p^2$, while $d_{beam} \propto L_p^4$ (for a given simply supported beam), this becomes an important constraint as pier spacings increase. Note that the parameter of interest is the dynamic beam deflection, not the beam weight.

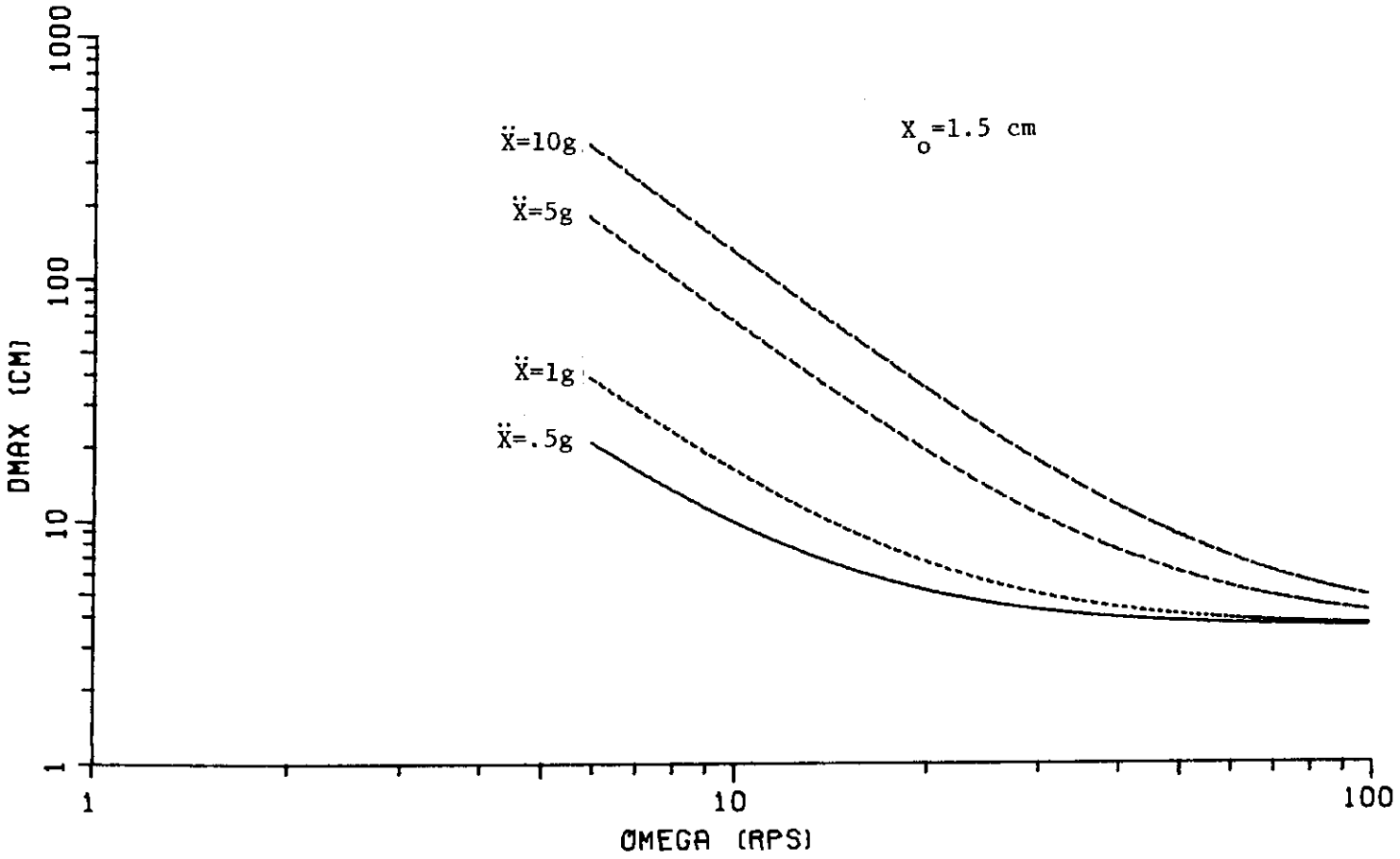

FIGURE 26
MAXIMUM DEFLECTION VS. PIER SPACING

An Example

For vehicle/guideway interactions, we require the magnet accelerations to be approximately equal to $\ddot{X}_{max}$. Equations 6.14 and 6.15 can then be used to define the control system parameters β and γ and the guideway amplitude which will cause vehicle/guideway reactions to be likely for a sinusoidal guideway shape. For the specific case of absolute velocity and gap feedback given in Section 6.1.4, the parameters ω_n and ξ can be varied. Figure 27 shows an example of a parameter study with α and X_e/X_o as a function of ω_n and $\dddot{X}$ for the following parameters

$$X_o = 15 \text{ mm}$$
$$g_o = 98 \text{ m/s}^2$$
$$\omega = 40 \text{ rps}$$
$$\xi = \sqrt{2}/2$$

which correspond to $\Delta\varepsilon = .2248$.

The upper pair of curves give α and X_e/X_o for $\ddot{X} = \ddot{X}_{max}$, the lower pair for $\ddot{X} = \frac{1}{2}\ddot{X}_{max}$. Note that α cannot become less than $\frac{1}{2}$ for the case $\ddot{X} = \ddot{X}_{max}$, regardless of the ω_n chosen. Although this case could be synthesized by a general control system, as shown in Figure 24, it cannot be synthesized for the case in point. Weaker interactions are possible, however, if the magnet acceleration is decreased. For example, the lower pair of curves, for $\ddot{X} = 1/2\ \ddot{X}_{max}$, allows solutions for $X_e/X_o < 1$ and $\alpha < \frac{1}{2}$ if ω_n is greater than 150 rps.

6.3 Computer Programs

A pitch-heave simulation for five independently sprung magnets was programmed for a digital computer. For this model the rigid vehicle and a flexible guideway are coupled. Each magnet is sprung from the secondary mass by a passive spring and dashpot. Current feedback of the form in Equation 6.28, absolute velocity and gap, is

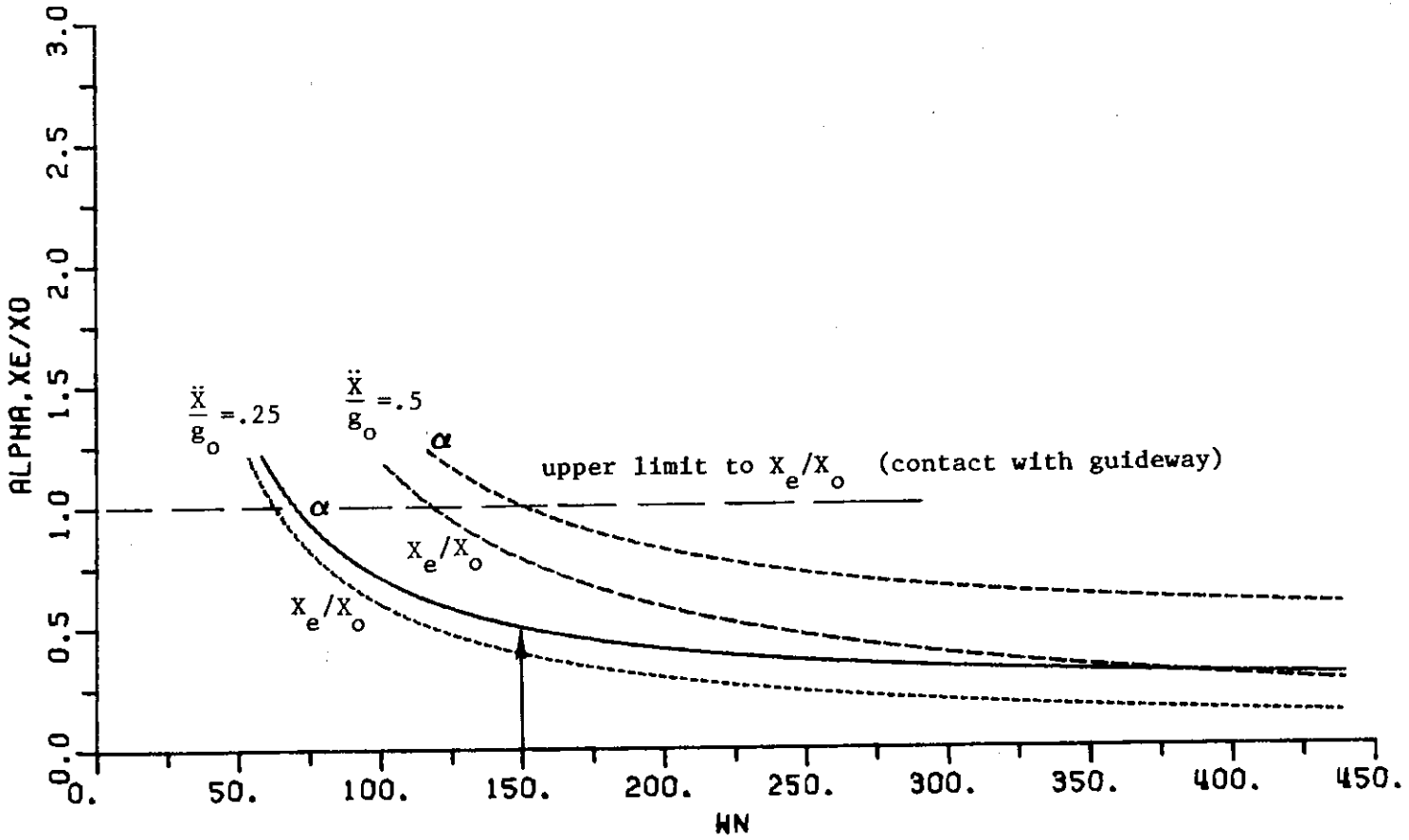

FIGURE 27
CONTROL SYSTEM PARAMETERS

included. The magnet force laws are quasi-linear, as given in Equation 6.6. This type of feedback control was discussed in a previous MITRE report [7].

7. SUMMARY

This report describes the correlation between theory and experiment of an analytical model of a maglev suspension. In addition, a brief discussion of the general conditions necessary for vehicle/guideway interactions (other than those predicted by a moving constant force distributed load) is given. A parameter study is also presented.

With respect to the model verification, reasonable correlation between theory and experiment was found for the vehicle to guideway gaps, poorer agreement was found for the vehicle accelerations and control voltages, especially for the higher speed tests. Due to the difficulty in obtaining "clean" signals for the accelerations and voltages, this poorer agreement is not necessarily significant. The prediction of collisions depends on the gaps, and the validity of gap prediction is the most significant point. The poorer correlation for accelerations and voltages, however, will result in some uncertainty in the validity of the use of the model for conditions which vary widely from the test conditions.

For the parameter study, it is shown that basic limits to the tracking ability of the suspension can be established, regardless of the control system used. For a rigid guideway of the shape shown in Figure 25, the largest amplitude than can be followed, d_{max}, is given roughly by,

$$d_{max} = 2.4\ (A_o + X_o) \tag{7.1}$$

where

$$A_o \triangleq \frac{g_o}{2\omega^2}\ (.55) \tag{7.2}$$

and

$$g_o \triangleq 2\frac{L}{W}g \tag{7.3}$$

where X_o is the bias gap, L/W is the lift to weight ratio of the magnet bogie, and g is the gravity acceleration. These conditions result in large fluctuations in the suspension forces, which indicate that vehicle guideway interactions are likely. When such interactions do occur, a more complex model, preferably for a nonlinear, coupled vehicle/flexible guideway, should be used to evaluate the particular case at hand. The extent such interactions improve or degrade the tracking ability of the suspension may depend on the ratio of pier spacing to vehicle length and the number of magnet bogies assumed, since the instantaneous acceleration of each magnet bogie will depend on its position along the span.

The current German approach to magnet control [4], using a decentralized control system hierarchy, will tend to decouple the response of the magnets. For fully decentralized control, only the motion of the secondary mass and the interaction with the guideway can couple the magnets. A decentralized magnet control scheme was therefore used as the basis of the parameter study in Section 6.0.

Recommendations for Future Work

Although not studied within the scope of this work, data for the magnet currents for the KOMET tests were obtained. The correlation of theory and experiment for these currents could help considerably to resolve the uncertainties noted in the correlations of theoretical and experimental accelerations and voltages. It is suggested that this be made the object of further study.

LIST OF REFERENCES

1. Geier, J.,"Test Runs with the KOMET on Flexible or Shaped Trackway on the LHP Trial Stretch in Manching," Transrapid-EMS Report 9254TB 2001, December 1976.

2. Meisinger, R., "Theoretical Research for the Test Runs with the KOMET on Flexible or Sine Shape Formed LHP Trackway," Transrapid-EMS Report 7624TB 2002, April 1977.

3. Private communication , L. Miller, Transrapid-EMS (9/7/77).

4. Gottzein, E., Miller, L., and Meisinger, R., "Magnetic Suspension Control System for High Speed Ground Transportation Vehicles," presented at the World Electrotechnical Congress in Moscow, June 21-25, 1977.

5. Meisinger, R., "The Structure and Gains of the Controller KOMET," Transrapid-EMS Document TN-RT21-131/76, July 1976.

6. Ravera, R.J., and Anderes, J.R., "Analysis and Simultation of Vehicle/Guideway Interactions with Application to a Tracked Air Cushion Vehicle," MITRE Corporation, MTR-6839, February 1975 (also available from NTIS, Springfield, Virginia PB 242 014).

7. Katz, R., "Attraction Maglev Guideway Follower Used for Non-Contacting Power Collection: Analytical and Experimental Treatment," MITRE Corporation, MTR-6575, December 1973.

APPENDIX A

Test 5 - Heave and Pitch Accelerations

SPEED: 129 km/hr

GUIDEWAY MODIFICATION: Sinusoidal

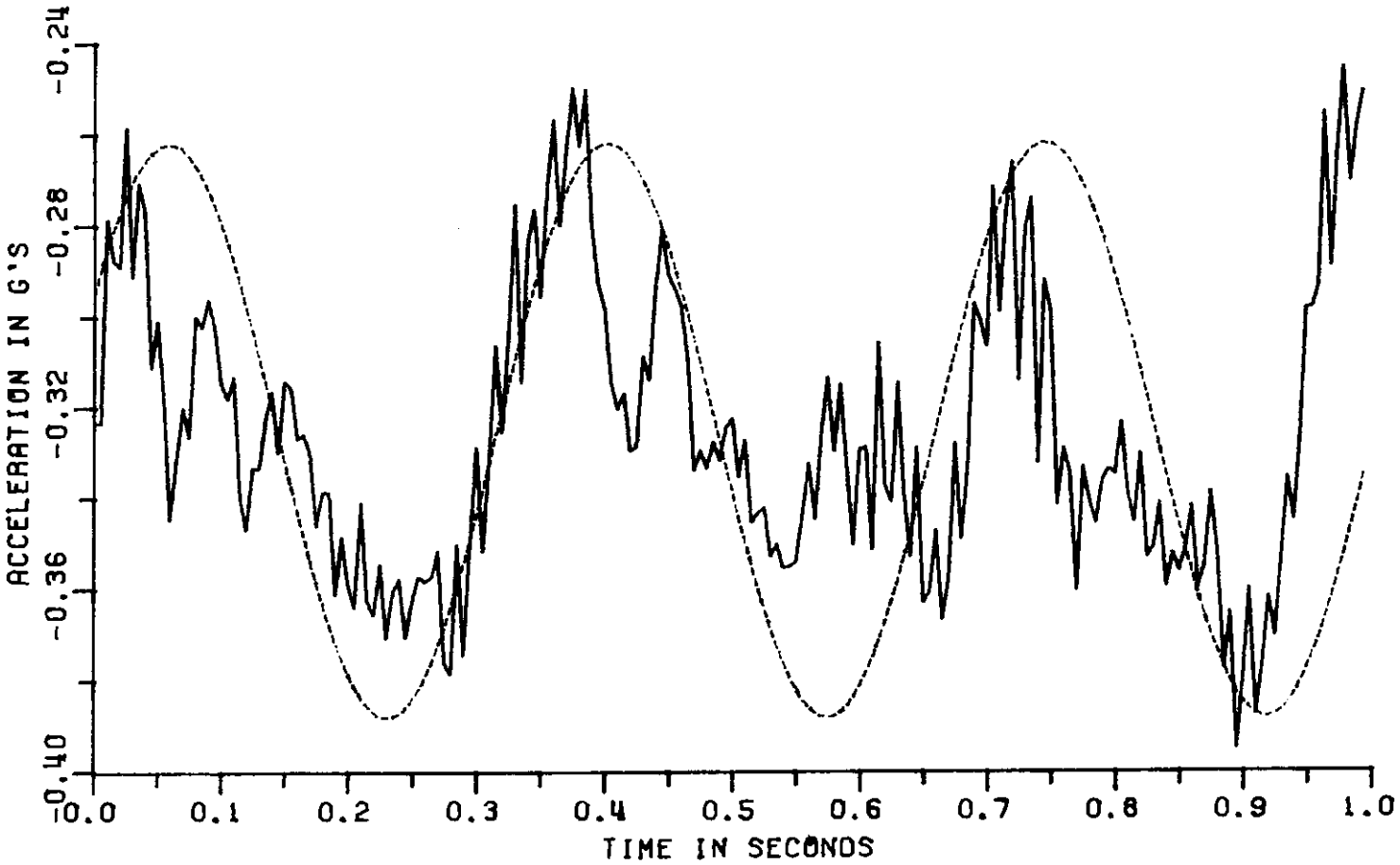

HEAVE ACC TEST 5

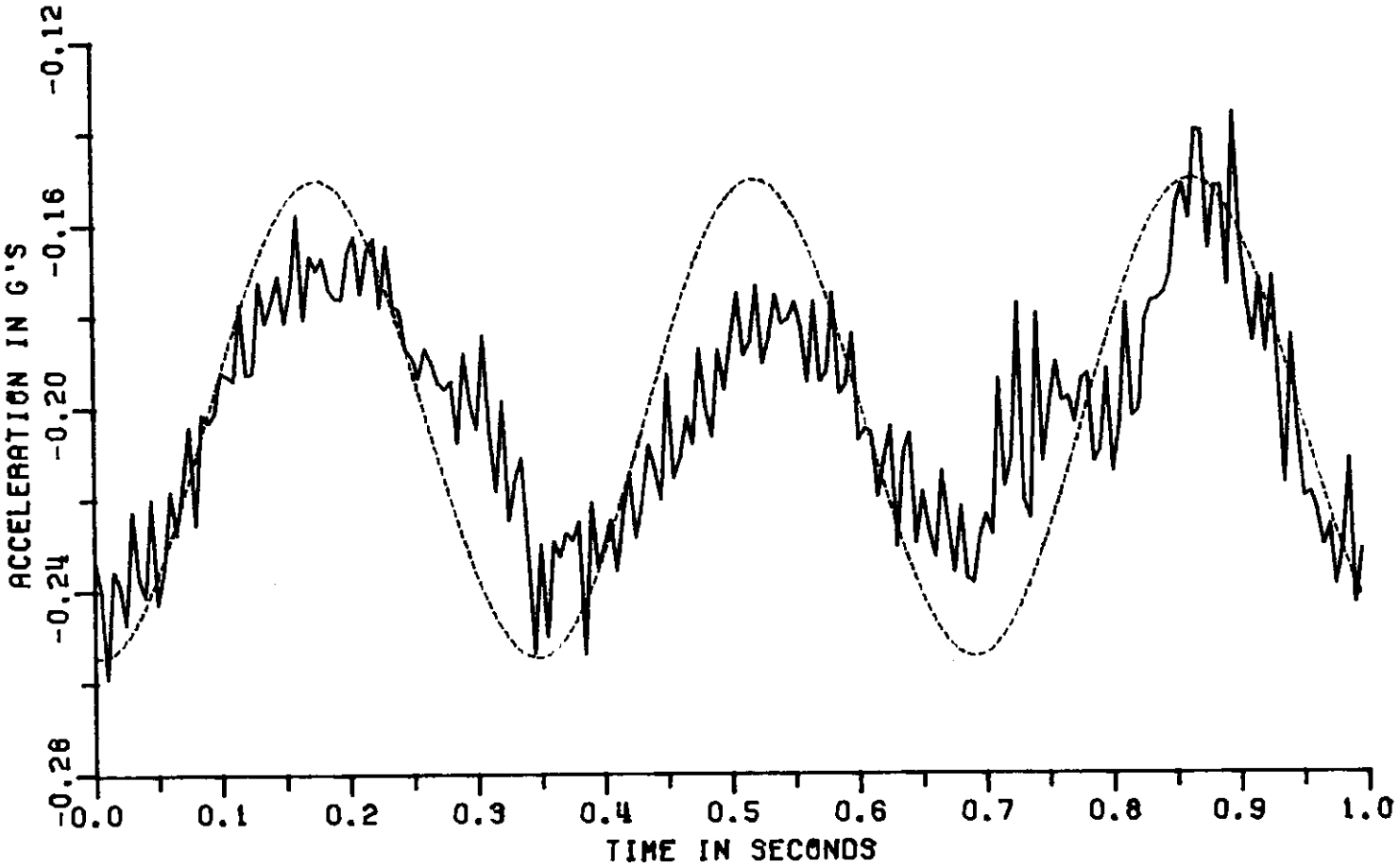

PITCH ACC TEST 5

APPENDIX B

Test 7 - Accelerations and Voltages

SPEED: 324 km/hr

GUIDEWAY MODIFICATION: Sinusoidal

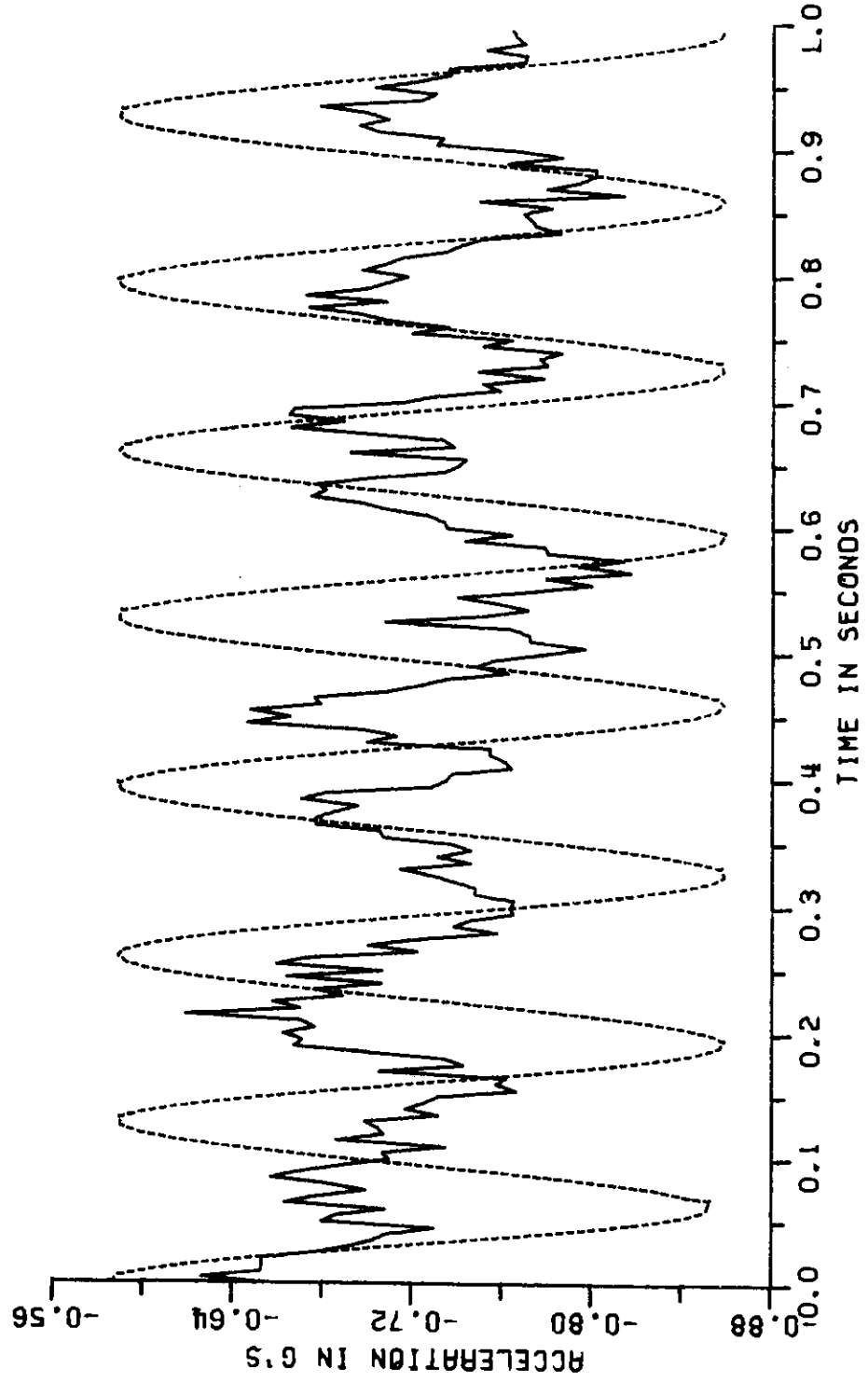

FRONT ACC TEST 7

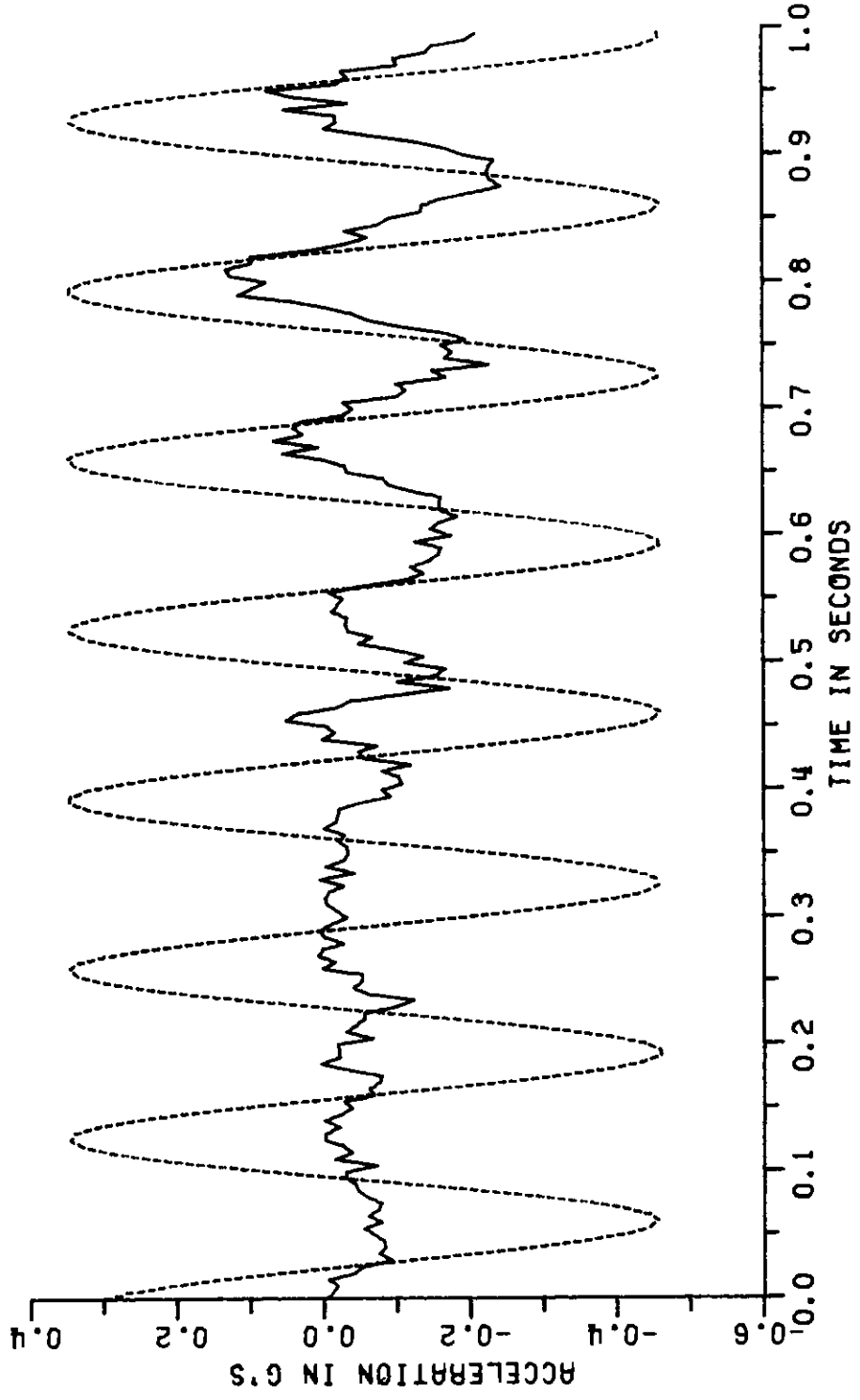

REAR ACC TEST 7

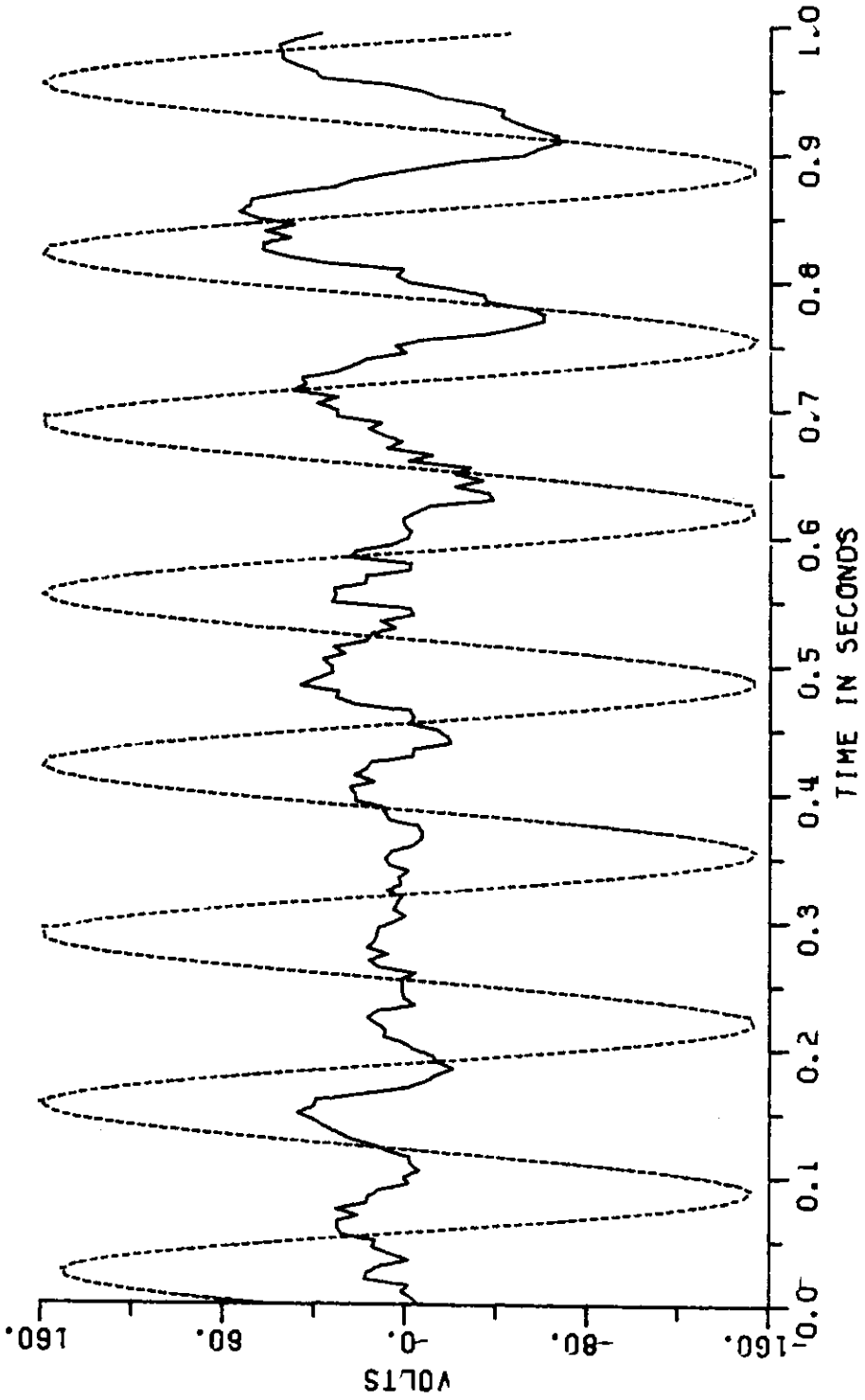

HEAVE VOLT TEST 7

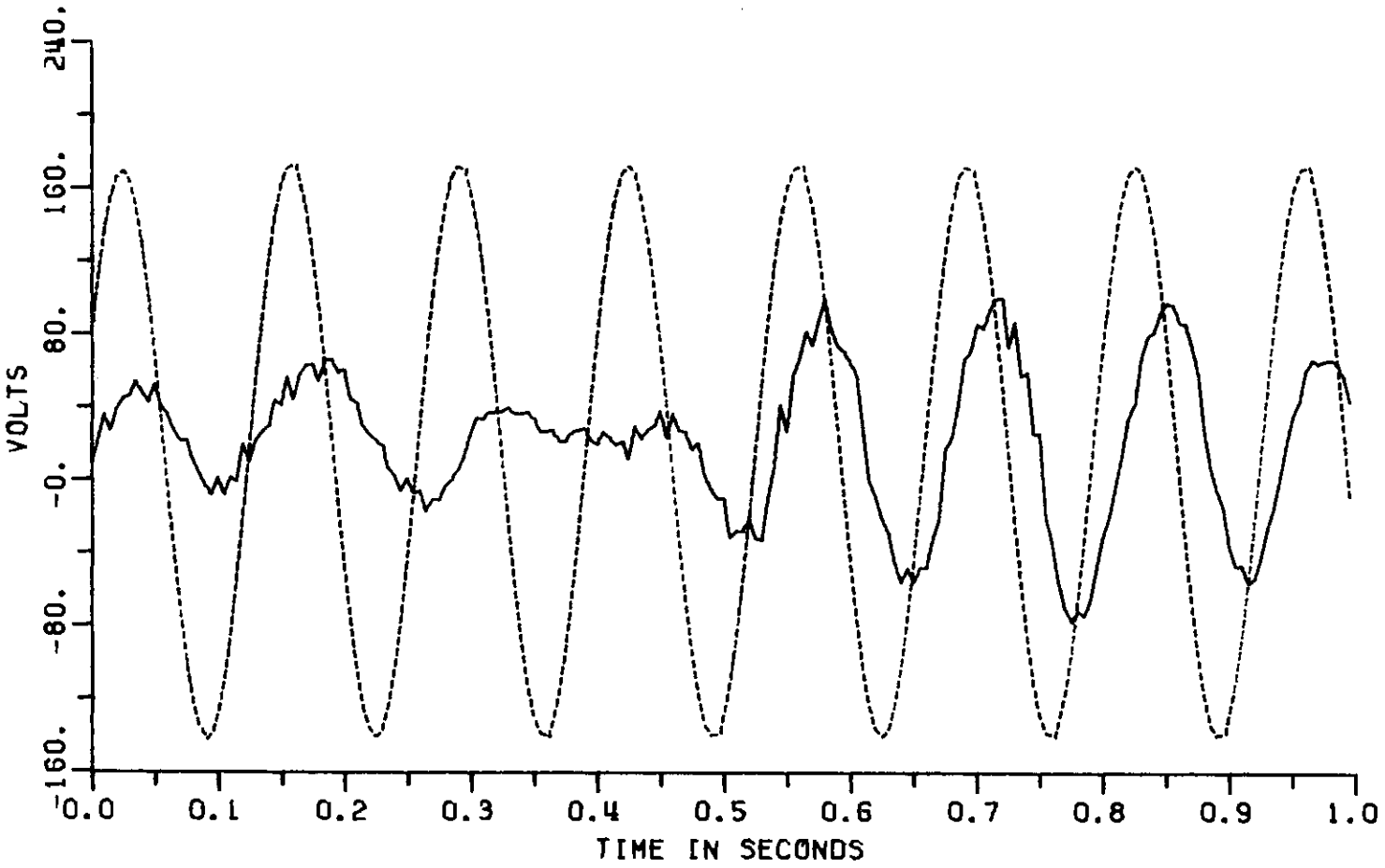

PITCH VOLT TEST 7

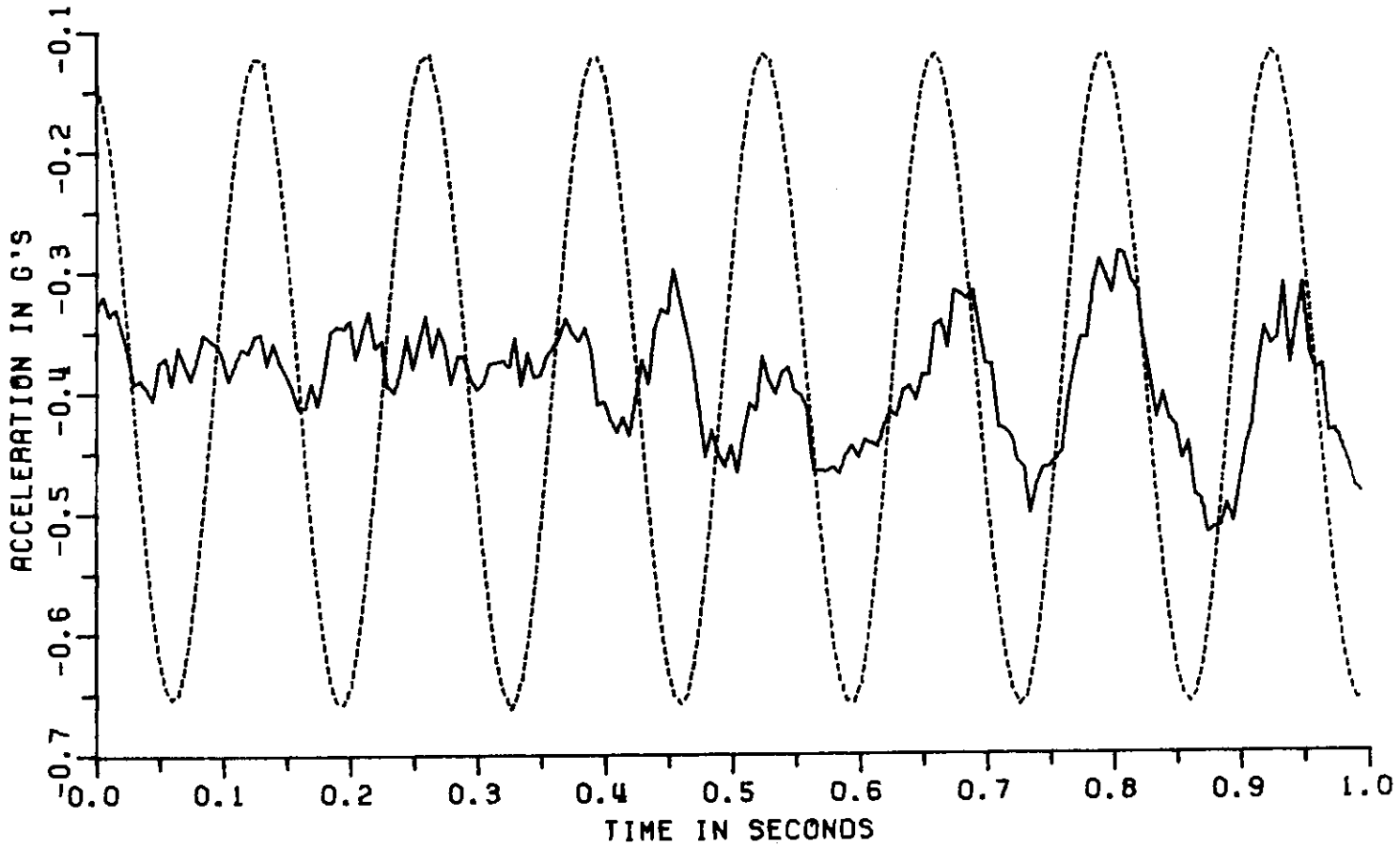

HEAVE ACC TEST 7

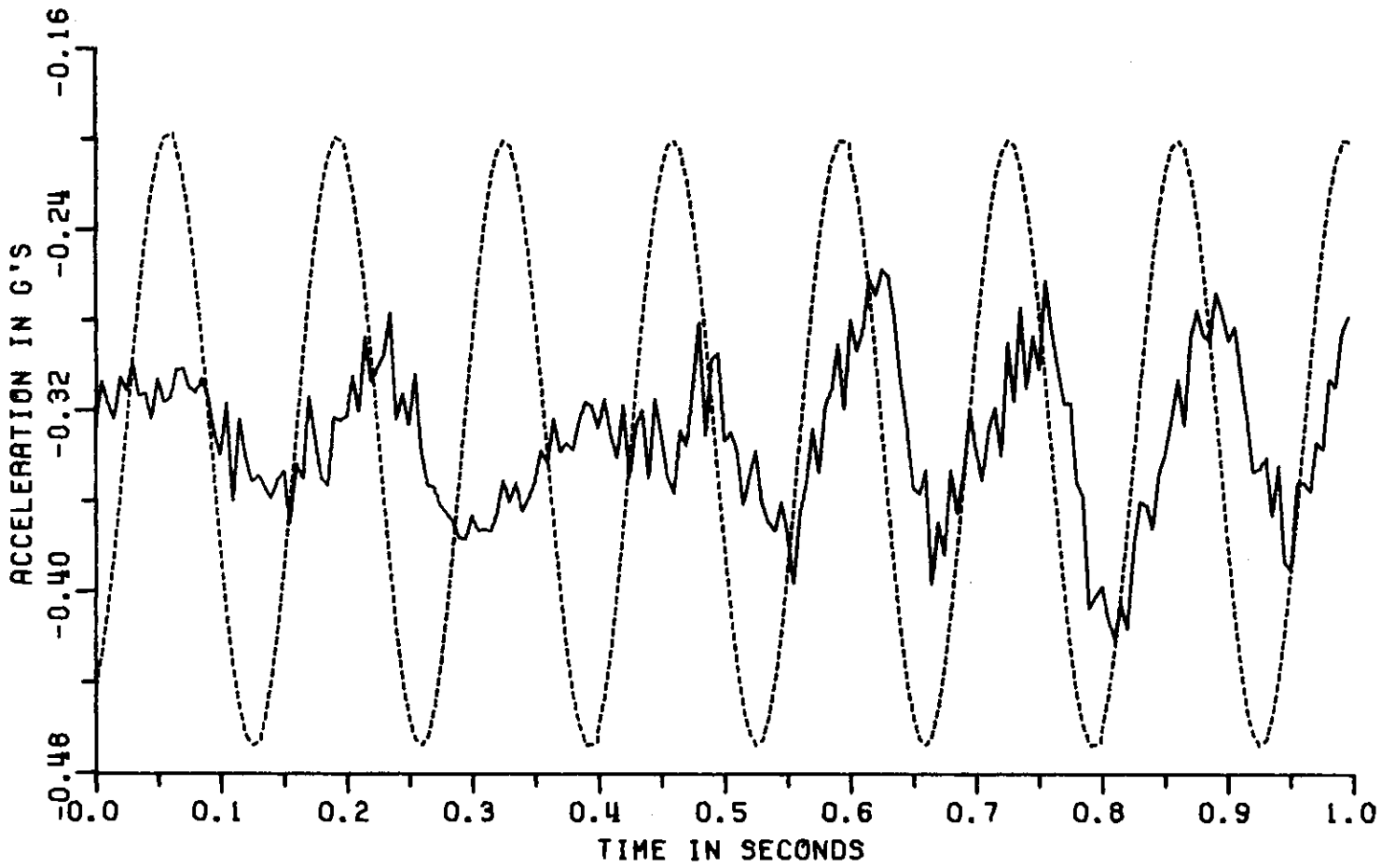

PITCH ACC TEST 7

APPENDIX C

Test 6 - Gaps, Accelerations and Voltages

SPEED: 258 km/hr

GUIDEWAY MODIFICATION: Sinusoidal

COMMENT: The time synchronization between theory and experiment is apparently off by 22 ms. (See Section 4.1.1.)

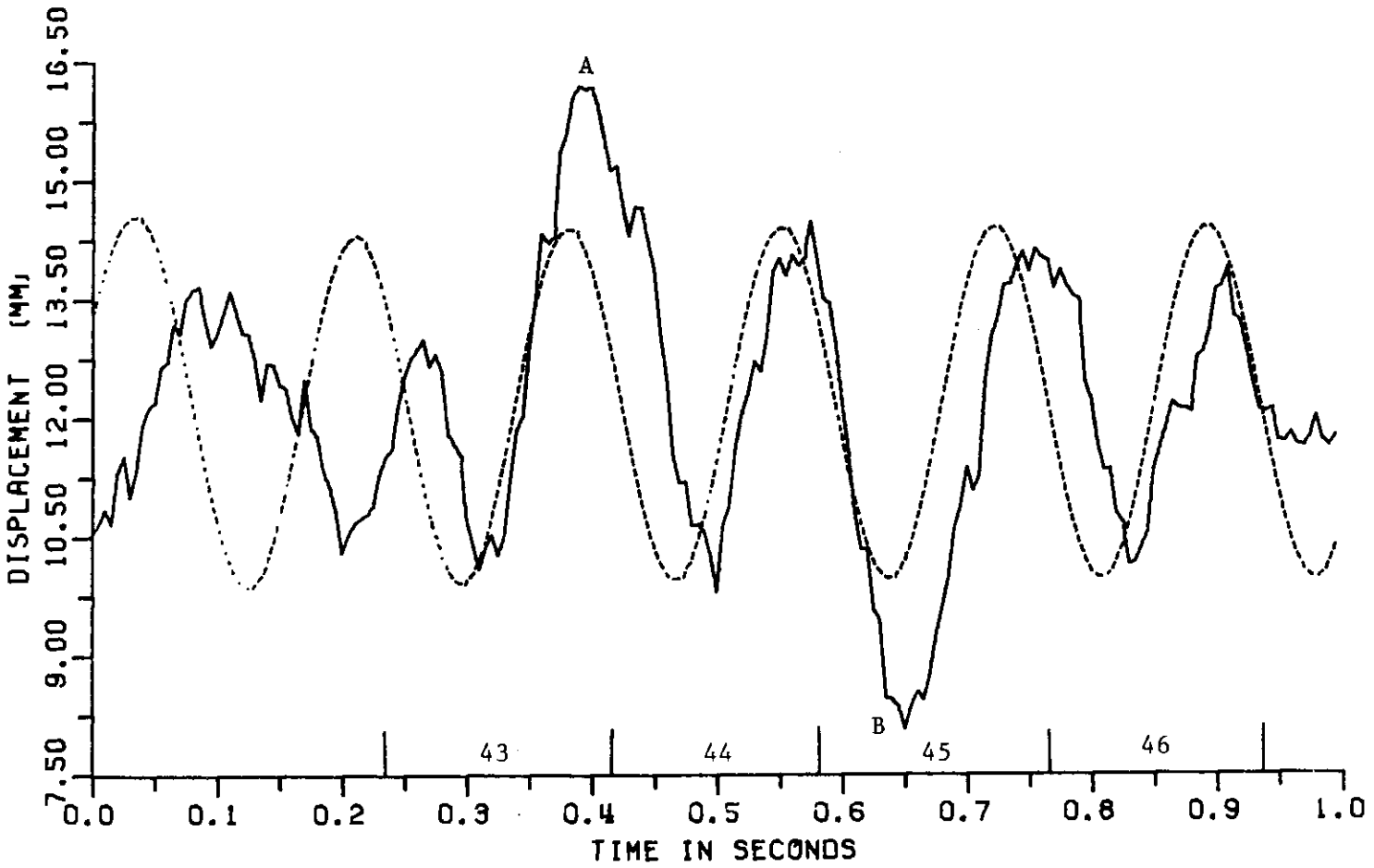

FRONT GAP TEST 6

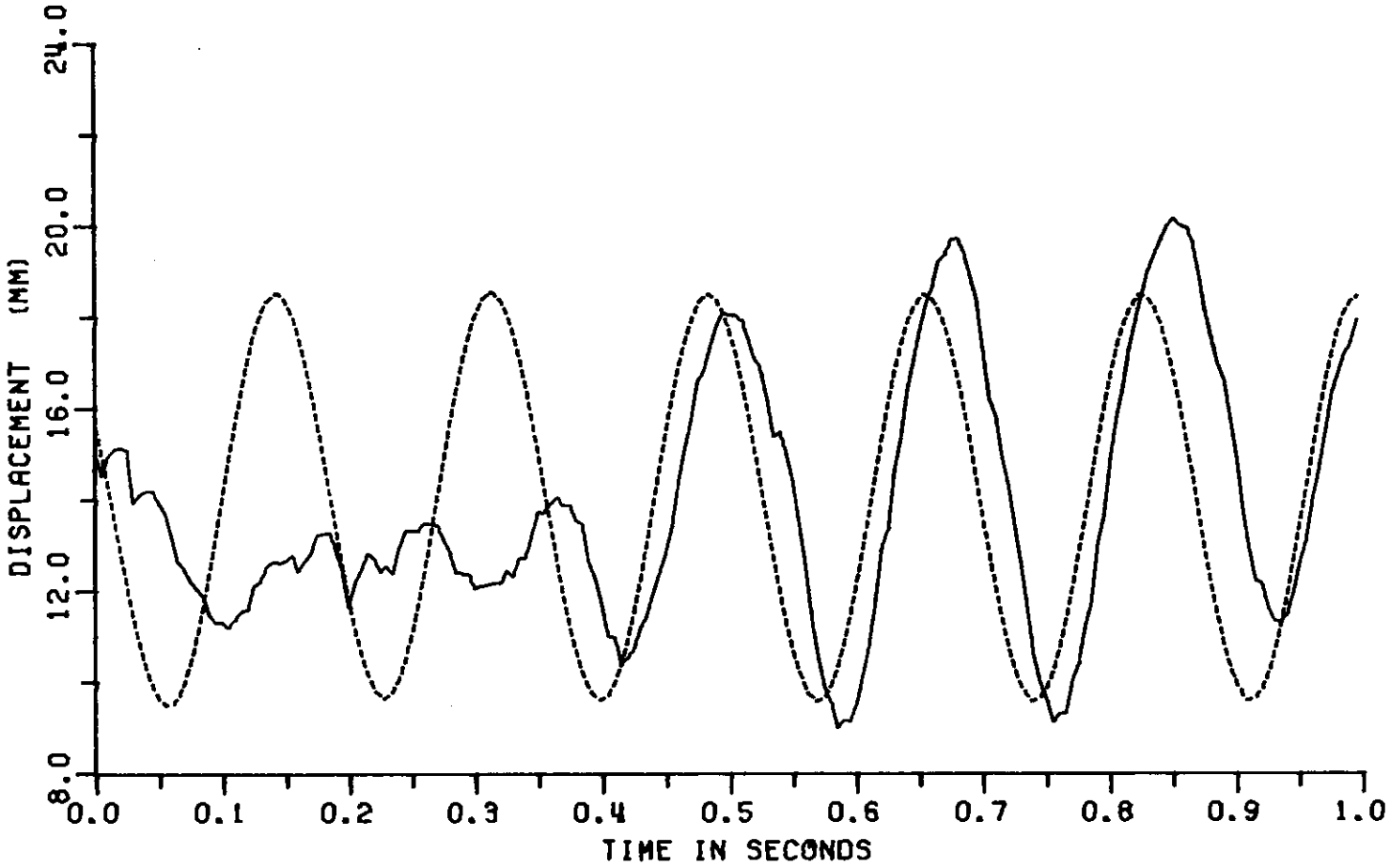

REAR GAP TEST 6

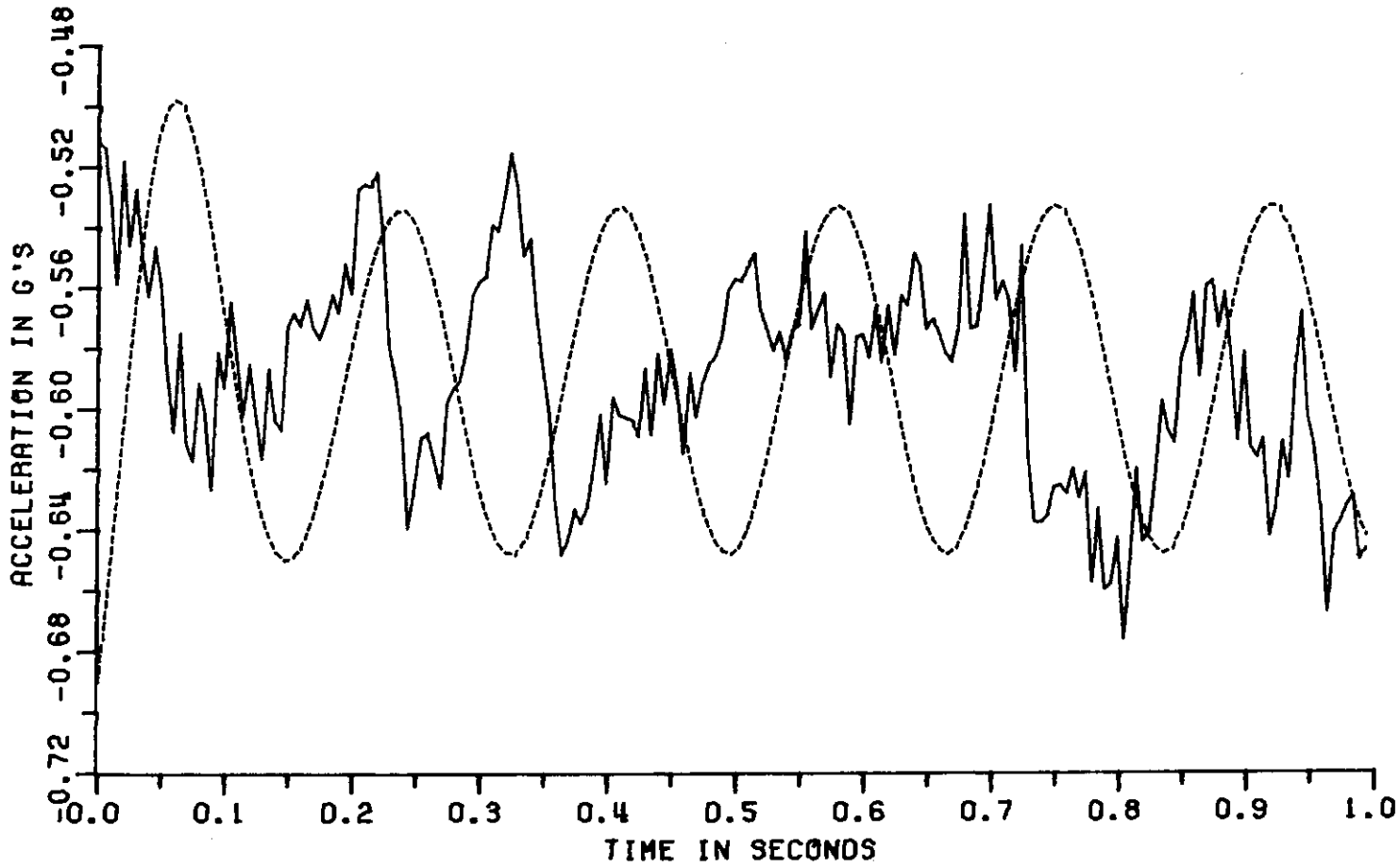

FRONT ACC TEST 6

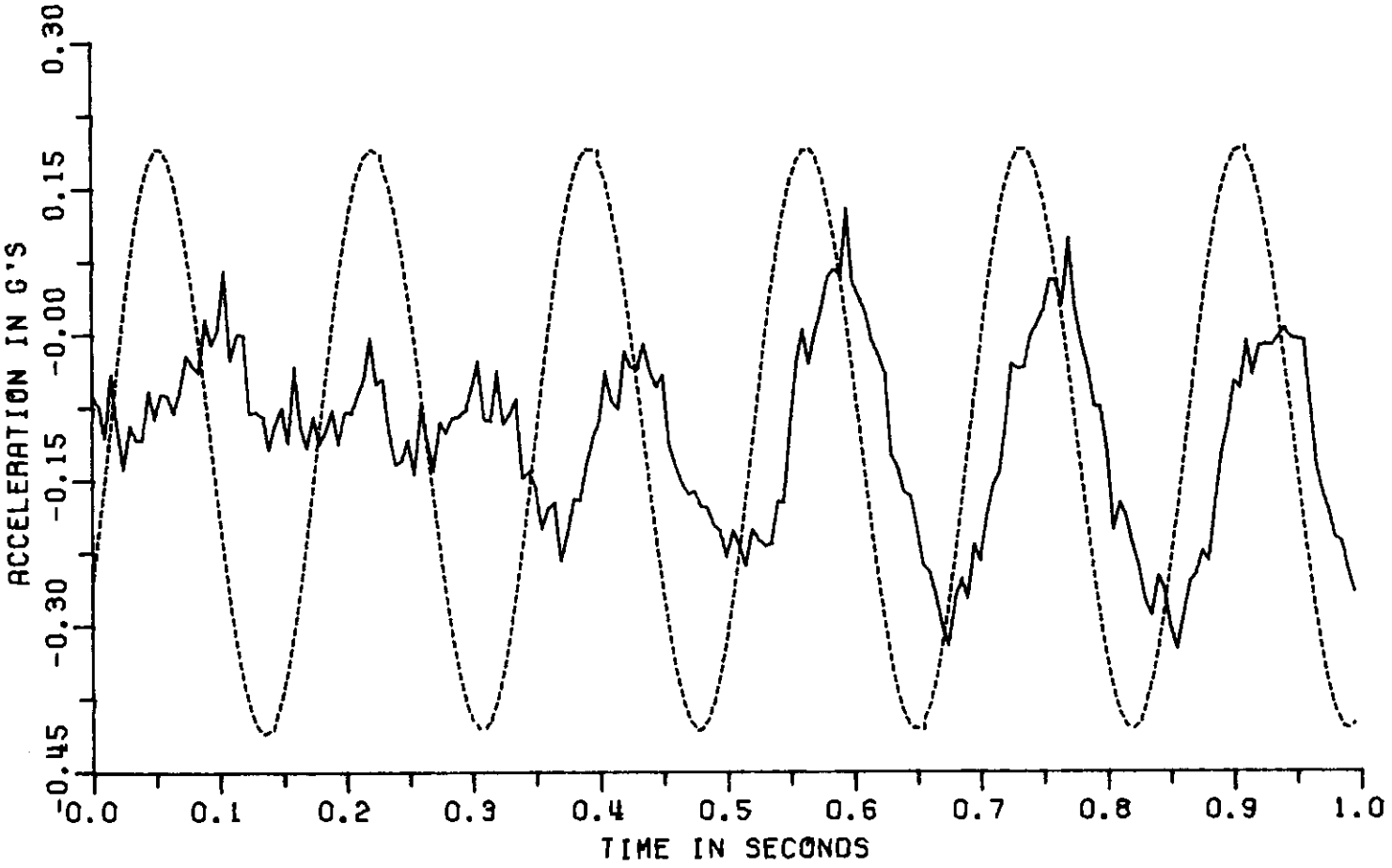

REAR ACC TEST 6

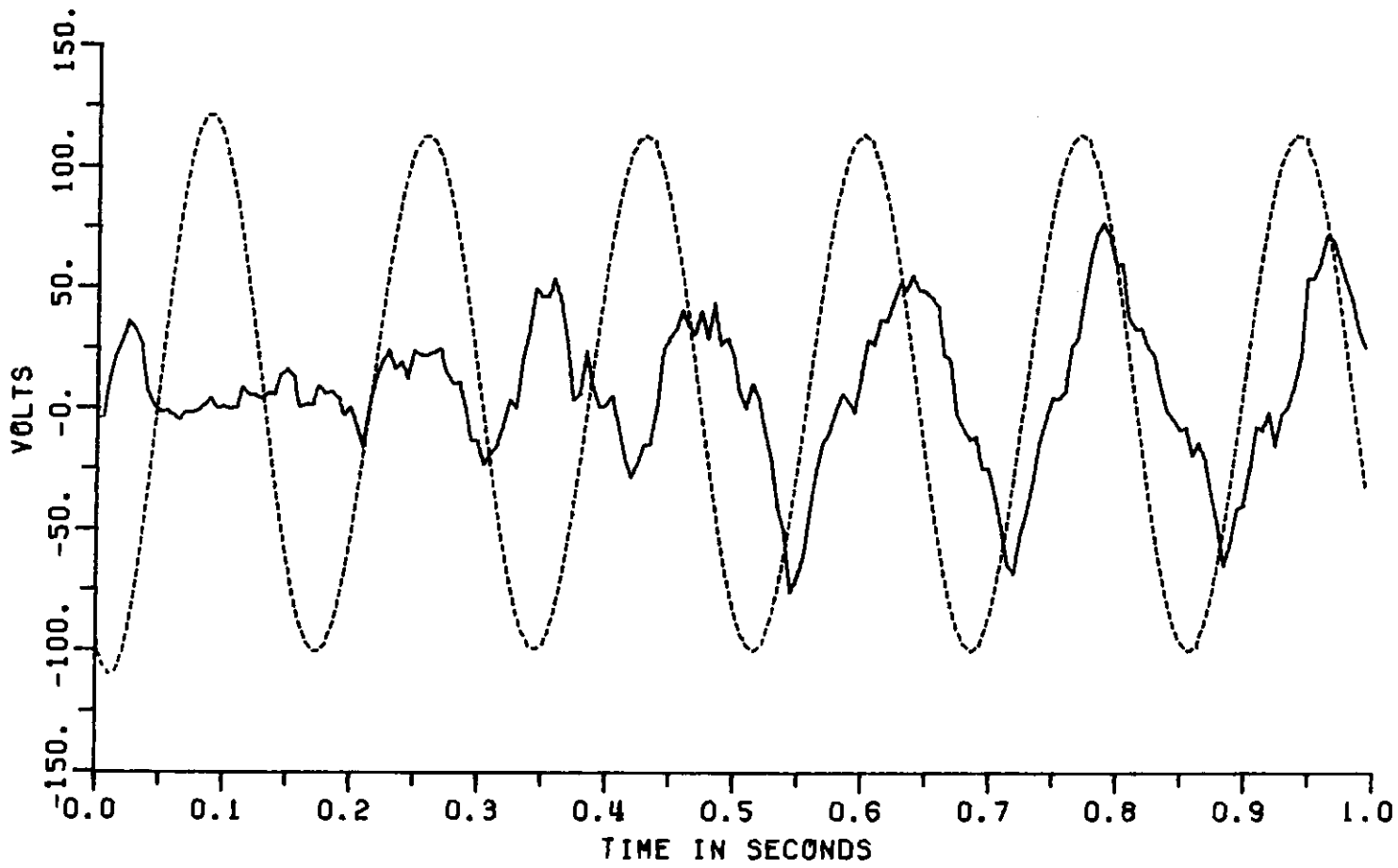

HEAVE VOLT TEST 6

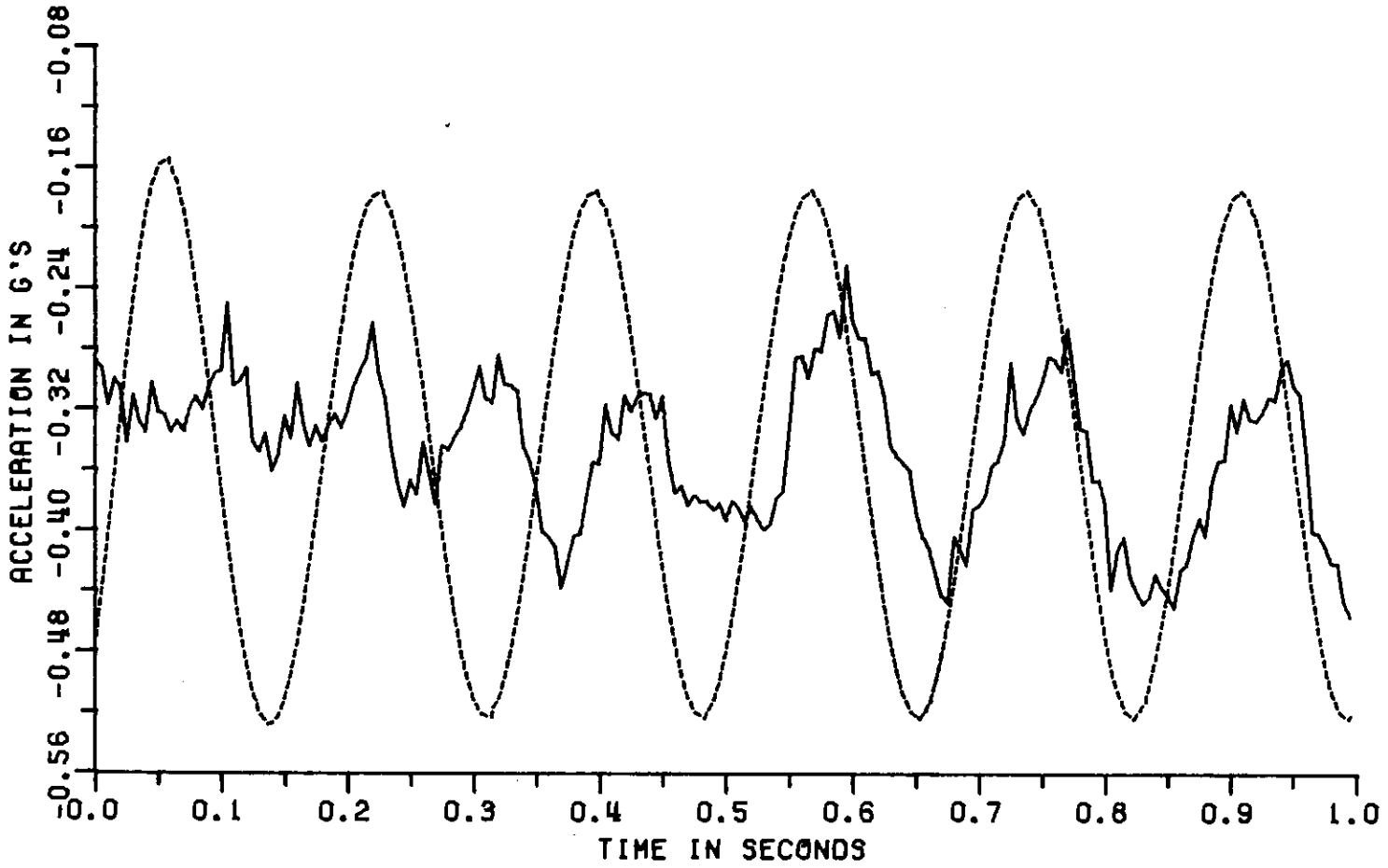

HEAVE ACC TEST 6

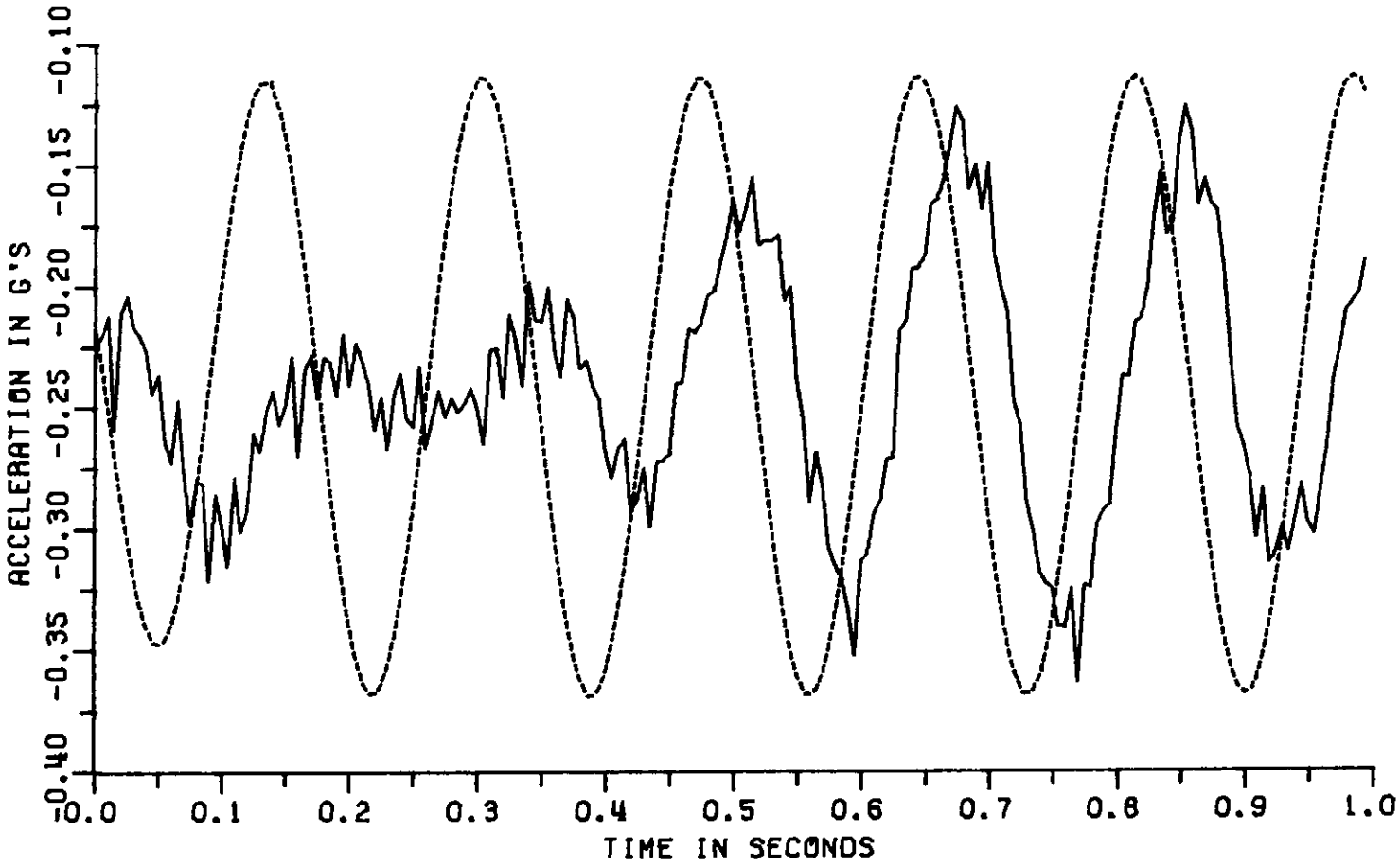

PITCH ACC TEST 6

APPENDIX D

Test 6 - Time Shifted by 22 ms

SPEED: 258 km/hr

GUIDEWAY MODIFICATION: Sinusoidal

COMMENTS: The theory was shifted in time an amount determined by visual inspection to align it with the experimental data. This was 22 ms different than indicated by the experimental synchronization signal.

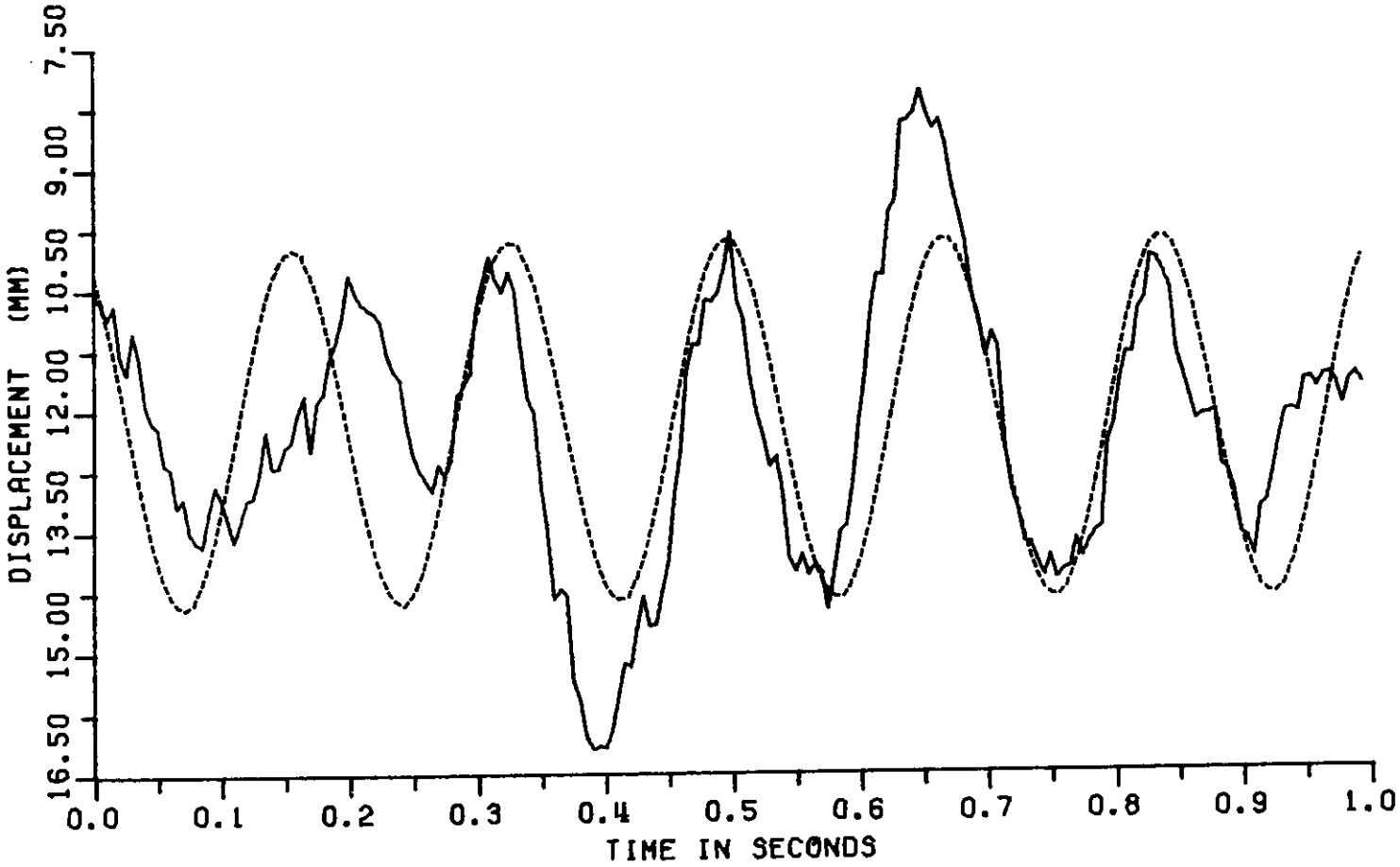

FRONT GAP TEST 6

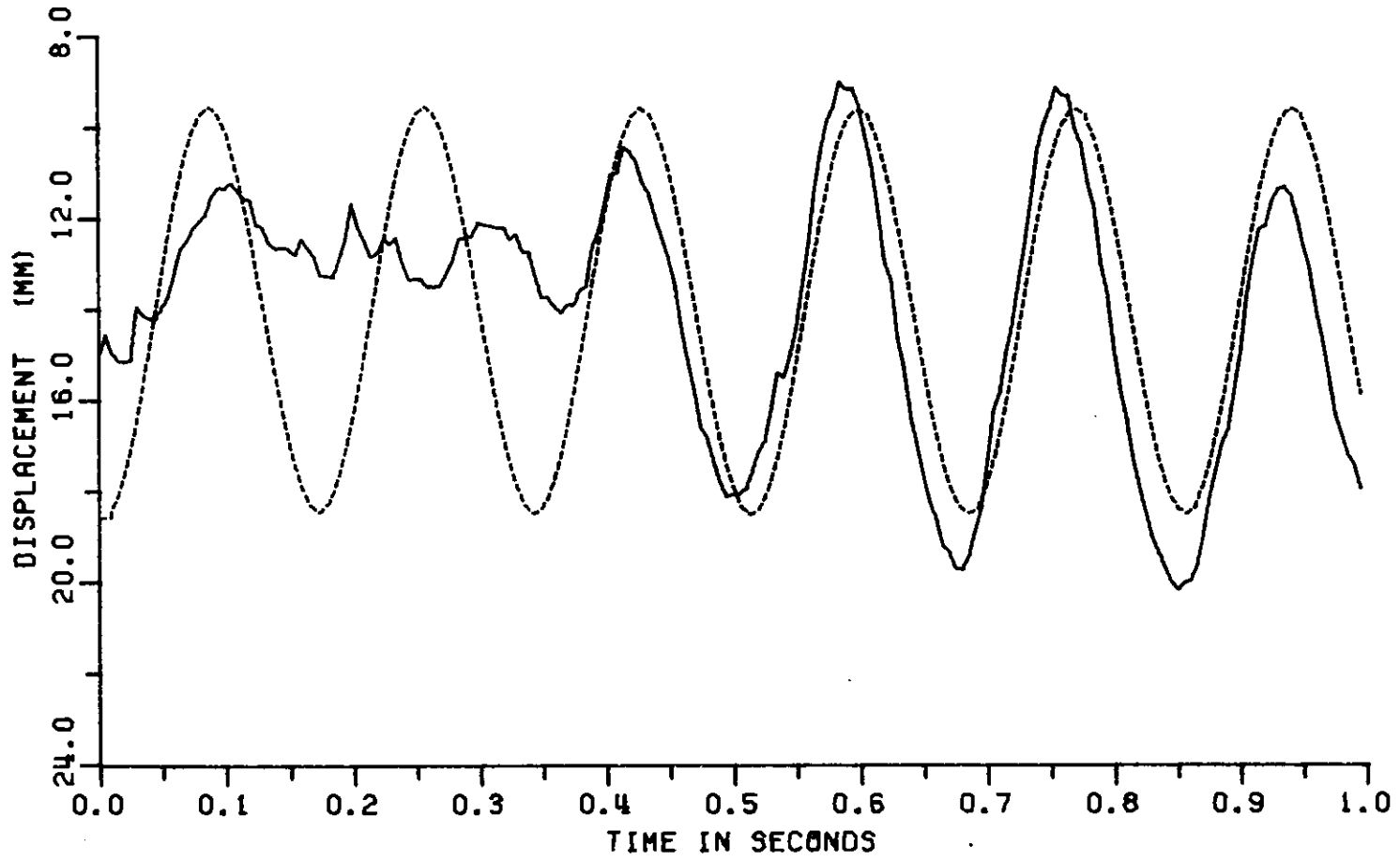

REAR GAP TEST 6

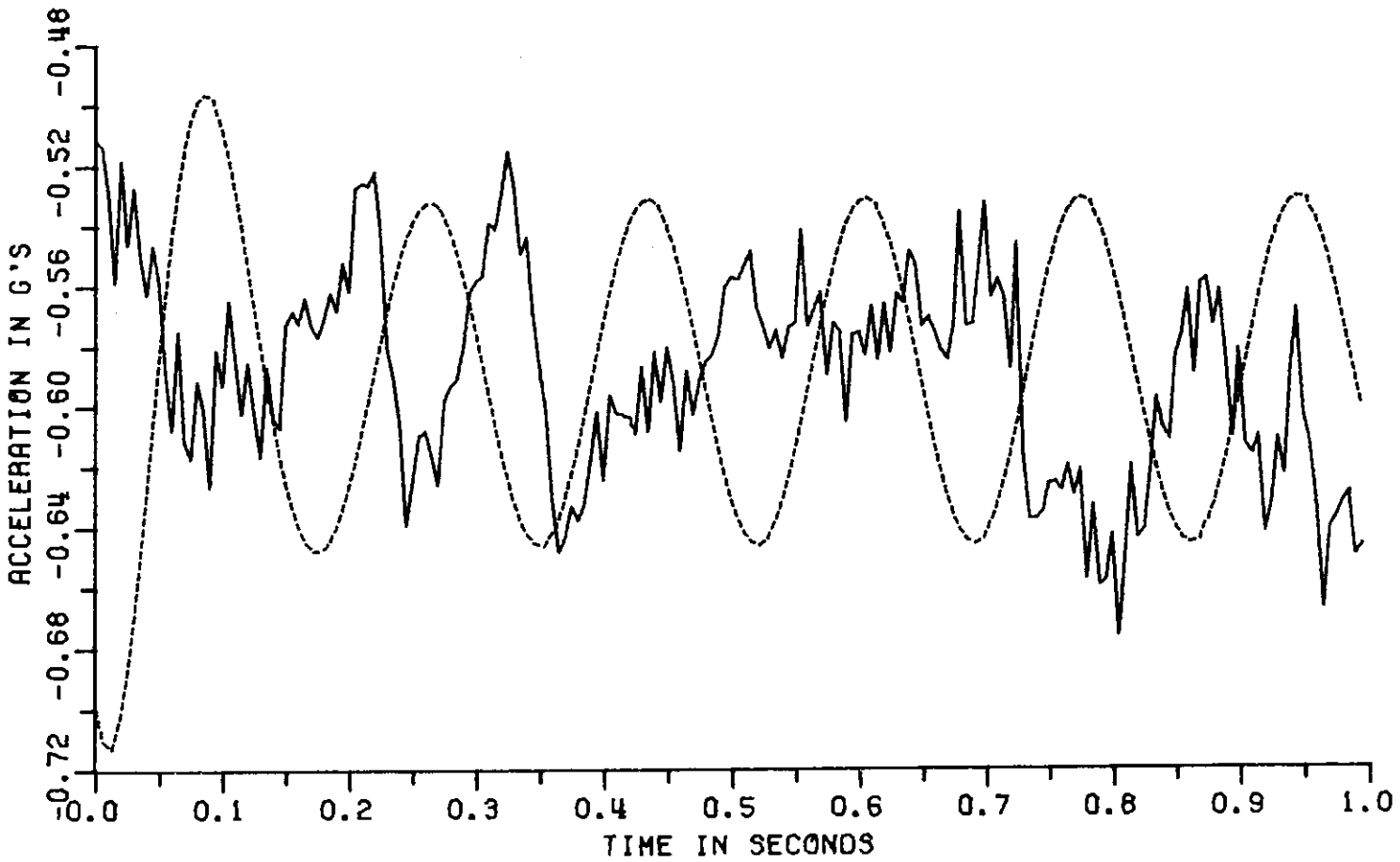

FRONT ACC TEST 6

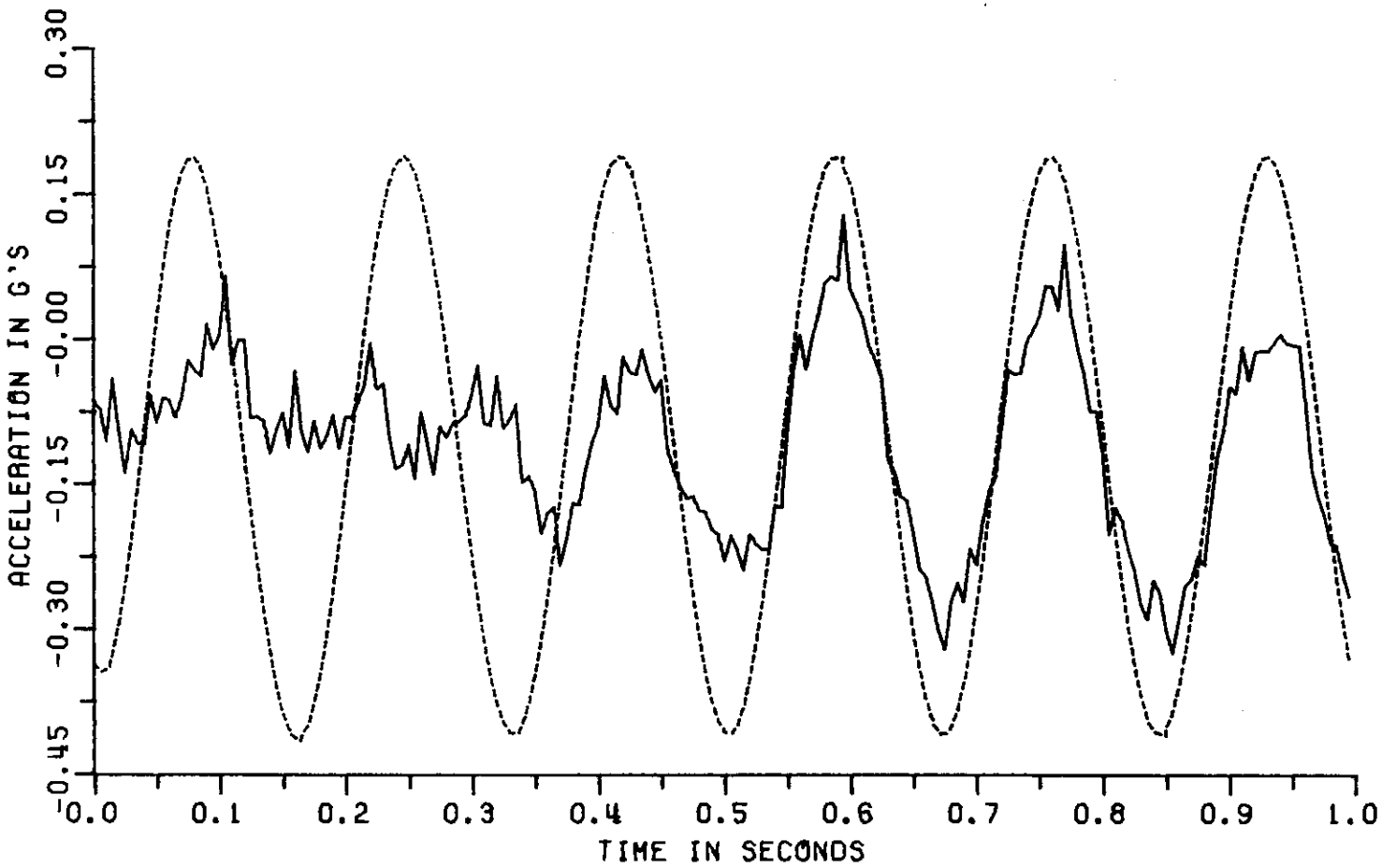

REAR ACCEL TEST 6

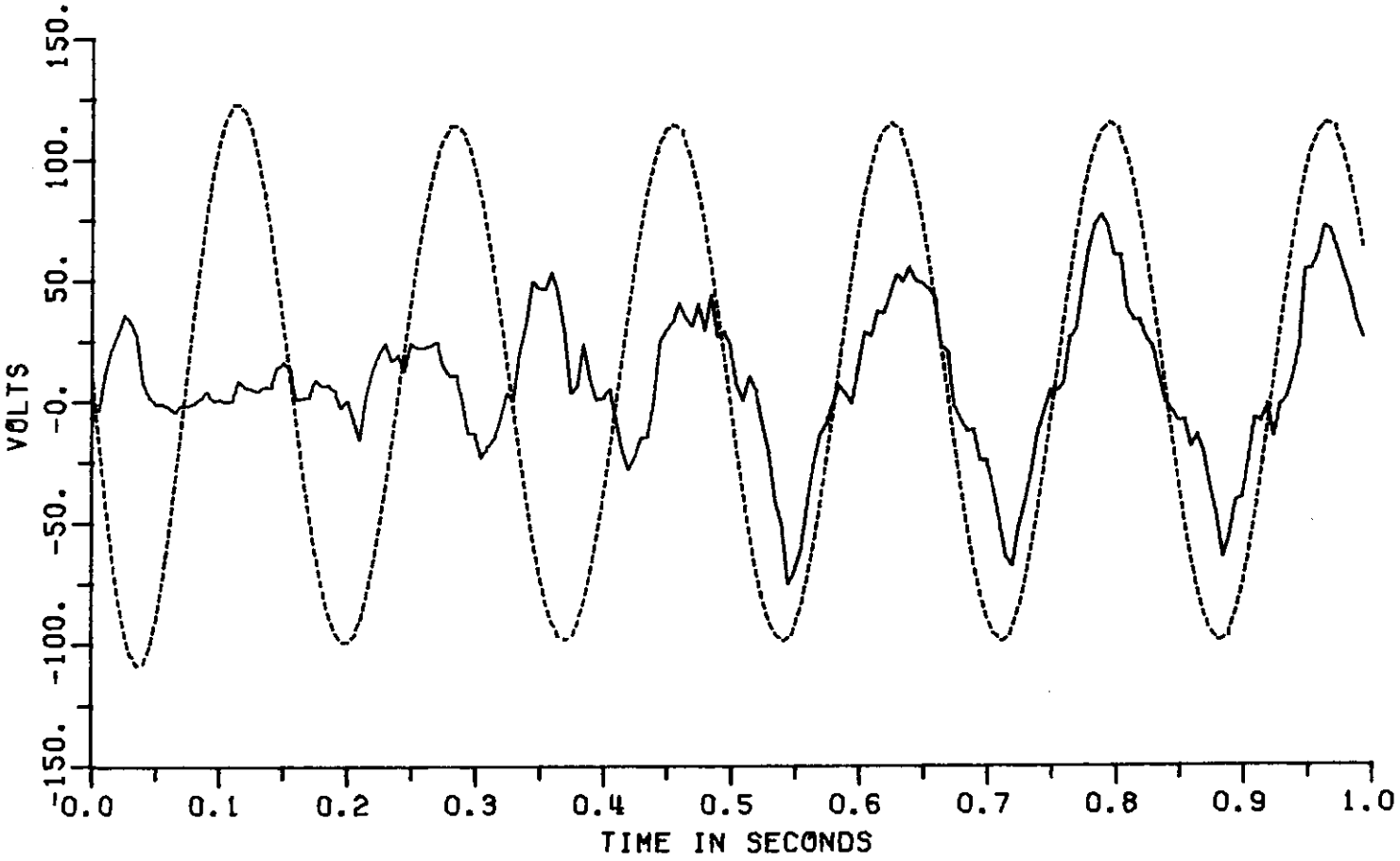

HEAVE VOLT TEST 6

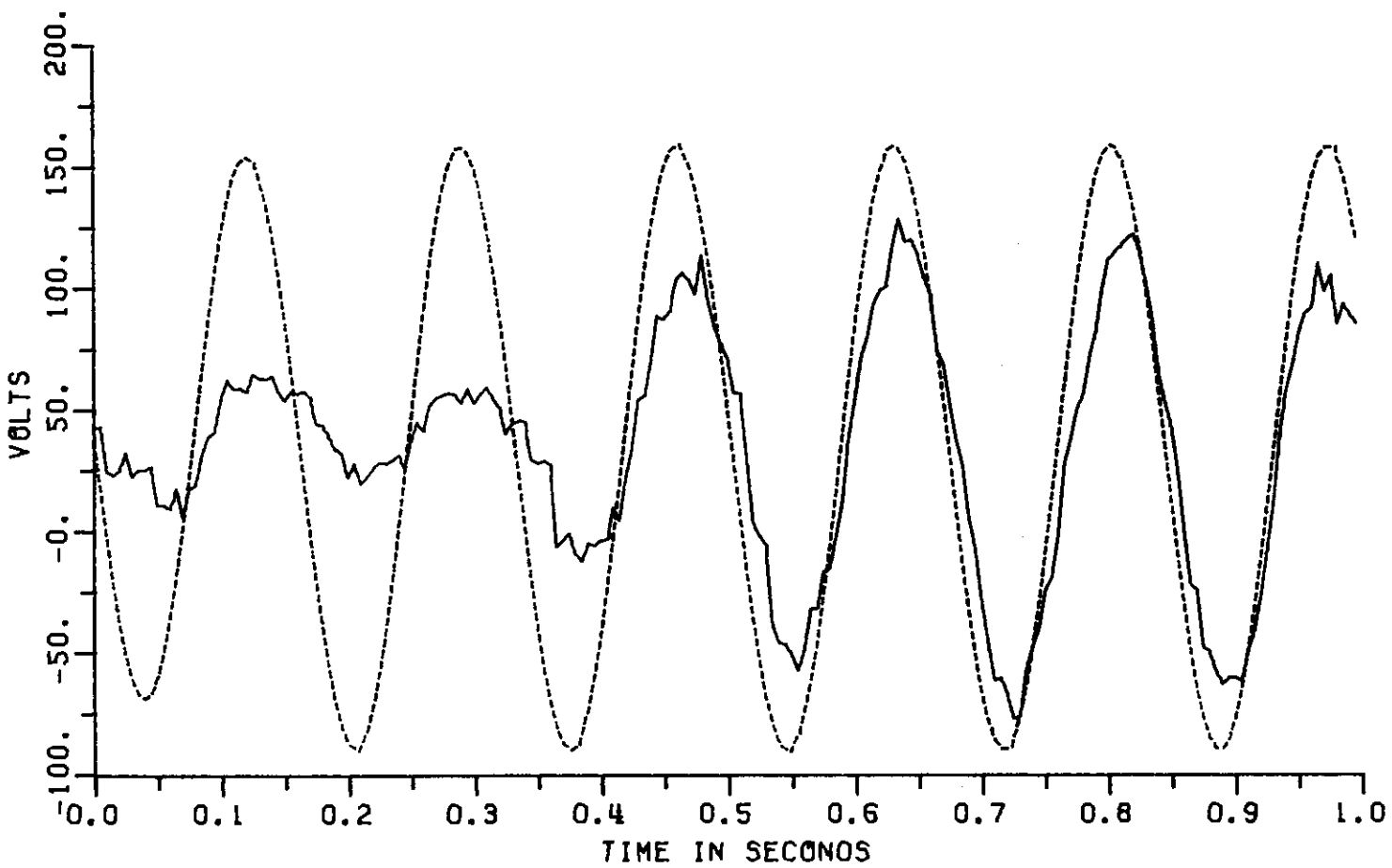

PITCH VOLTAGE TEST 6

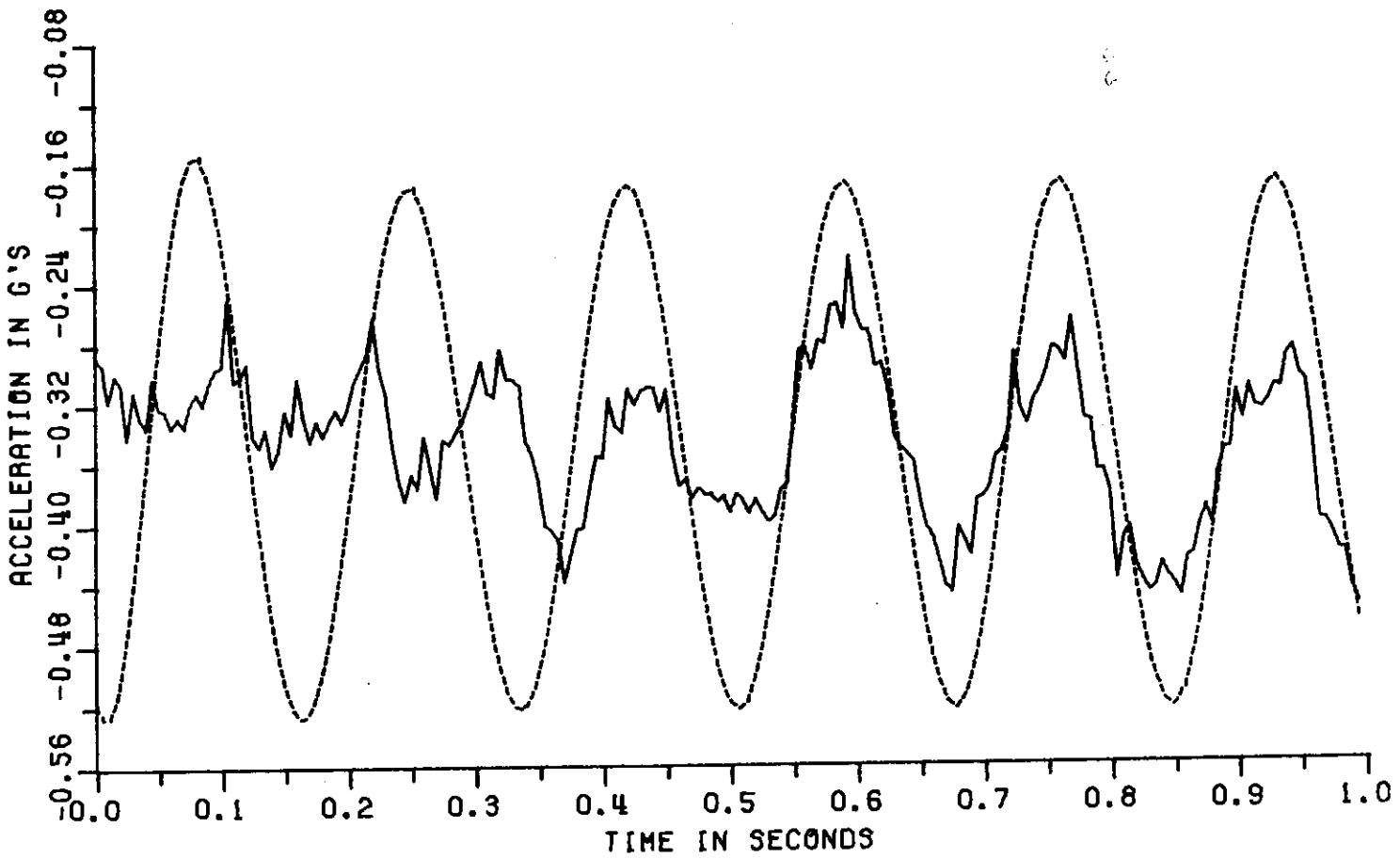

HEAVE ACC TEST 6

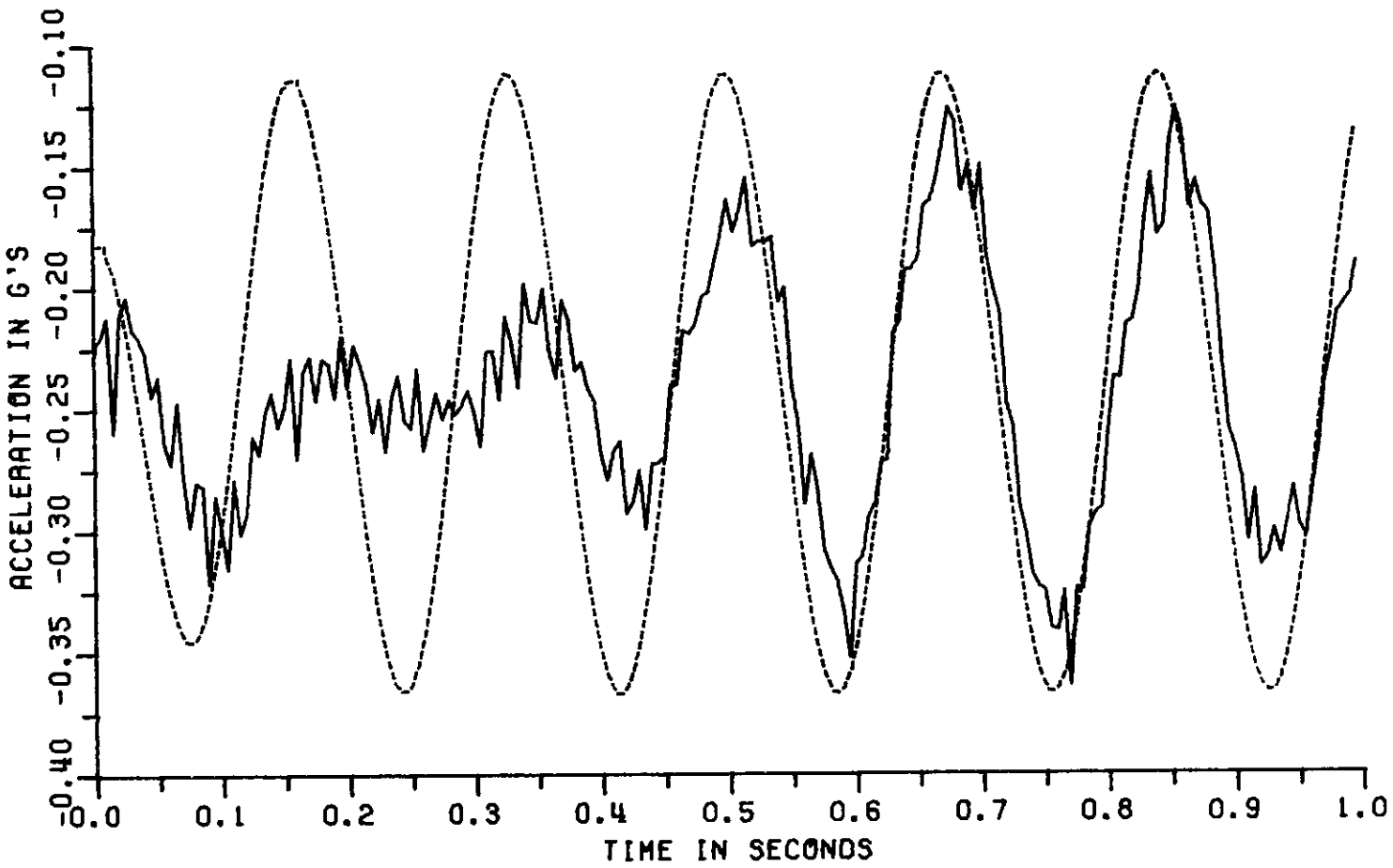

PITCH ACC TEST 6

APPENDIX E

Test 3 - Guideway Deflections

SPEED: 331 km/hr

GUIDEWAY MODIFICATION: elastic

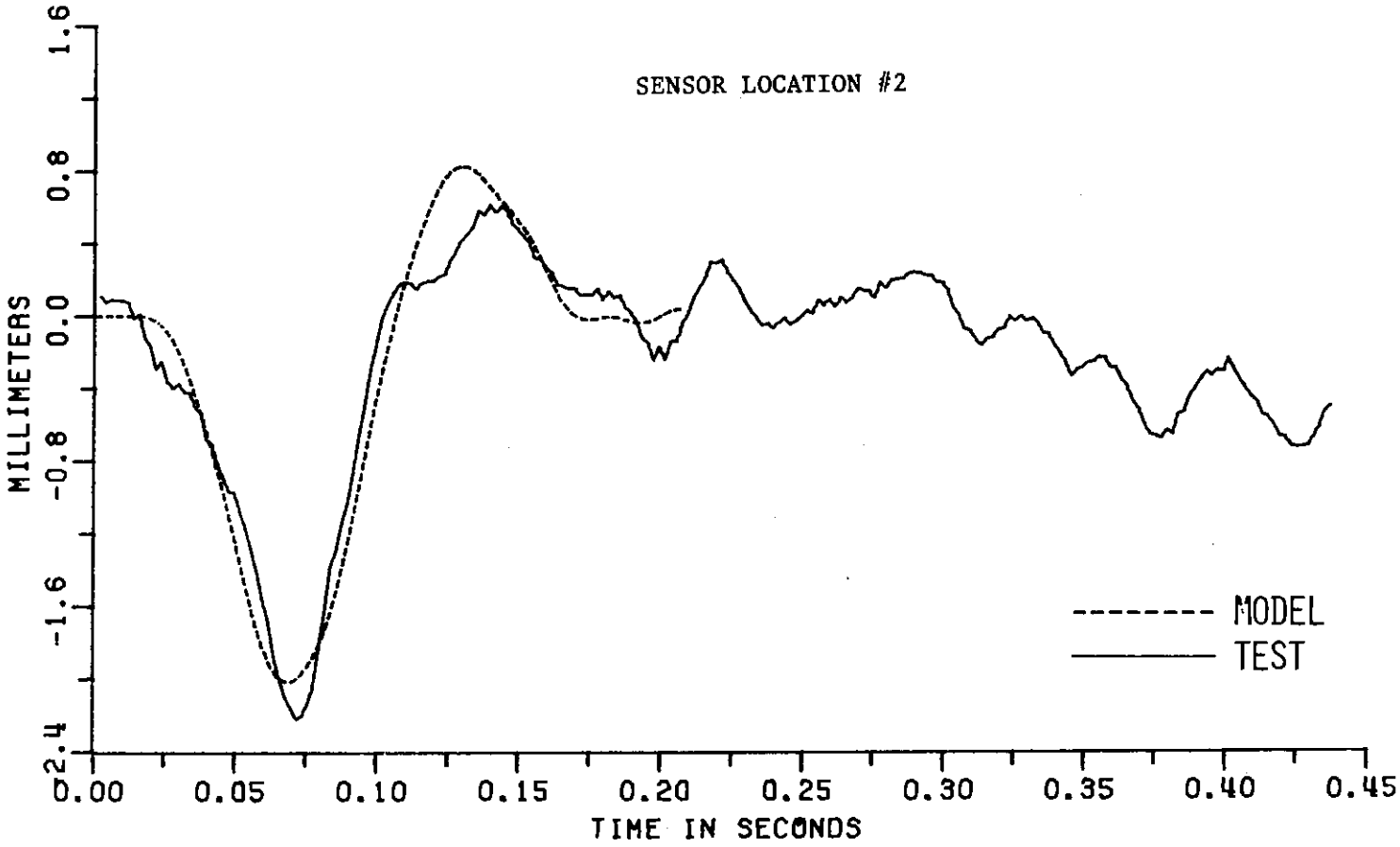
SENSOR LOCATION #2
MILLIMETERS
1.6
0.8
0.0
-0.8
-1.6
-2.4
0.00
0.05
0.10
0.15
0.20
0.25
0.30
0.35
0.40
0.45
TIME IN SECONDS
MODEL
TEST

KOMET TEST 3

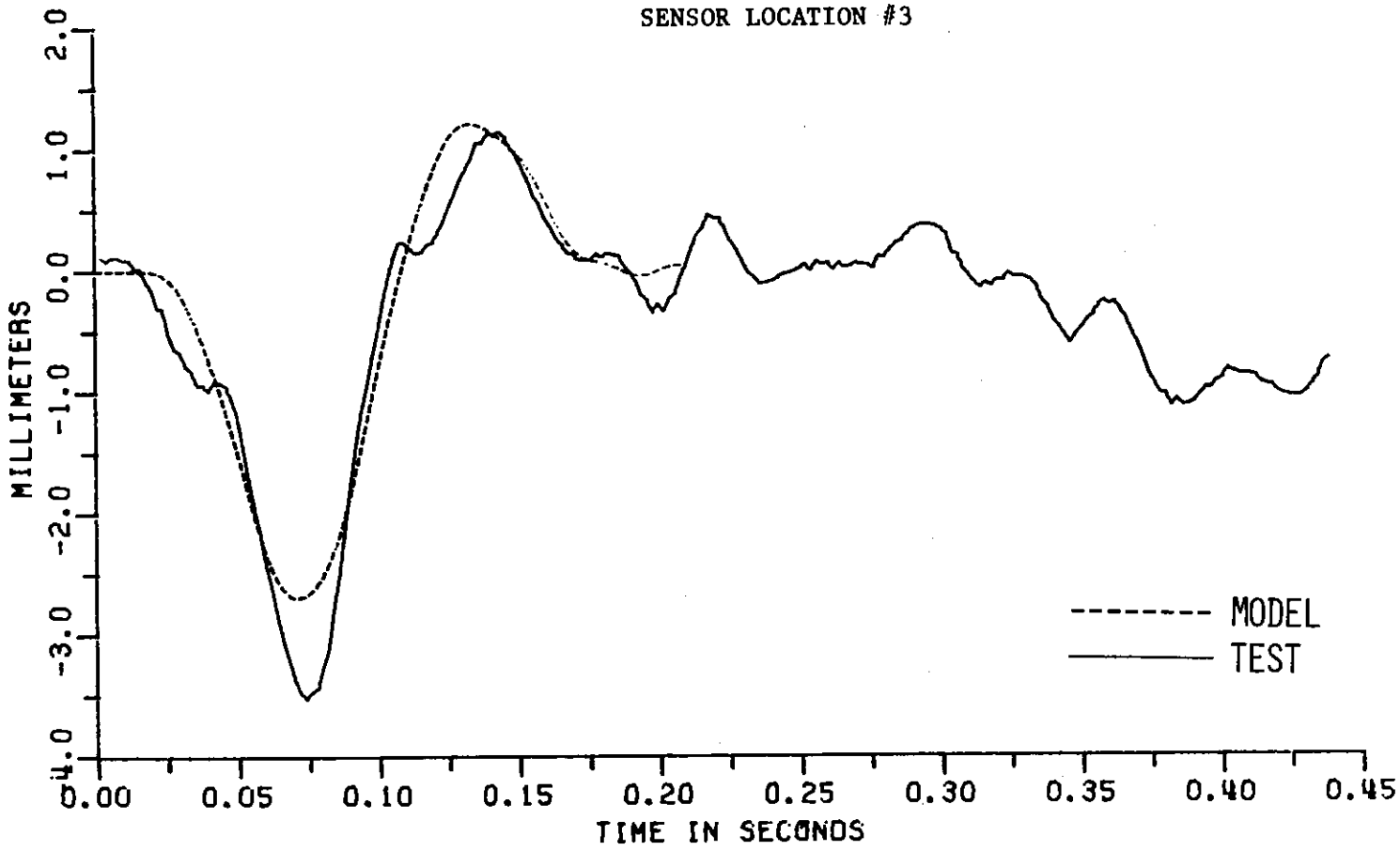
SENSOR LOCATION #3
MILLIMETERS
2.0
1.0
0.0
-1.0
-2.0
-3.0
-4.0
0.00
0.05
0.10
0.15
0.20
0.25
0.30
0.35
0.40
0.45
TIME IN SECONDS
MODEL
TEST

KOMET TEST 3

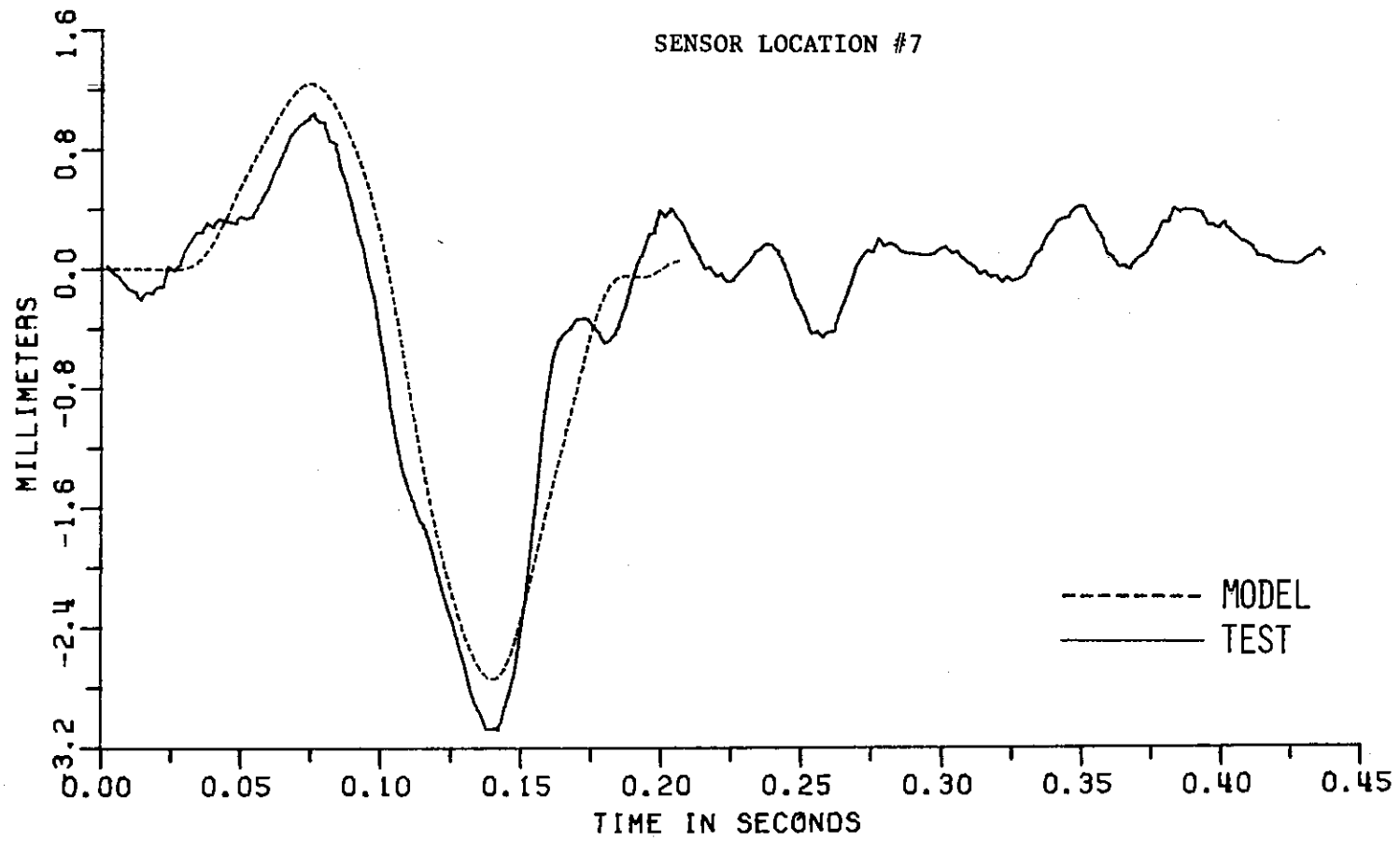
SENSOR LOCATION #7
MILLIMETERS
1.6
0.8
0.0
-0.8
-1.6
-2.4
-3.2
0.00
0.05
0.10
0.15
0.20
0.25
0.30
0.35
0.40
0.45
TIME IN SECONDS
MODEL
TEST

KOMET TEST 3

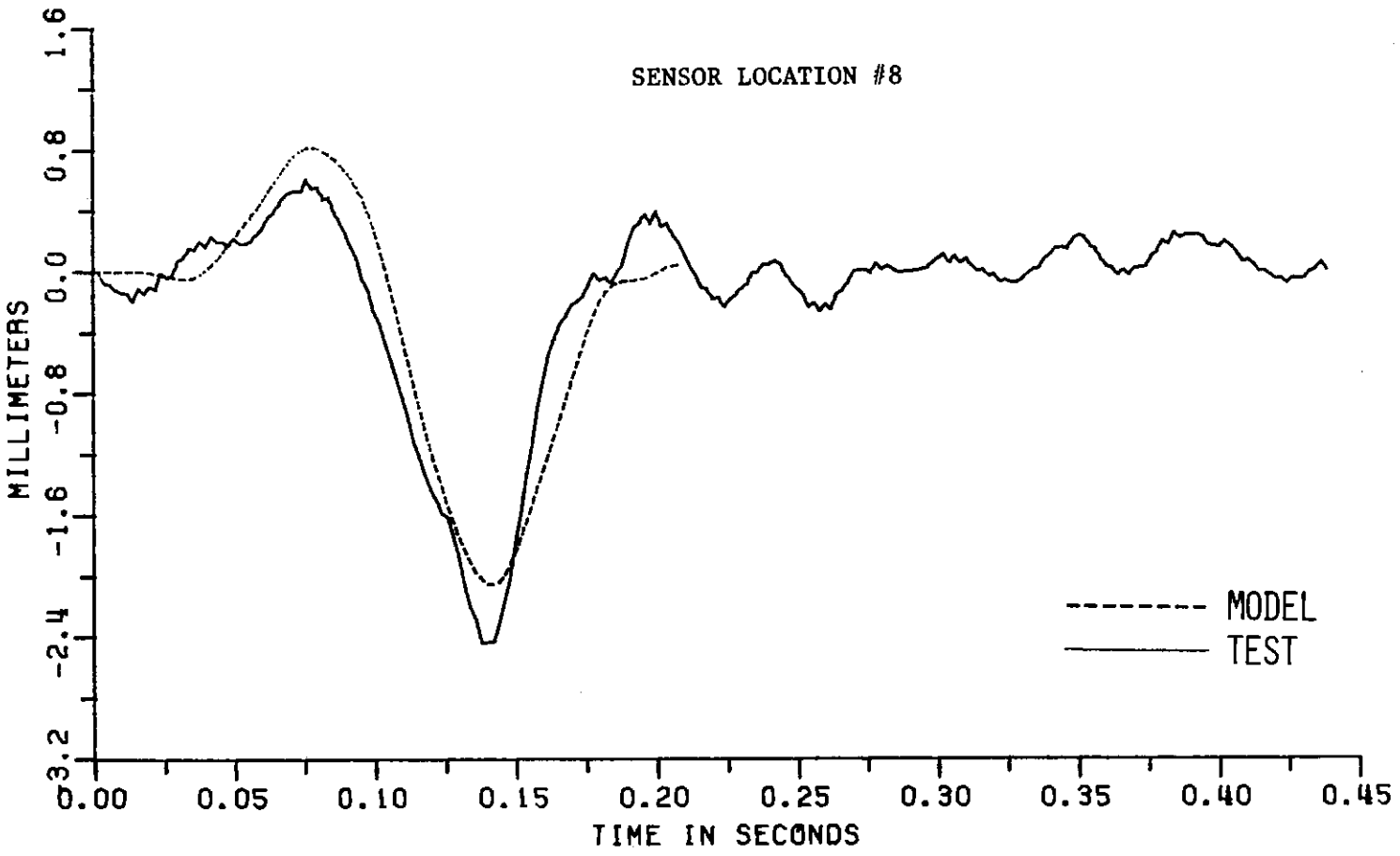
SENSOR LOCATION #8
MILLIMETERS
1.6
0.8
0.0
-0.8
-1.6
-2.4
-3.2
0.00
0.05
0.10
0.15
0.20
0.25
0.30
0.35
0.40
0.45
TIME IN SECONDS
MODEL
TEST

KOMET TEST 3

APPENDIX F

Test 3 - Accelerations and Voltages

SPEED: 331 km/hr

GUIDEWAY MODIFICATION: elastic

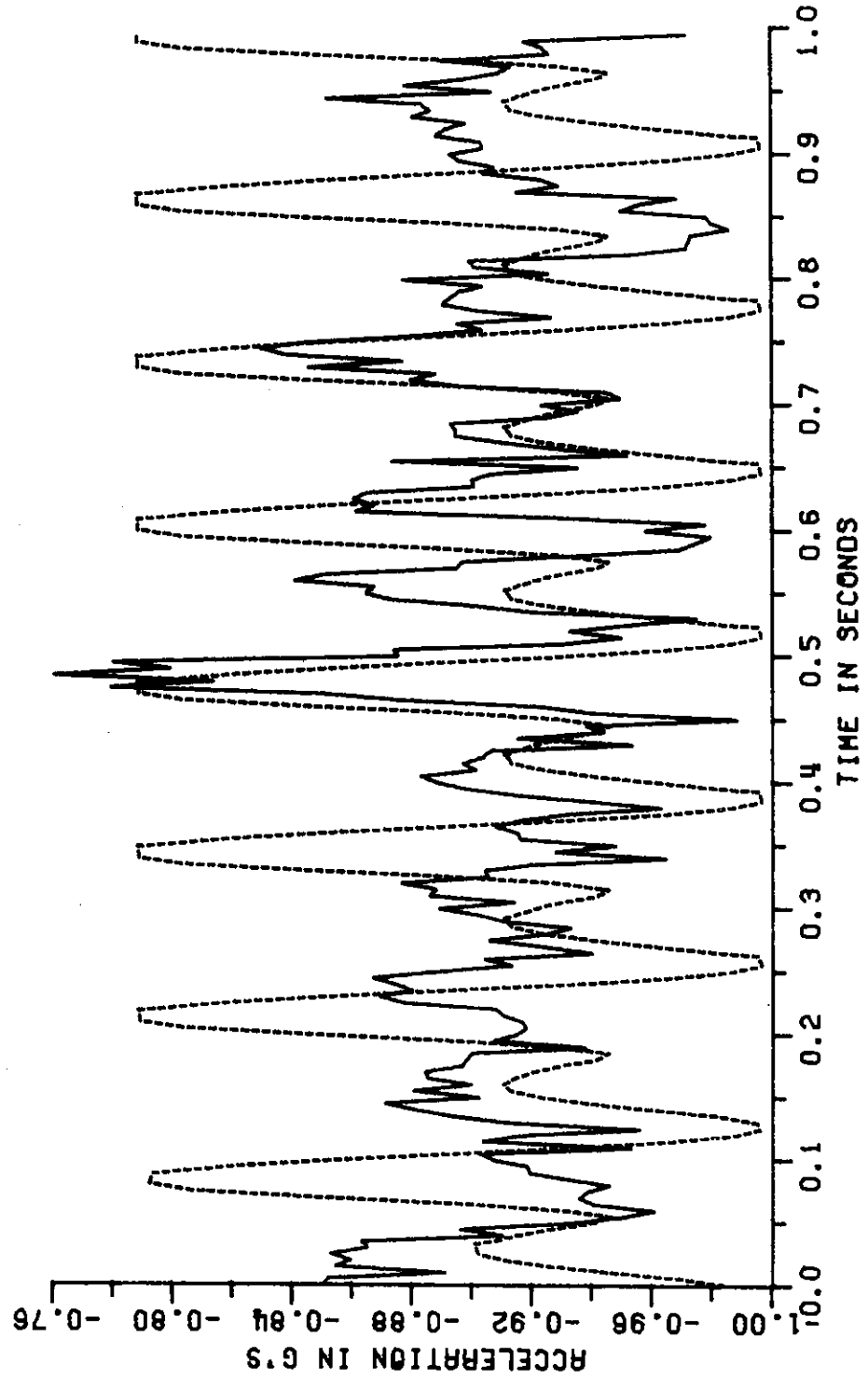

FRONT ACC TEST 3

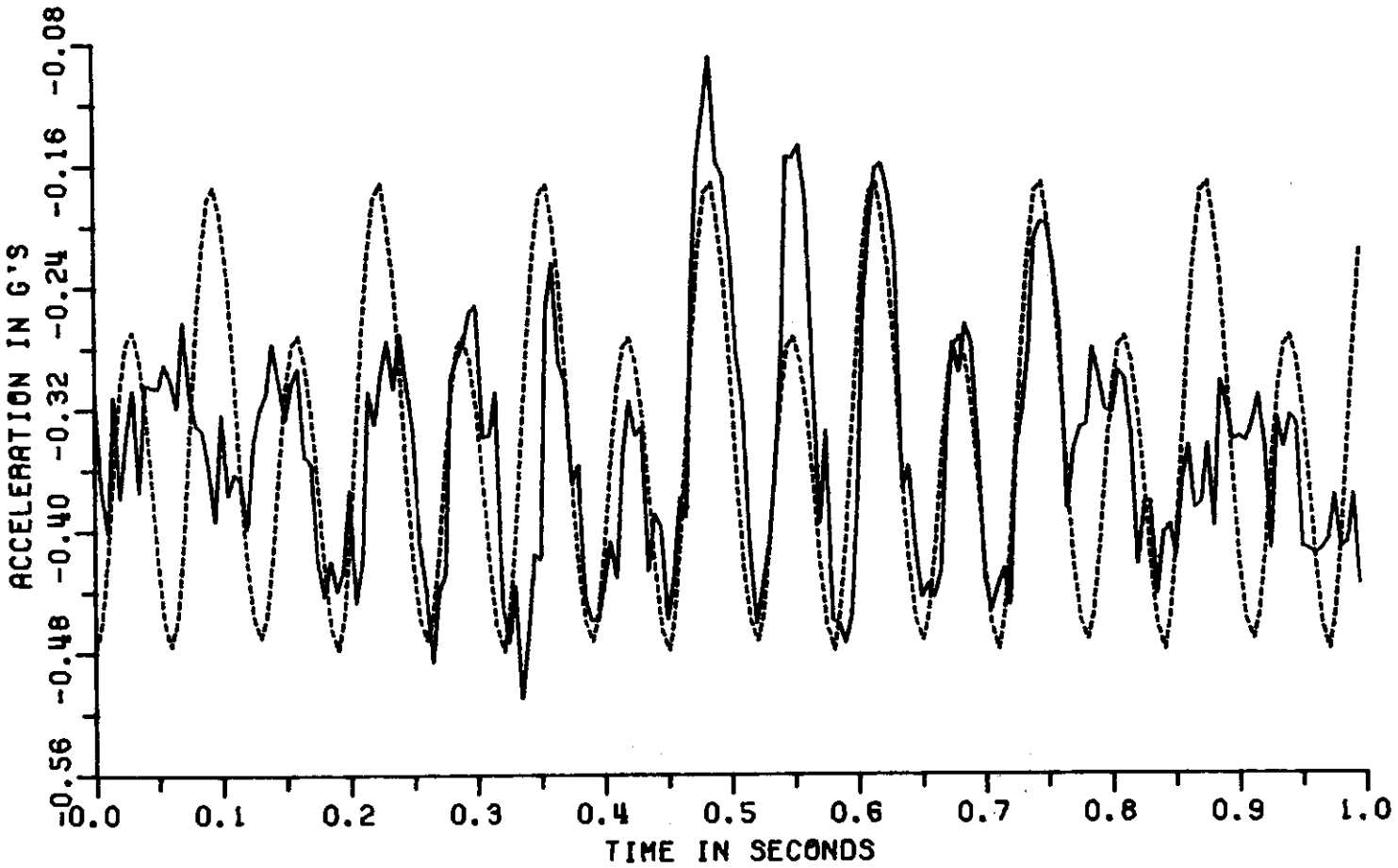

REAR ACC TEST 3

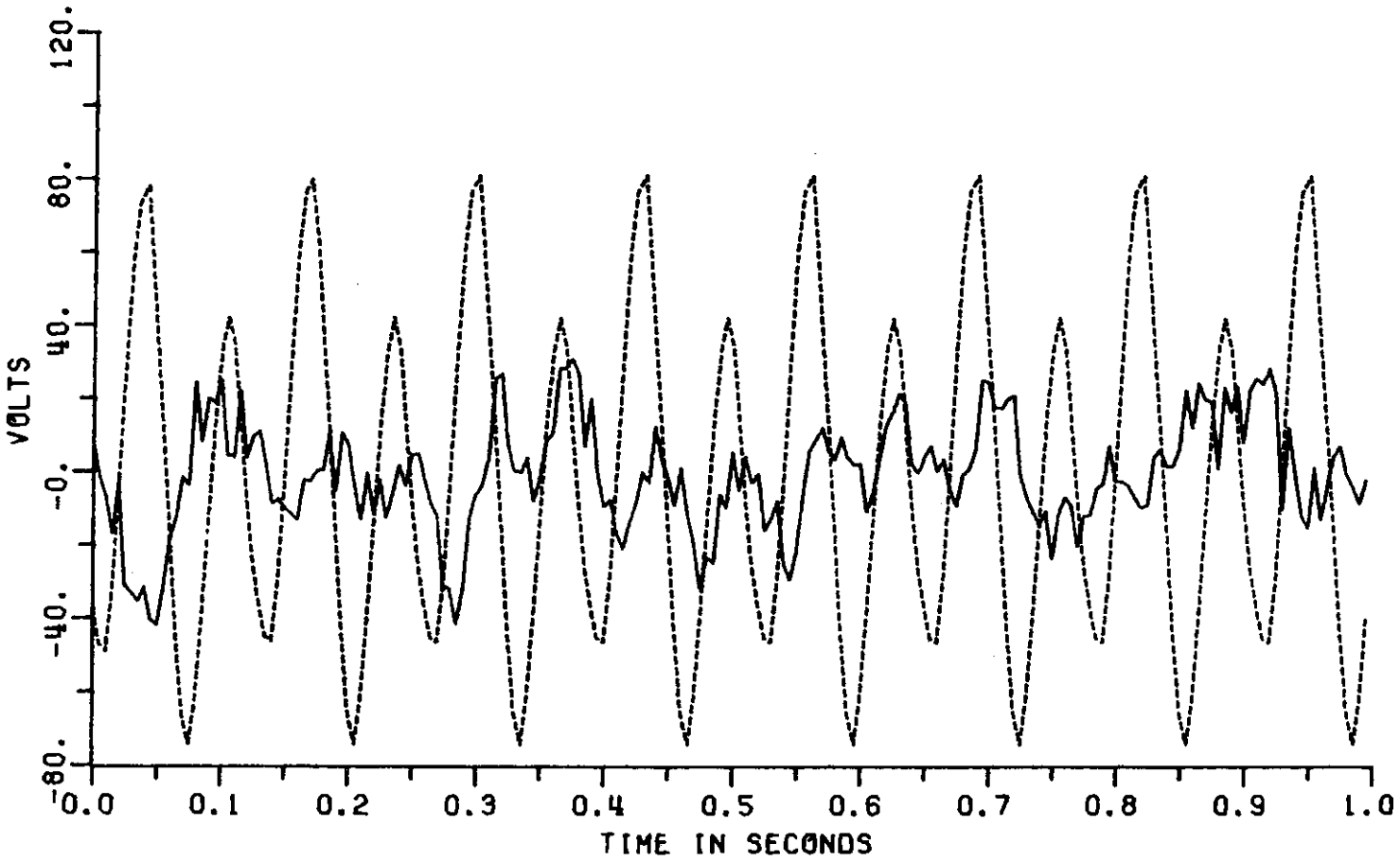

PITCH VOLT TEST 3

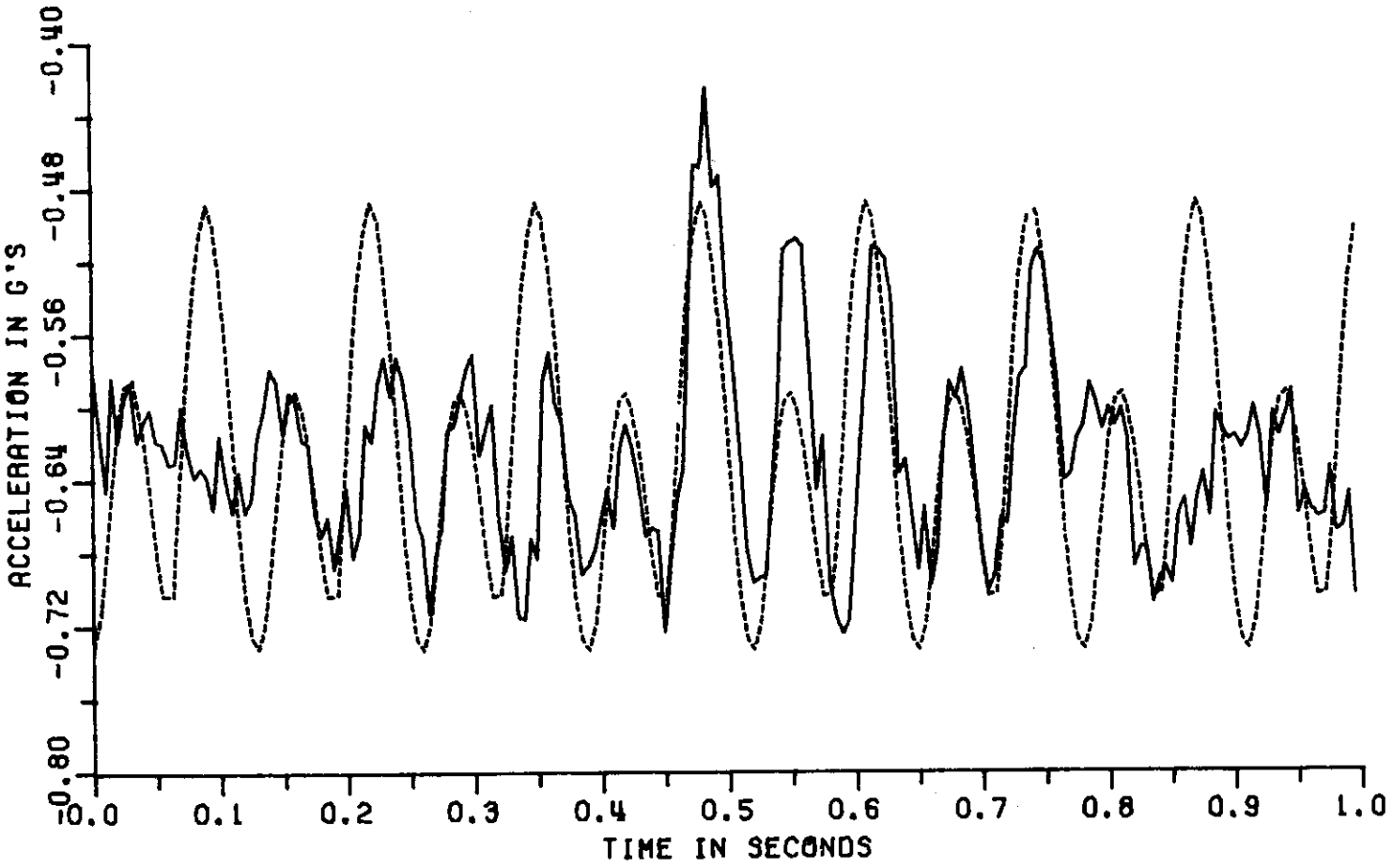

HEAVE ACC TEST 3

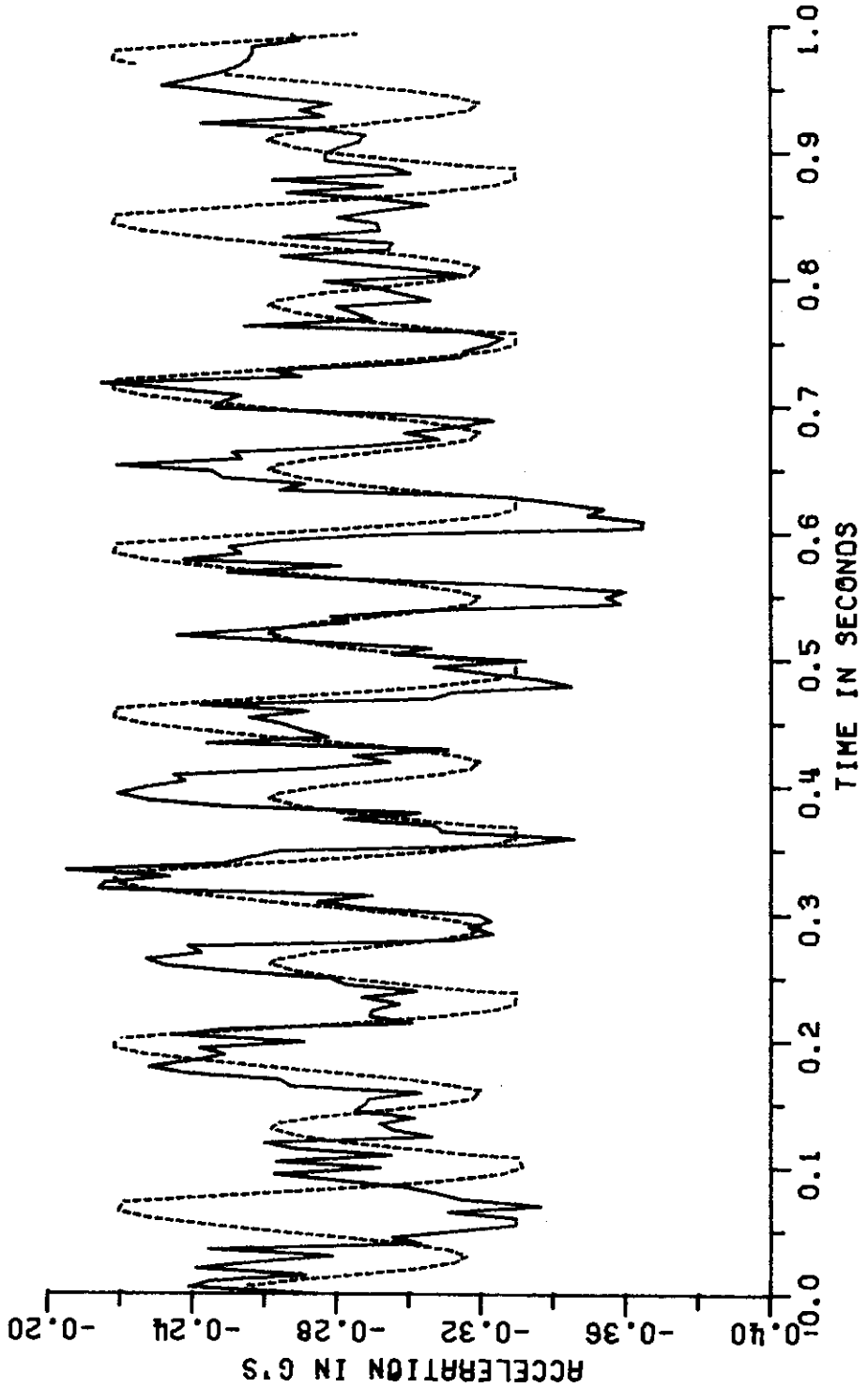

PITCH ACC TEST 3

APPENDIX G

Test 1 - Gaps, Accelerations and Voltages

SPEED: 188 km/hr

GUIDEWAY MODIFICATION: elastic

COMMENT: The time synchronization between theory and experiment is apparently off by 20 ms. (See Section 4.1.2.)

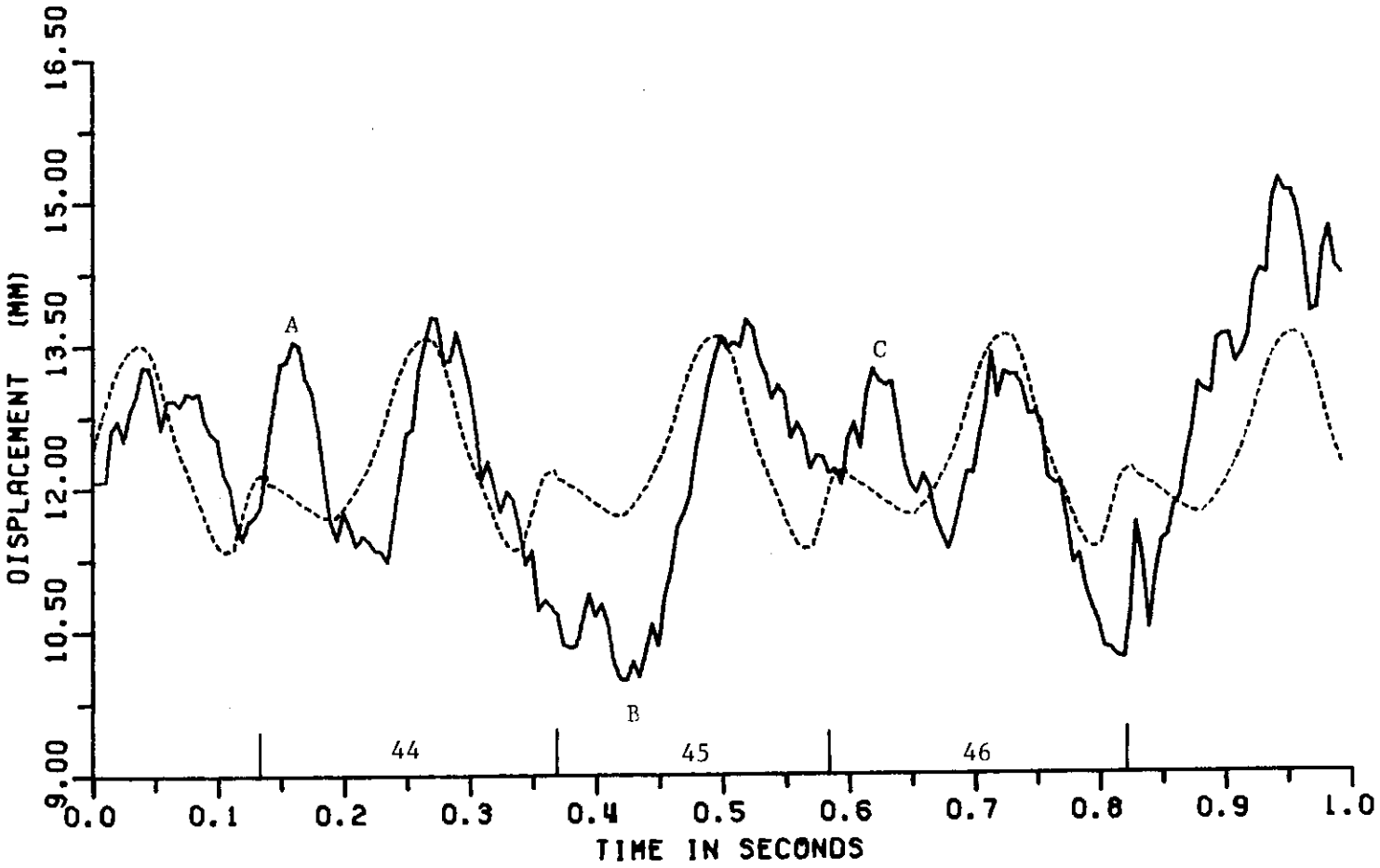

FRONT GAP TEST 1

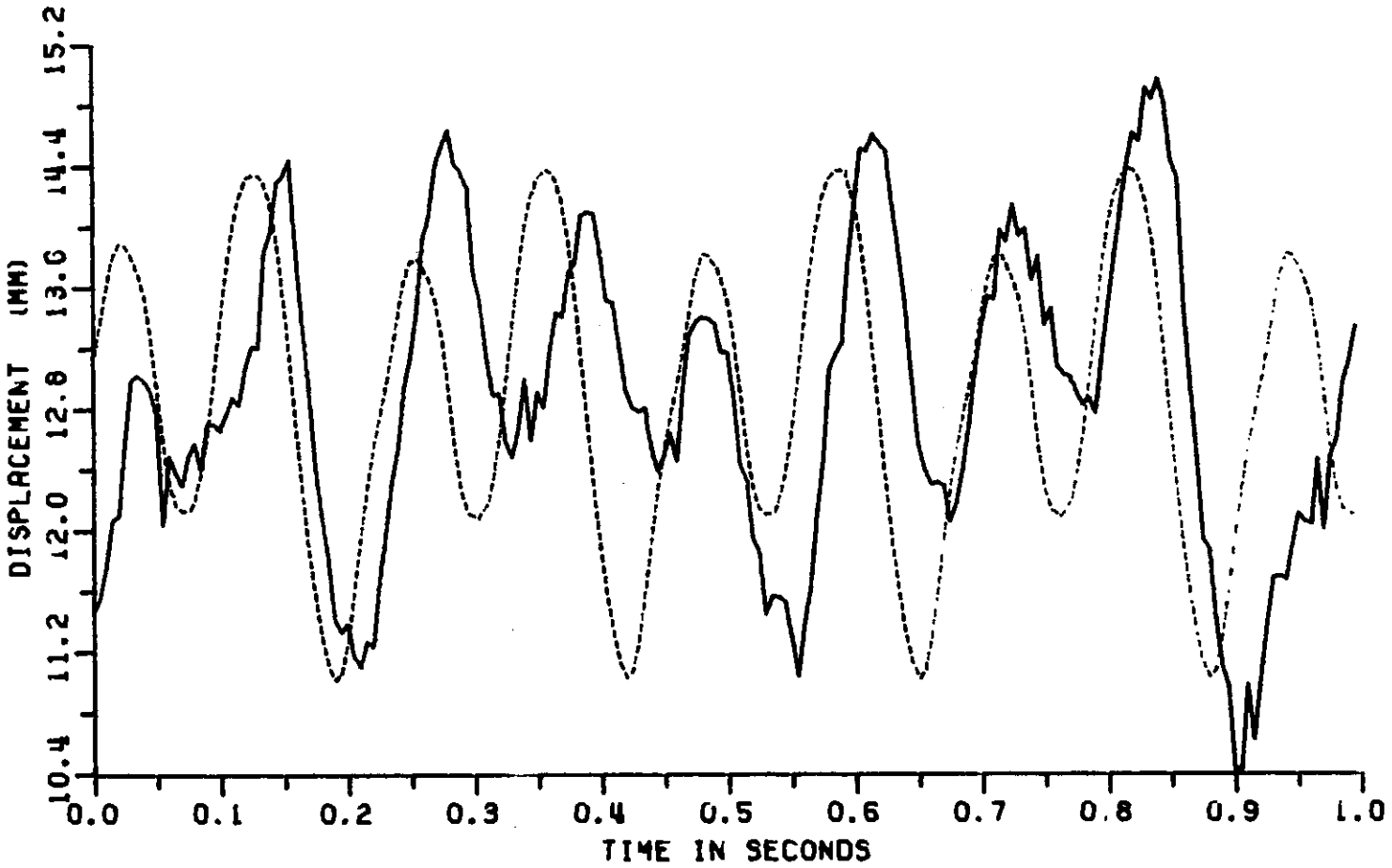

REAR GAP TEST 1

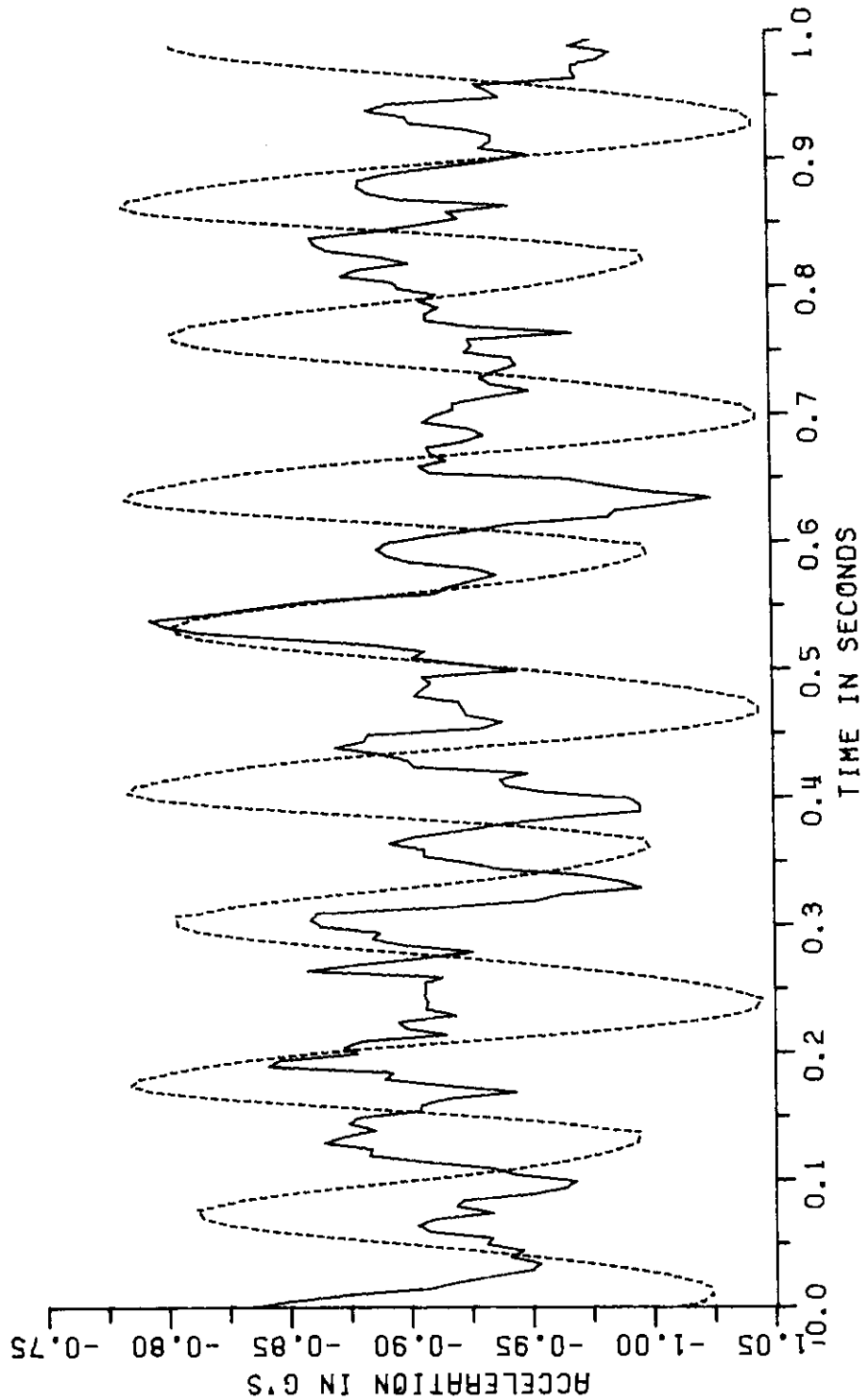

FRONT ACC TEST 1

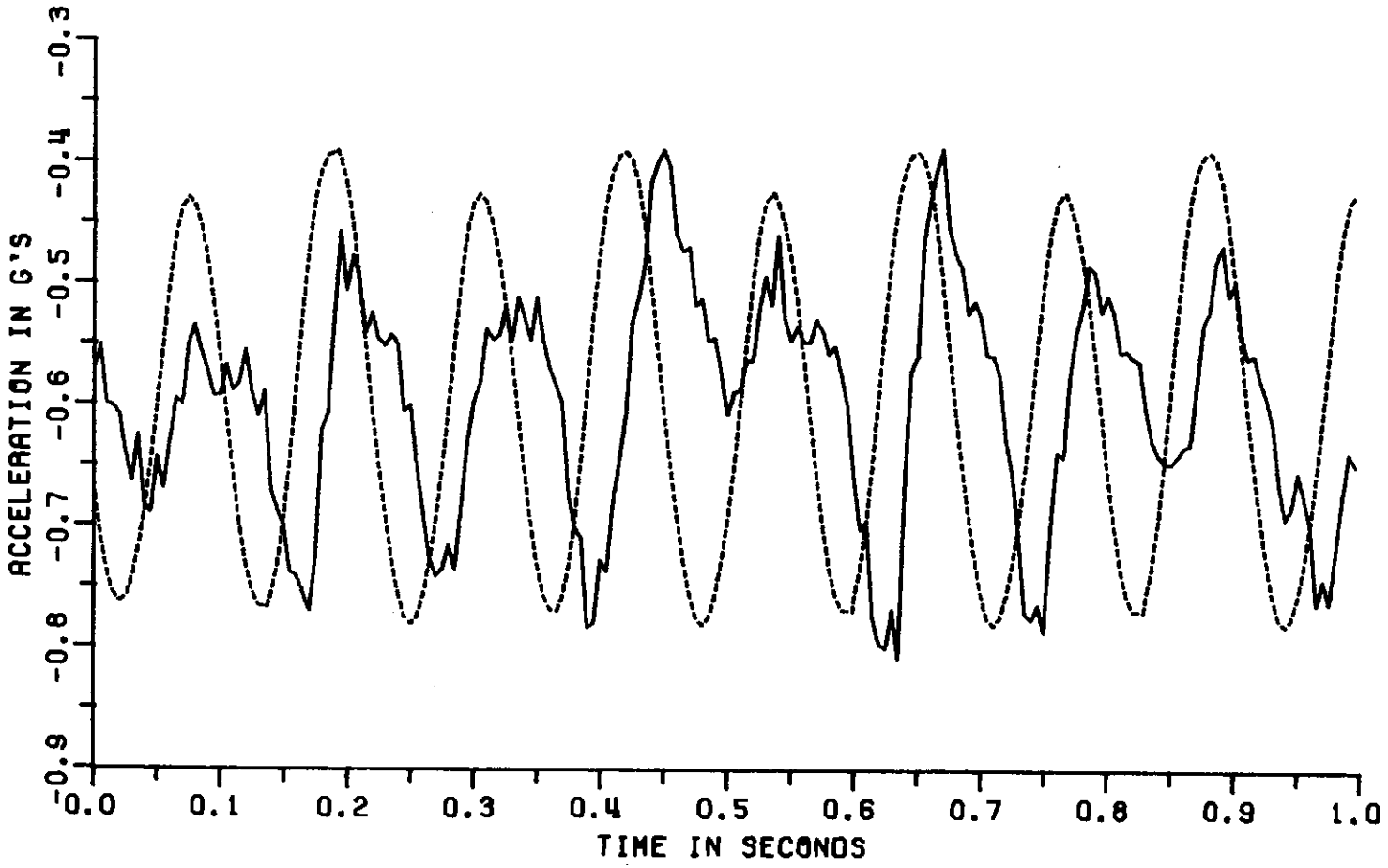

REAR ACC TEST 1

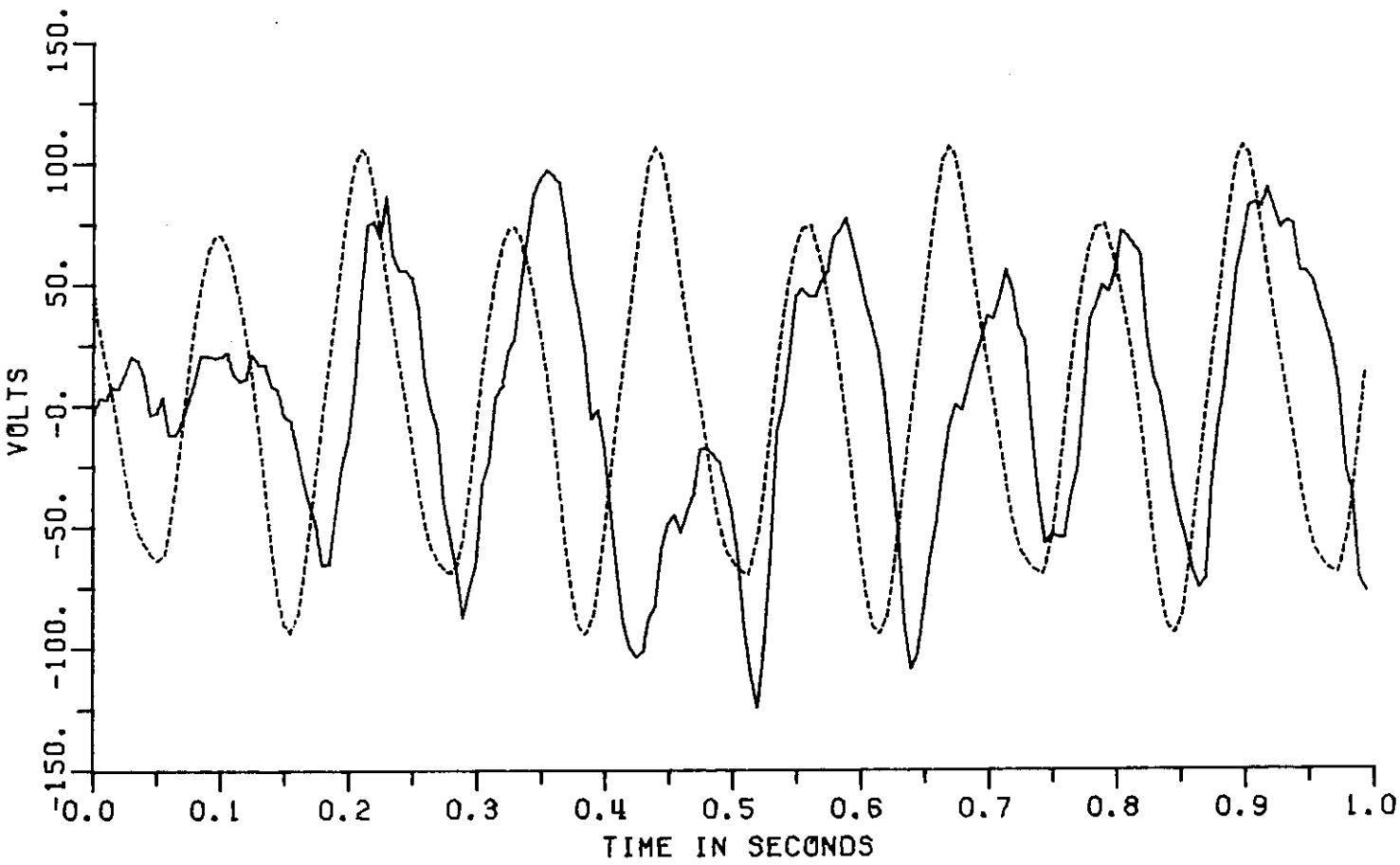

HEAVE VOLT TEST 1

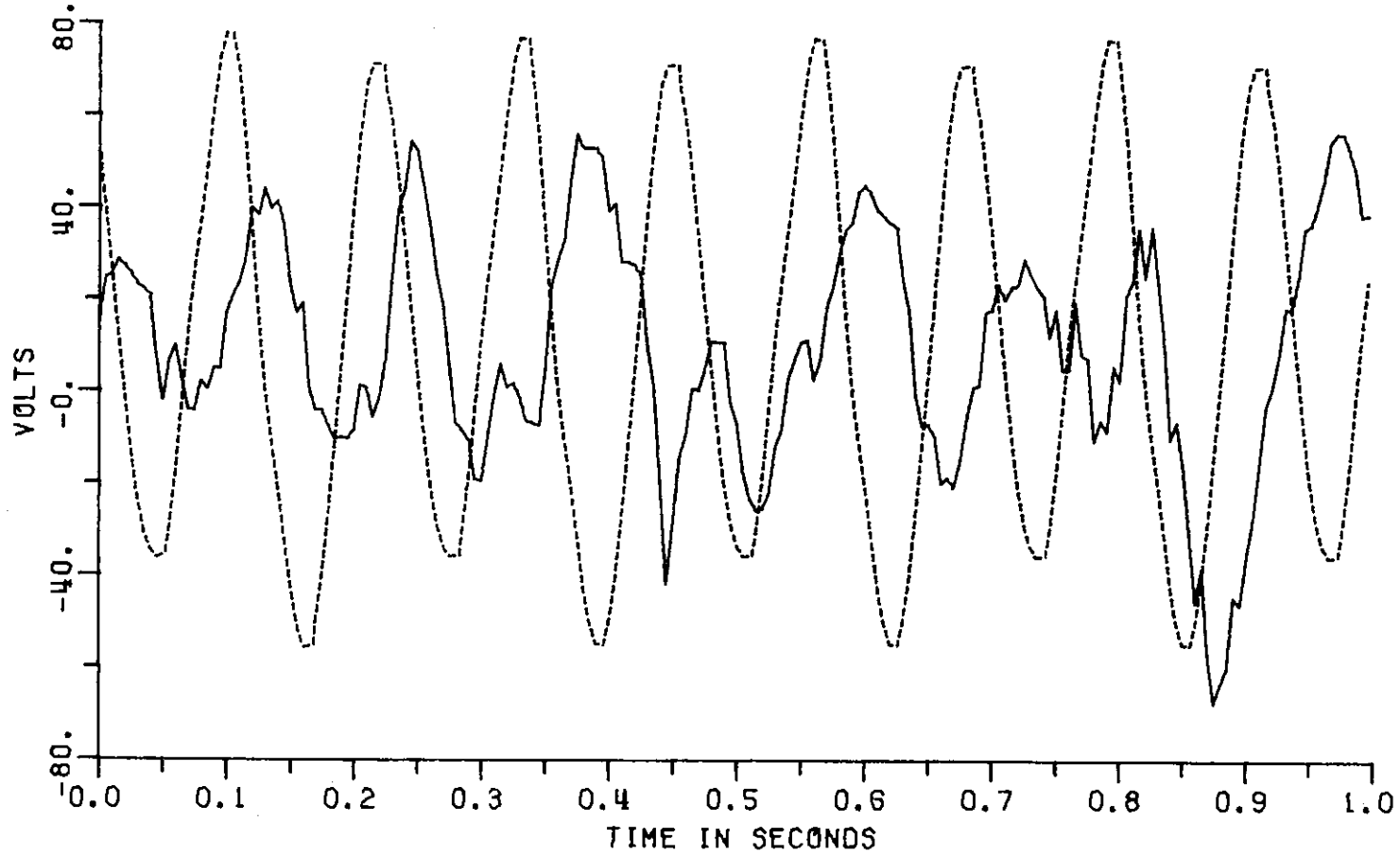

PITCH VOLT TEST 1

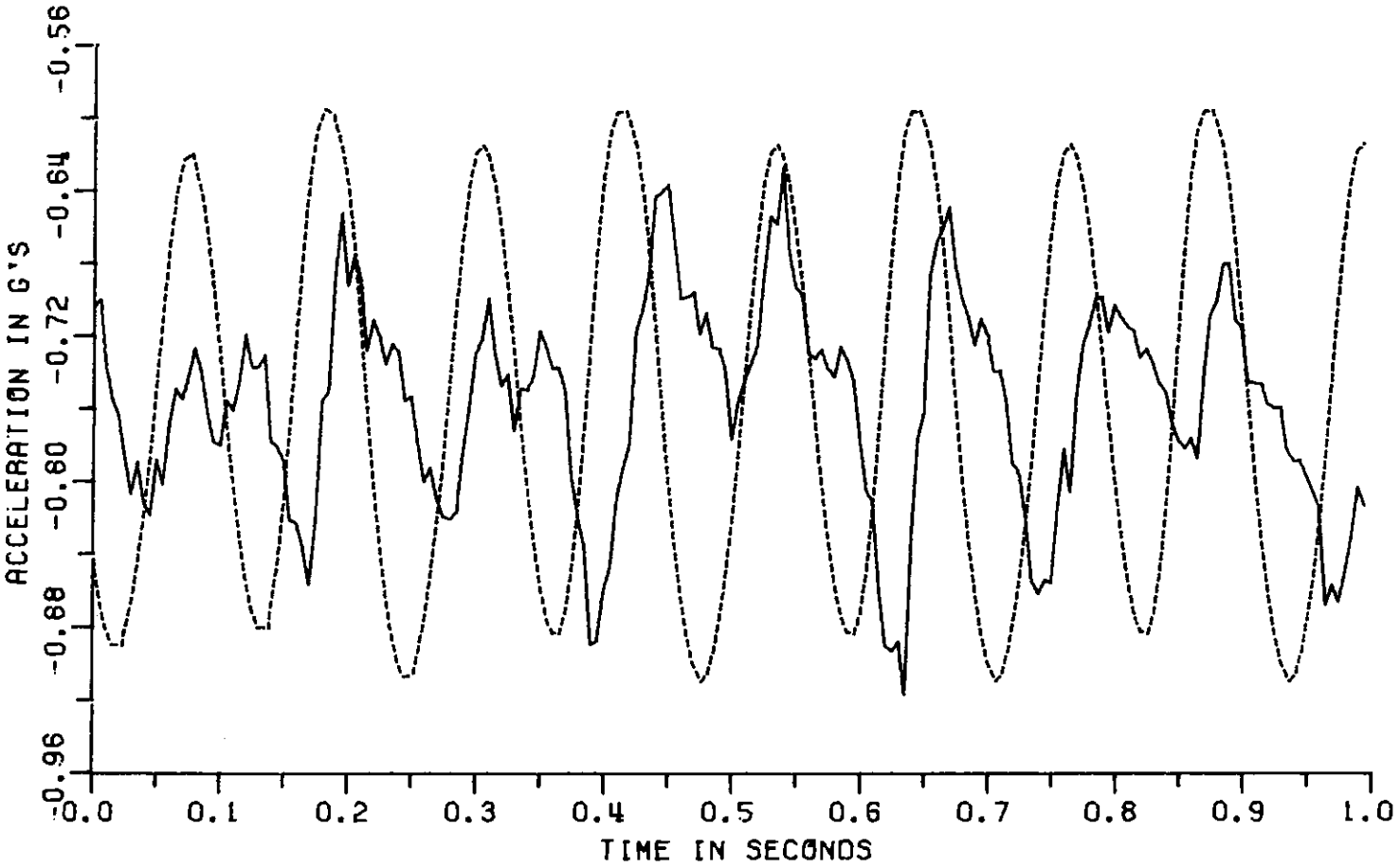

HEAVE ACC TEST 1

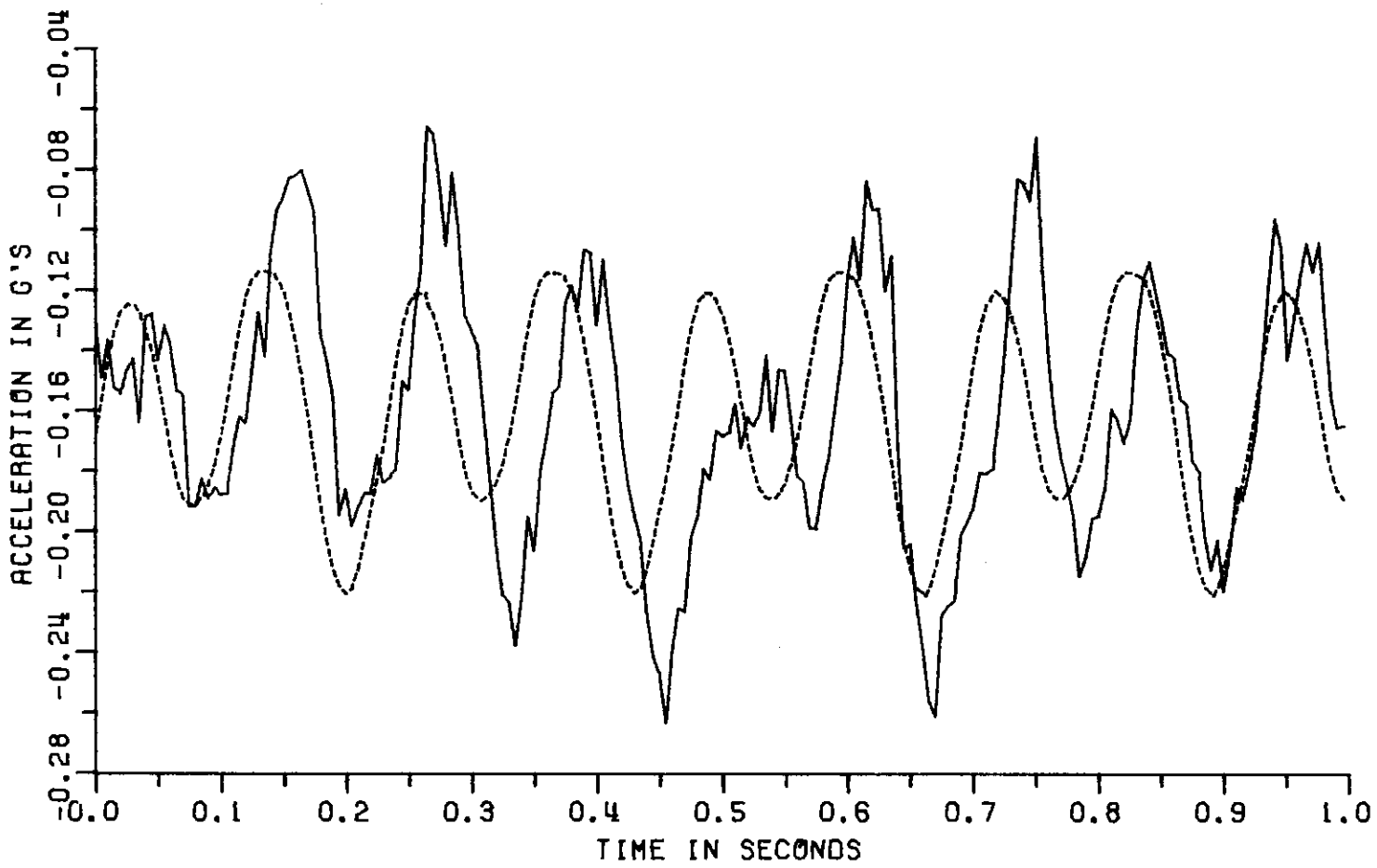

PITCH ACC TEST 1

APPENDIX H

Test 2 - Gaps, Accelerations and Voltages

SPEED: 261 km/hr

GUIDEWAY MODIFICATION: elastic

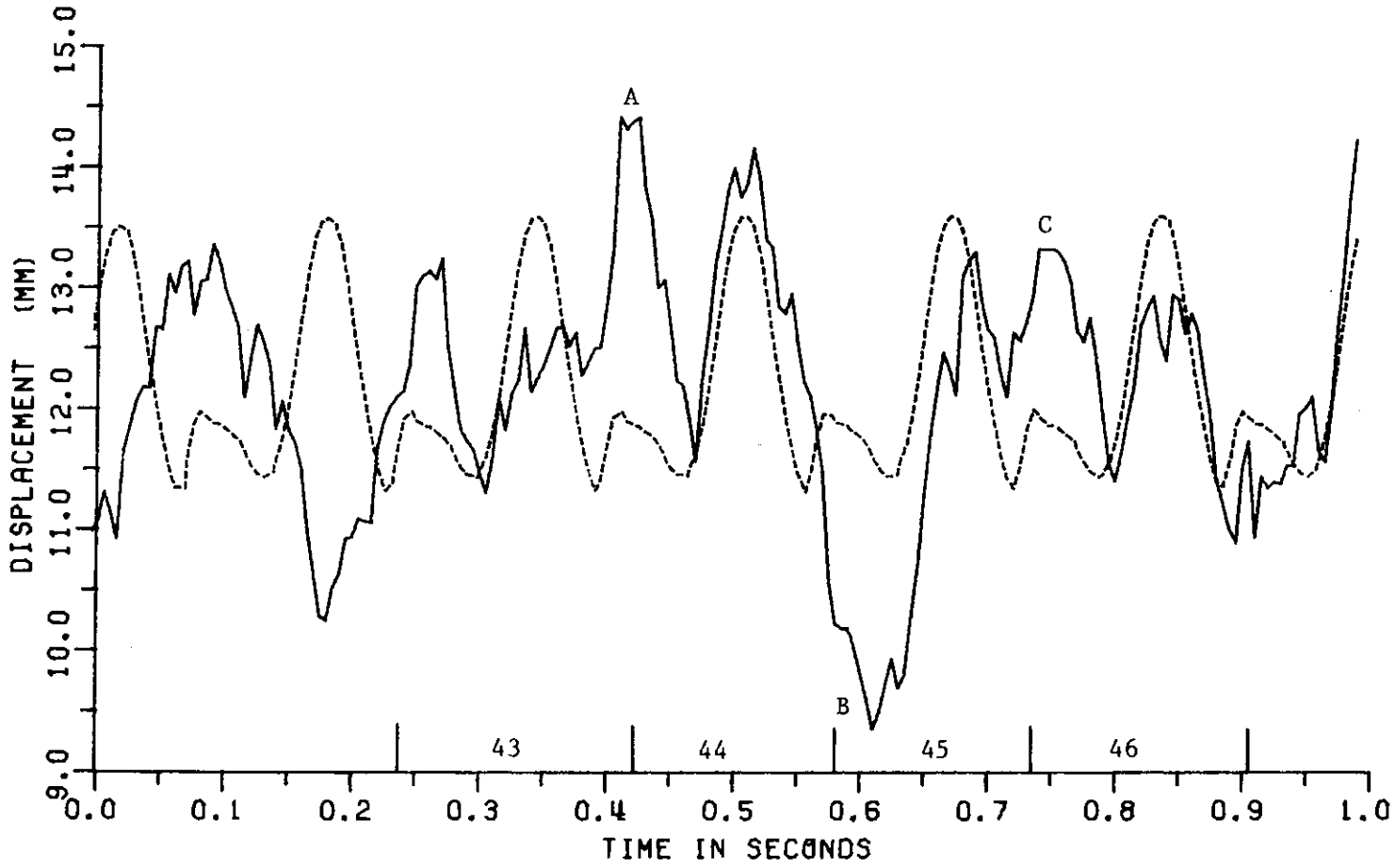

FRONT GAP TEST 2

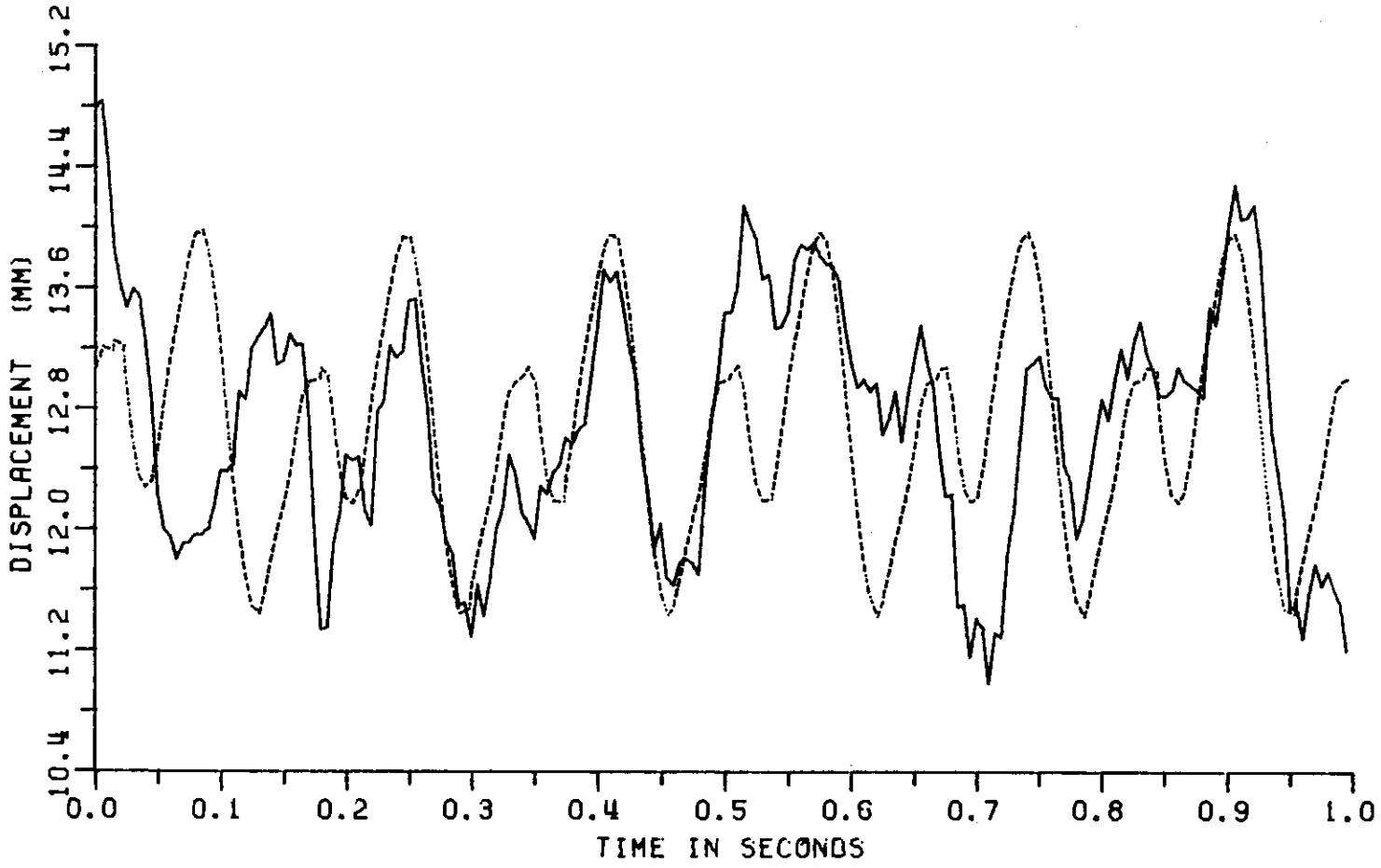

REAR GAP TEST 2

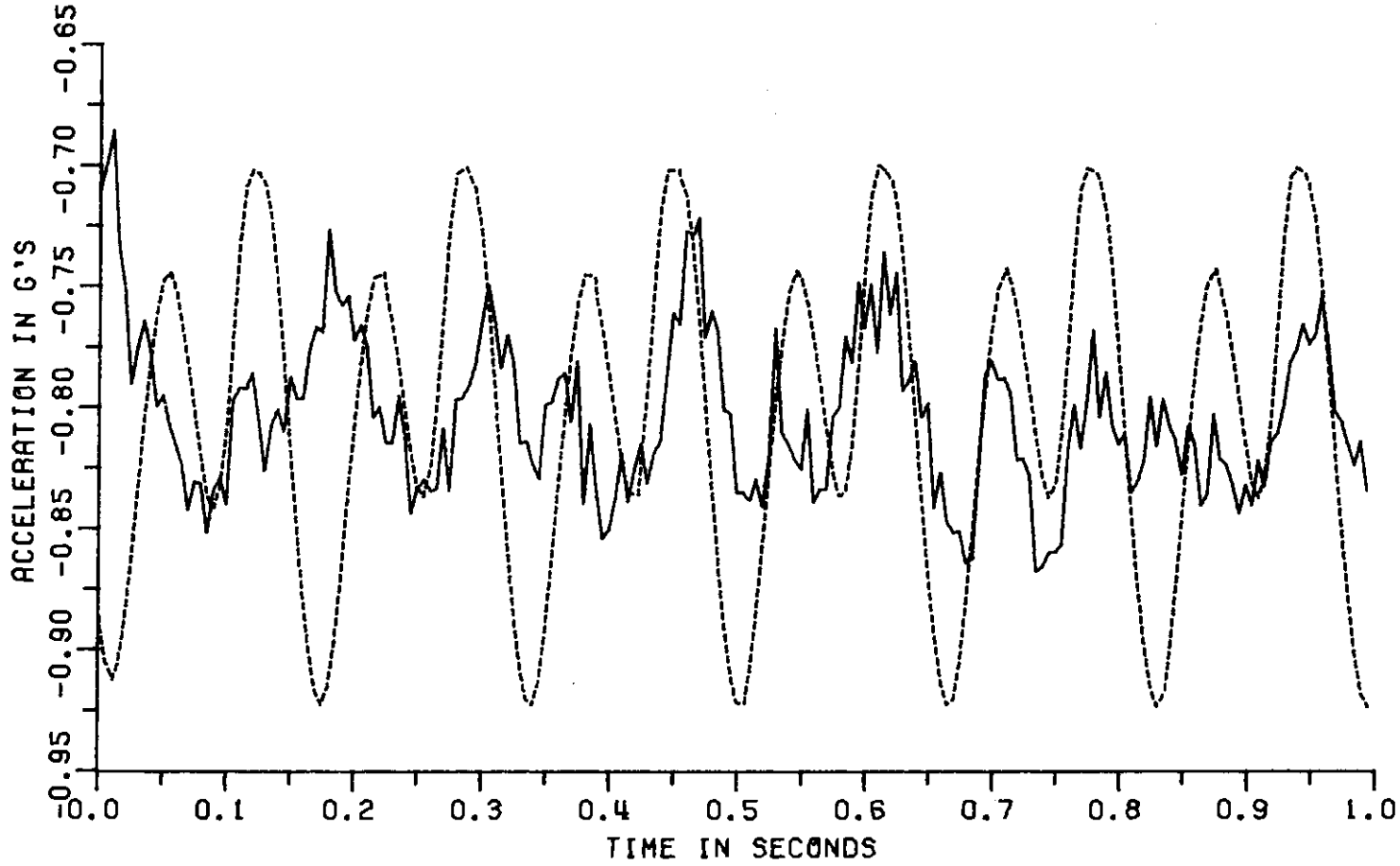

FRONT ACC TEST 2

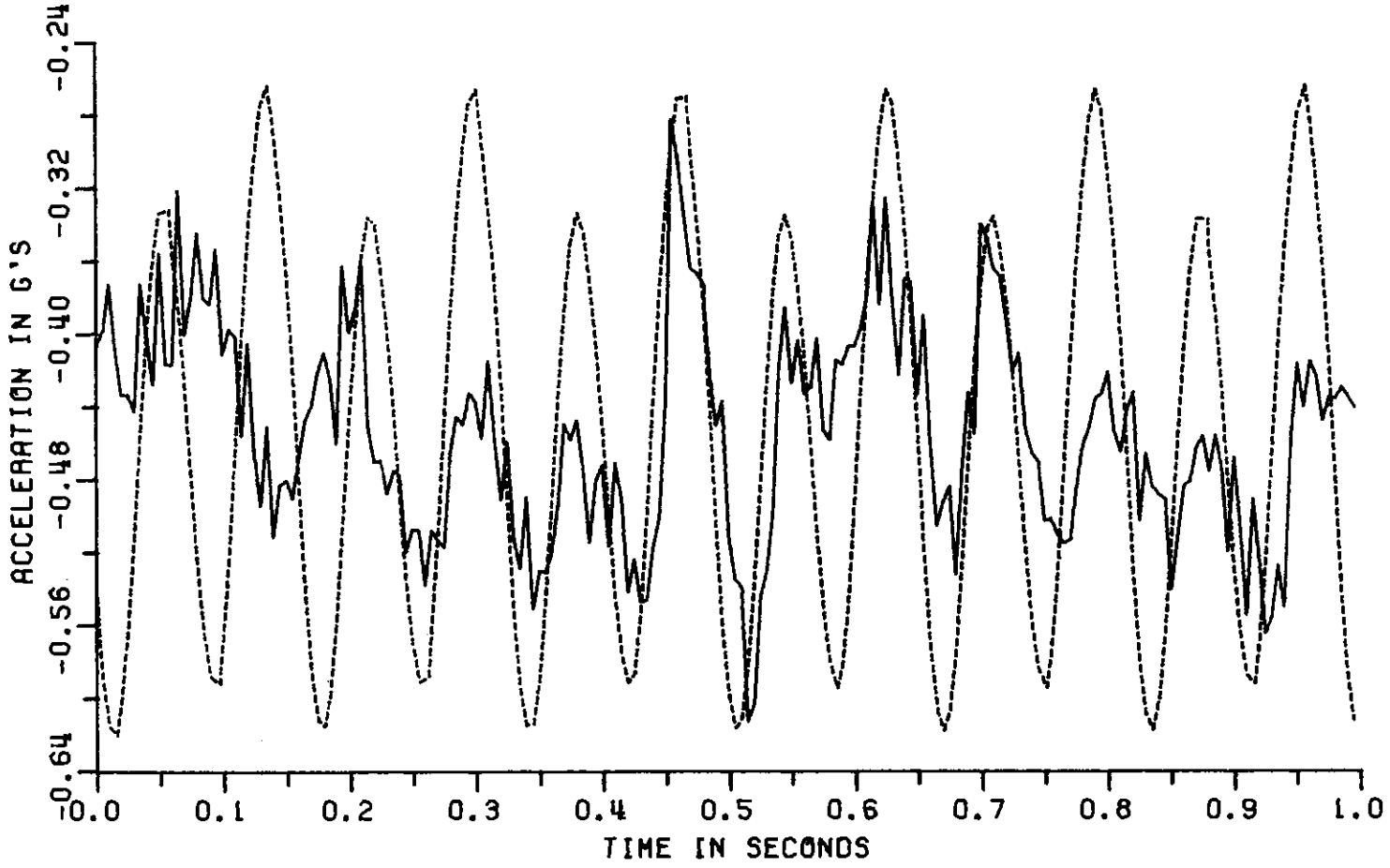

REAR ACC TEST 2

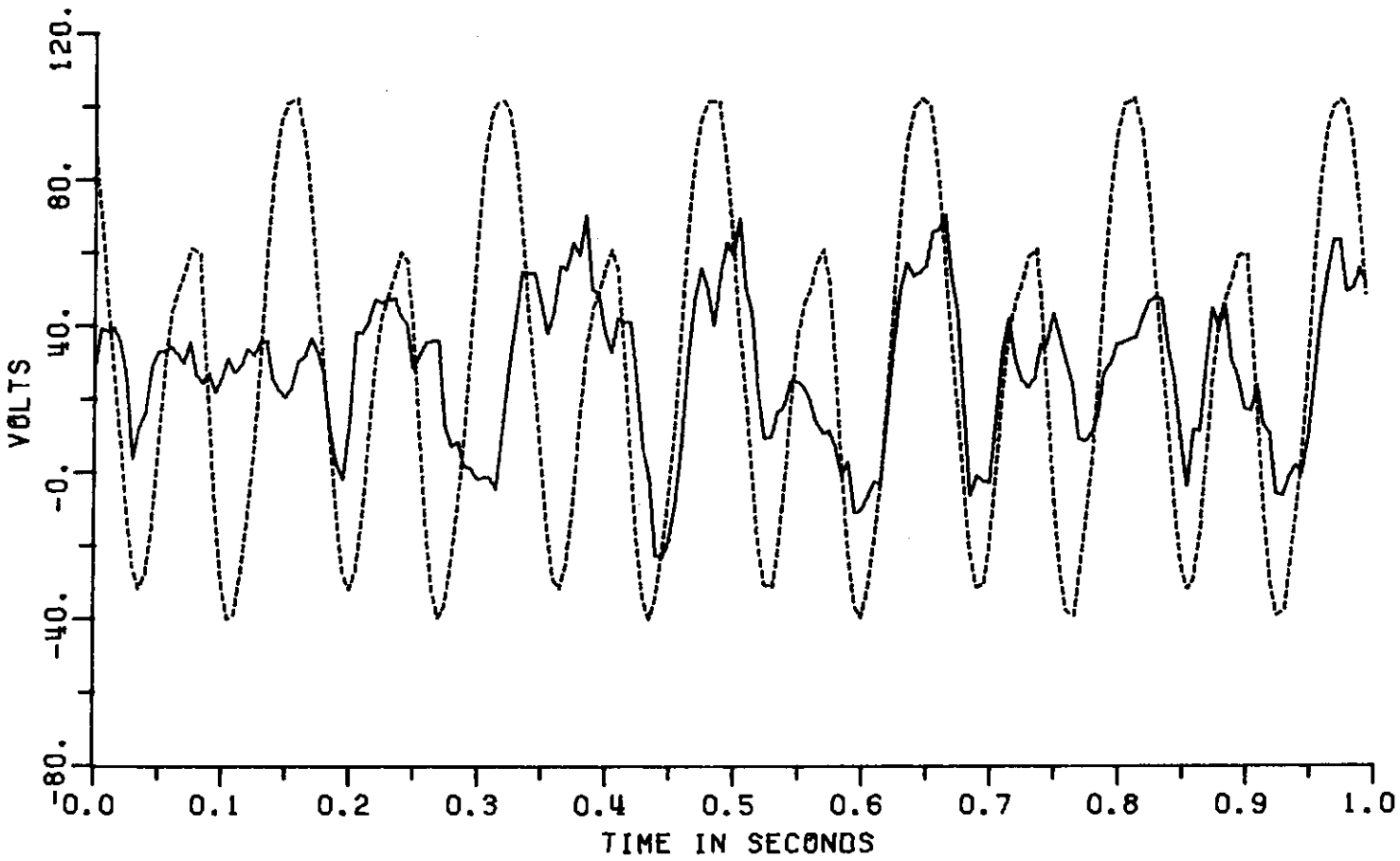

HEAVE VOLT TEST 2

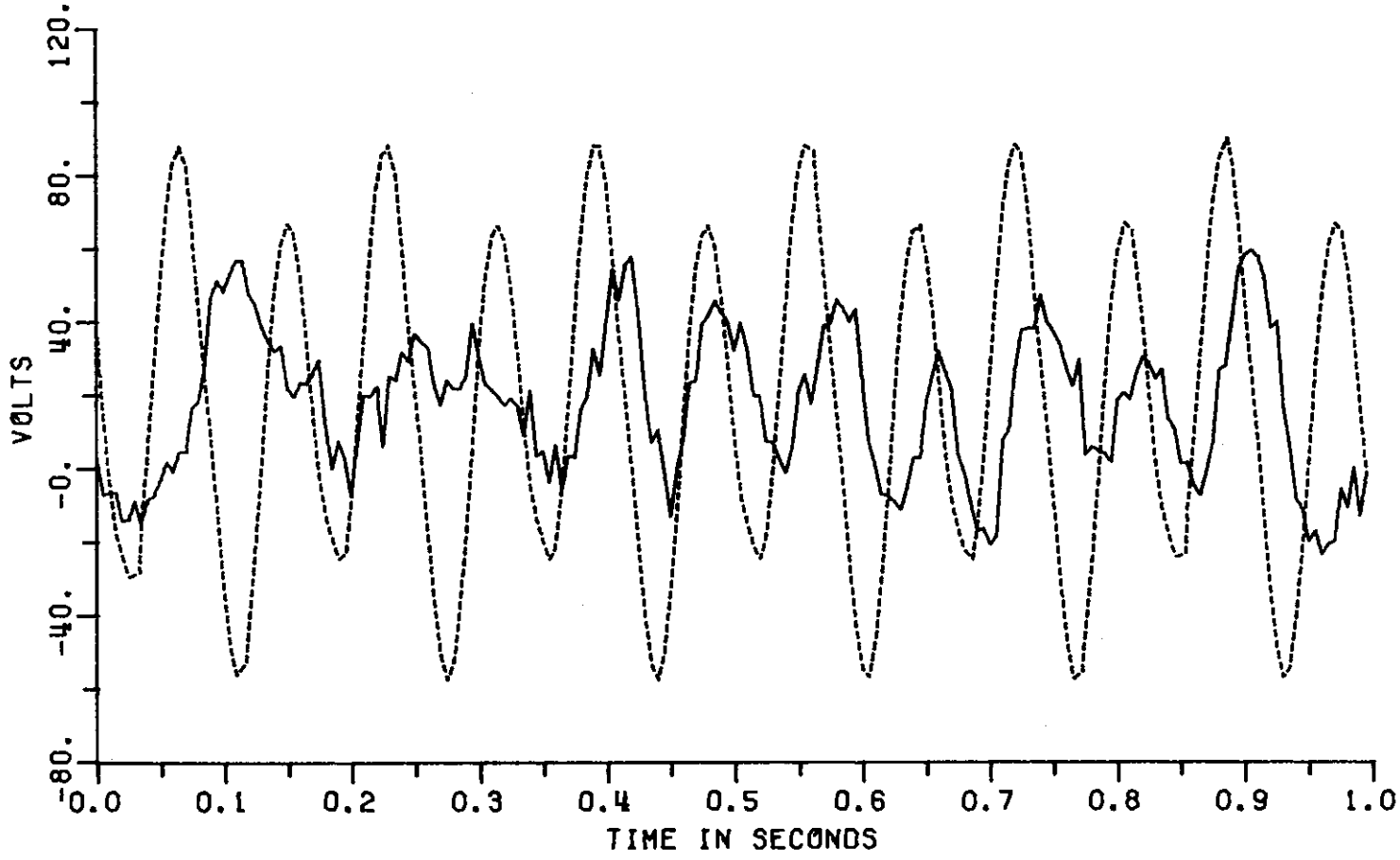

PITCH VOLT TEST 2

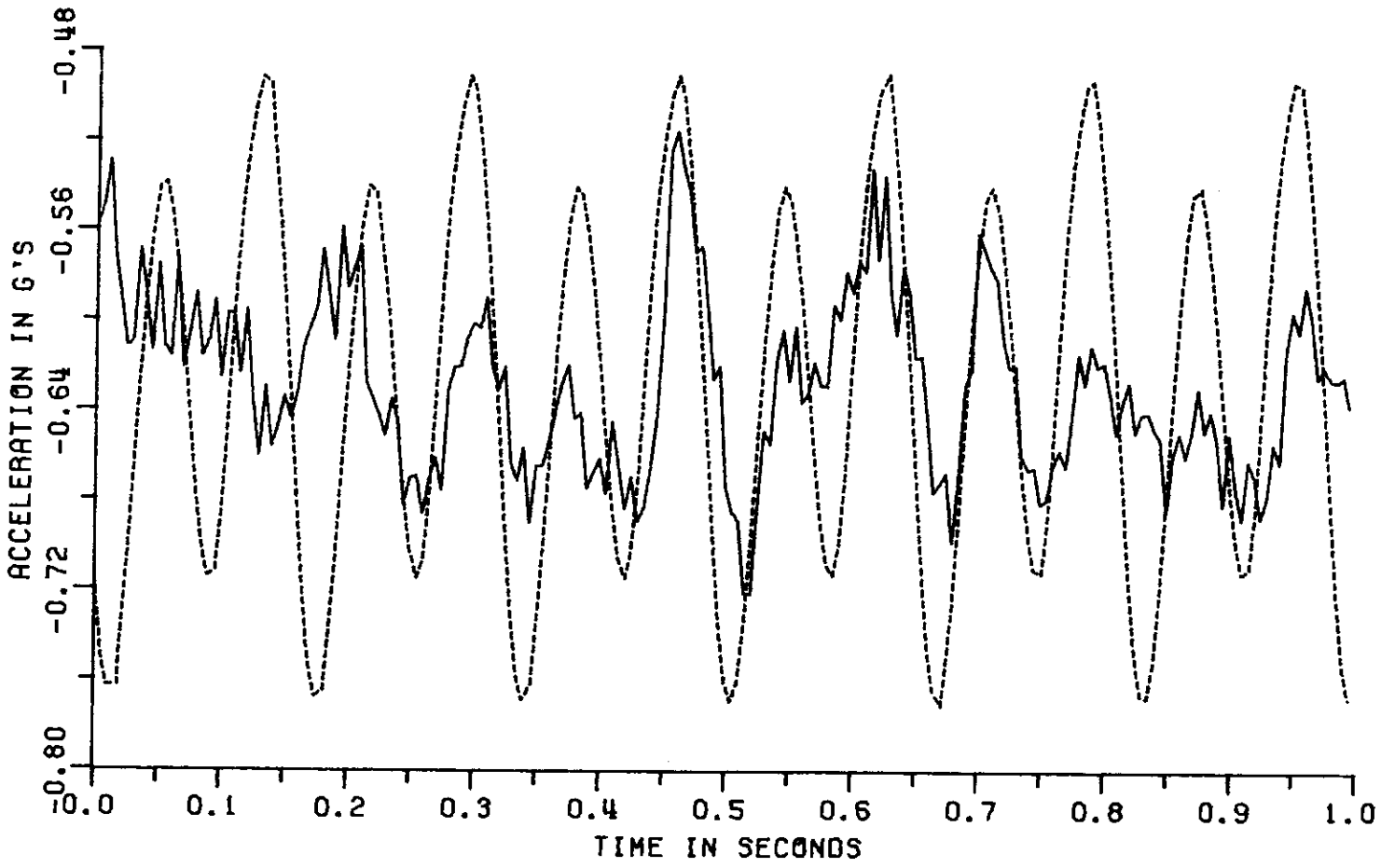

HEAVE ACC TEST 2

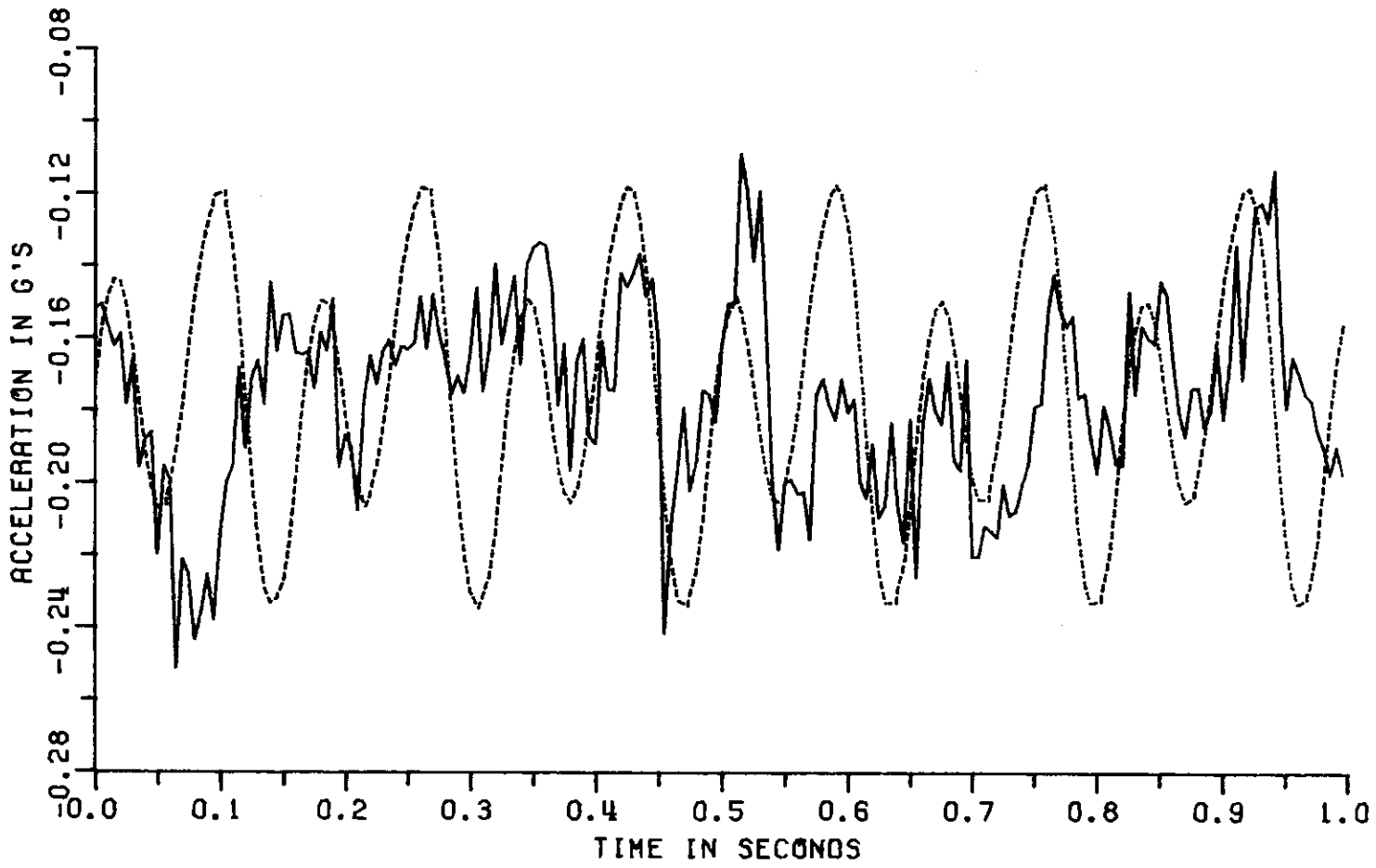

PITCH ACC TEST 2

APPENDIX I

Test 1 - Time Shifted by 20 ms

SPEED: 188 km/hr

GUIDEWAY MODIFICATION: elastic

COMMENT: The theory was shifted in time an amount determined by visual inspection to align it with the experimental data. This was 20 ms different than indicated by the experimental synchronization signal.

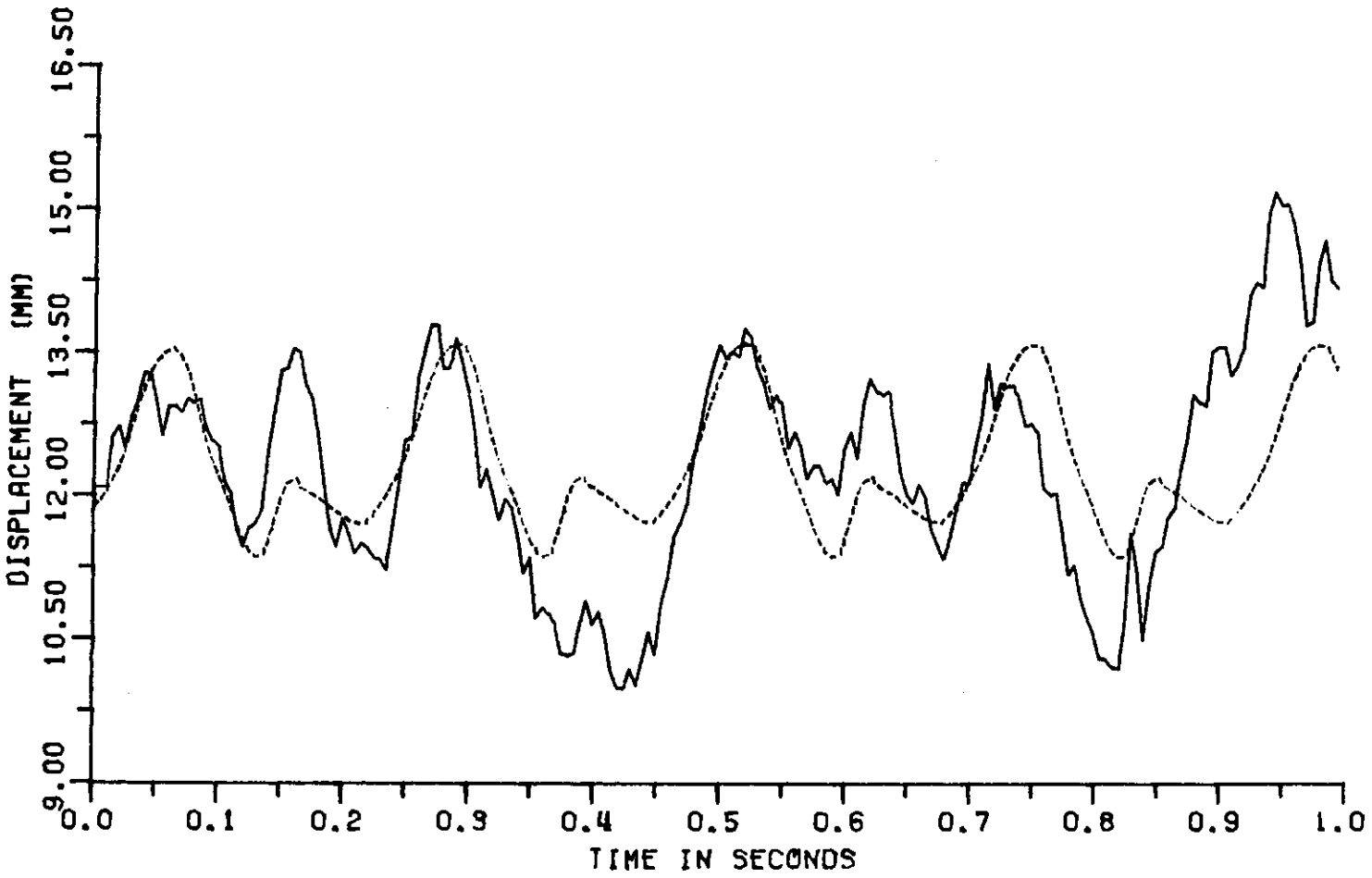

FRONT GAP TEST 1

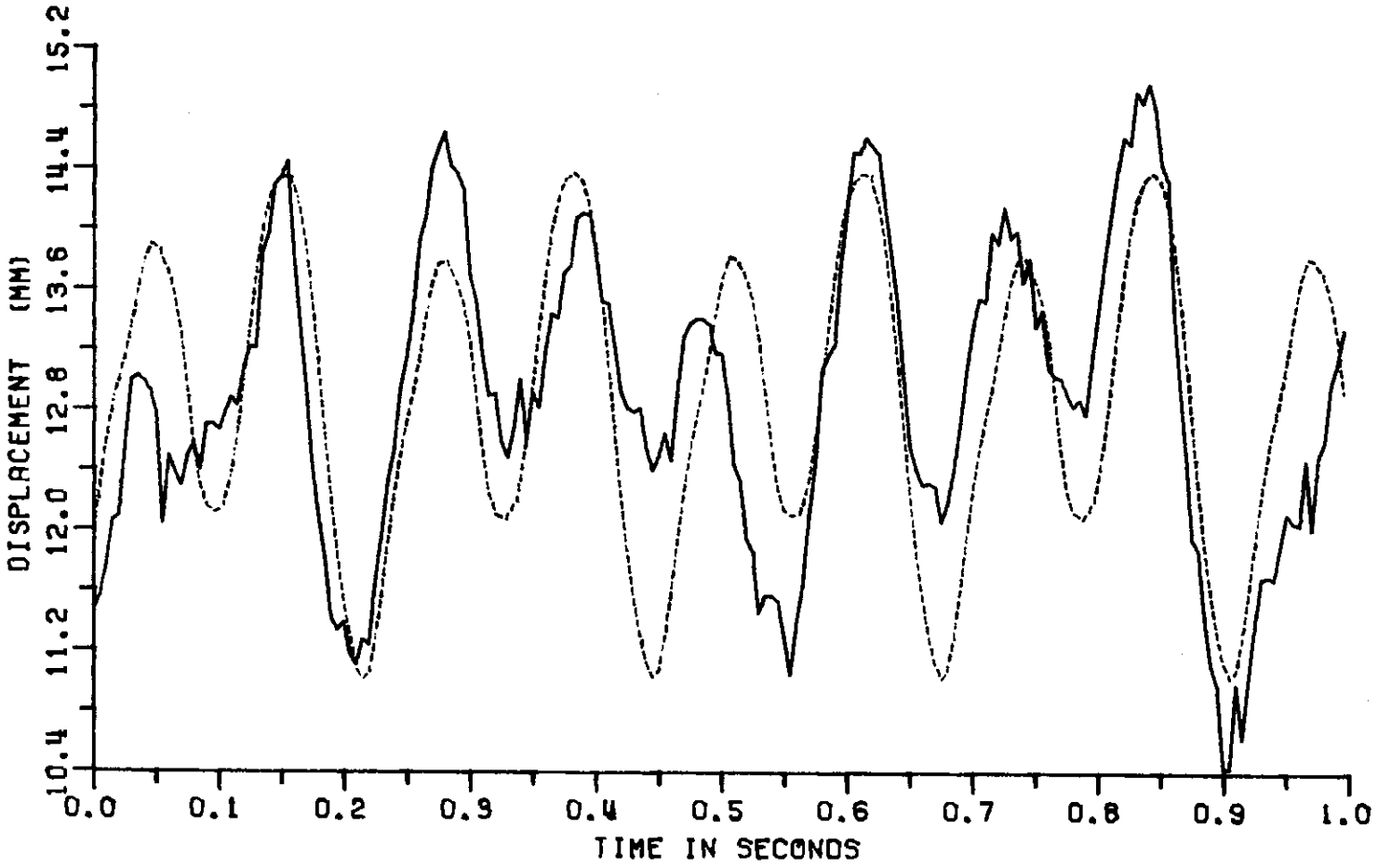

REAR GAP TEST 1

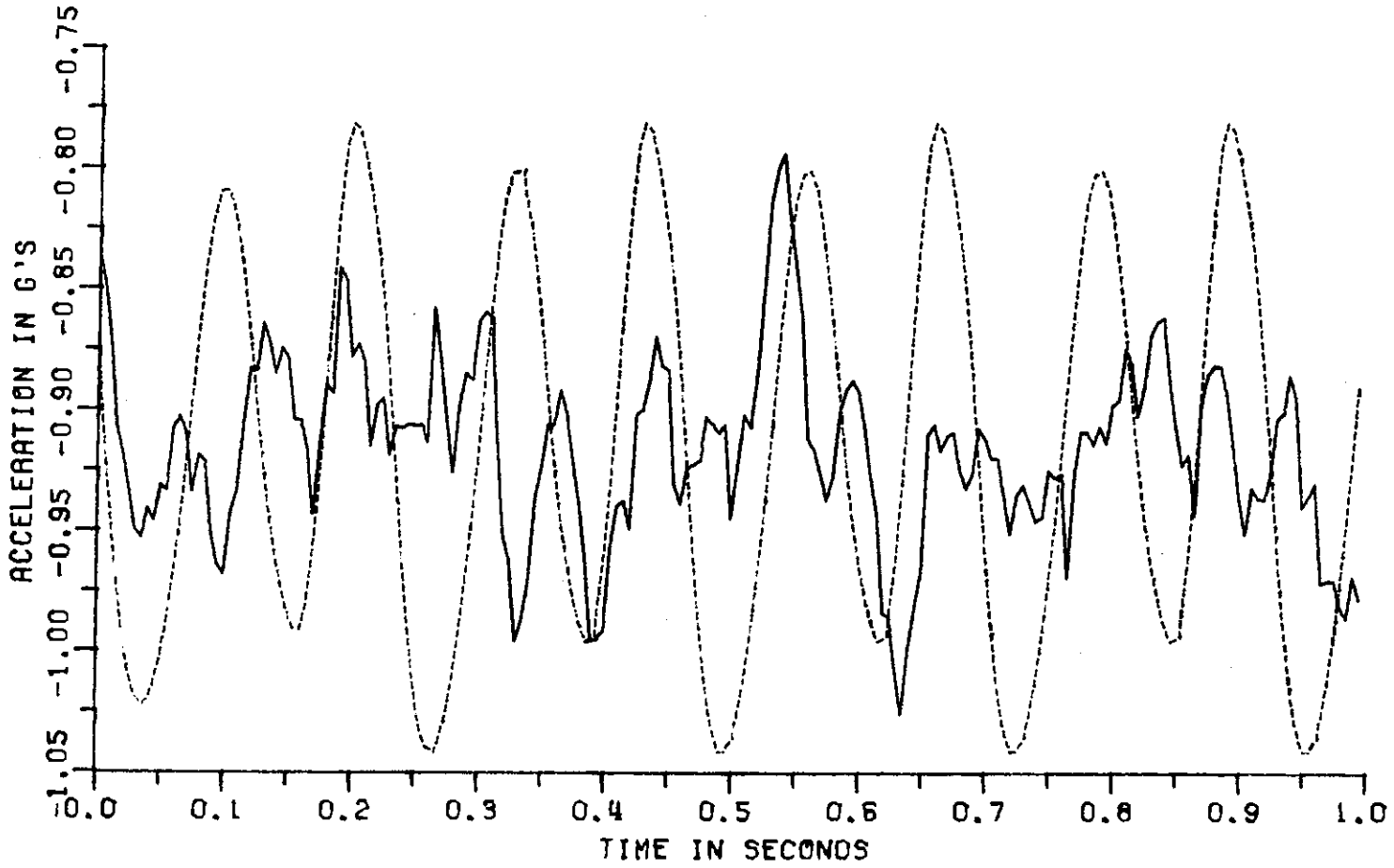

FRONT ACC TEST 1

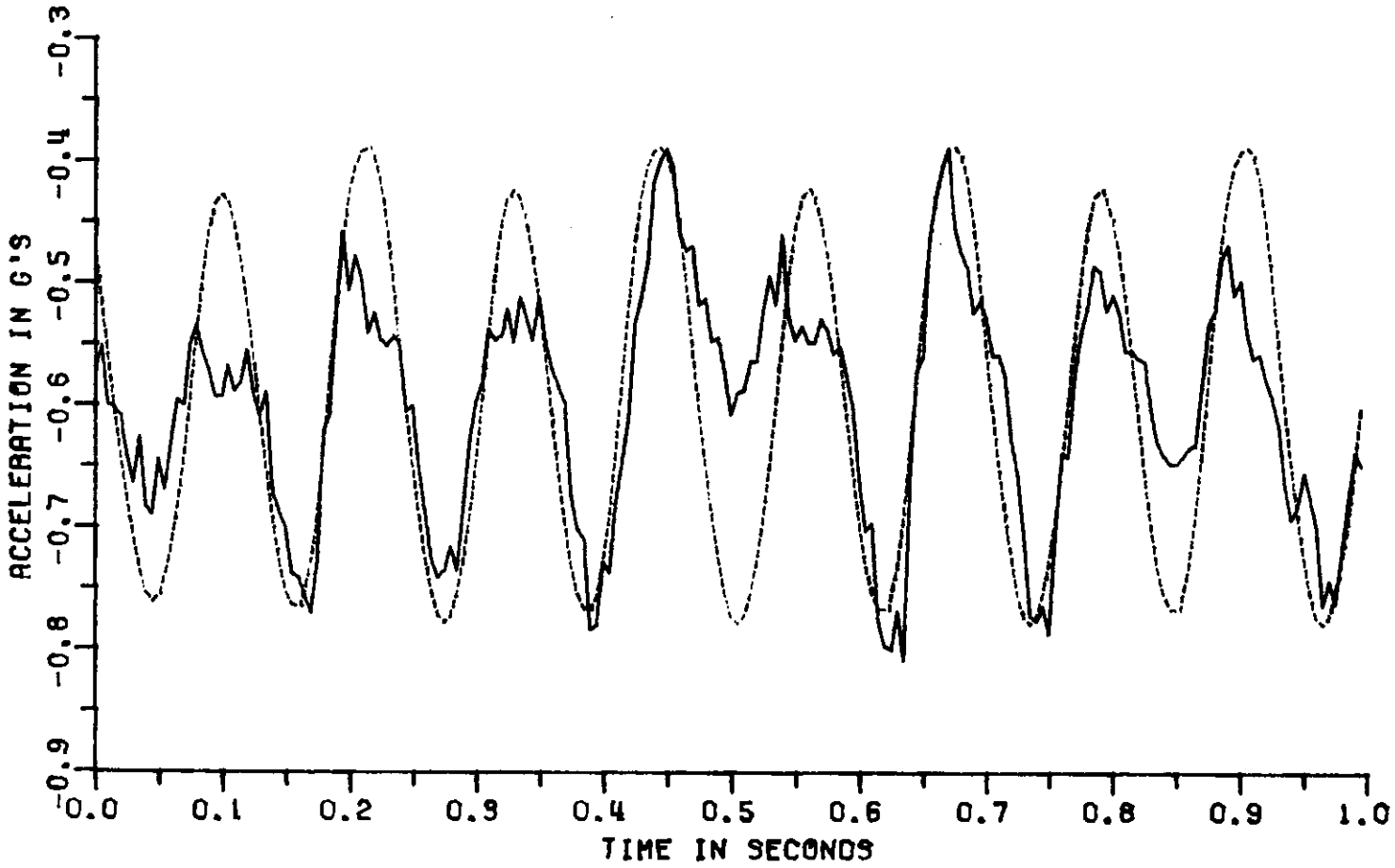

REAR ACC TEST 1

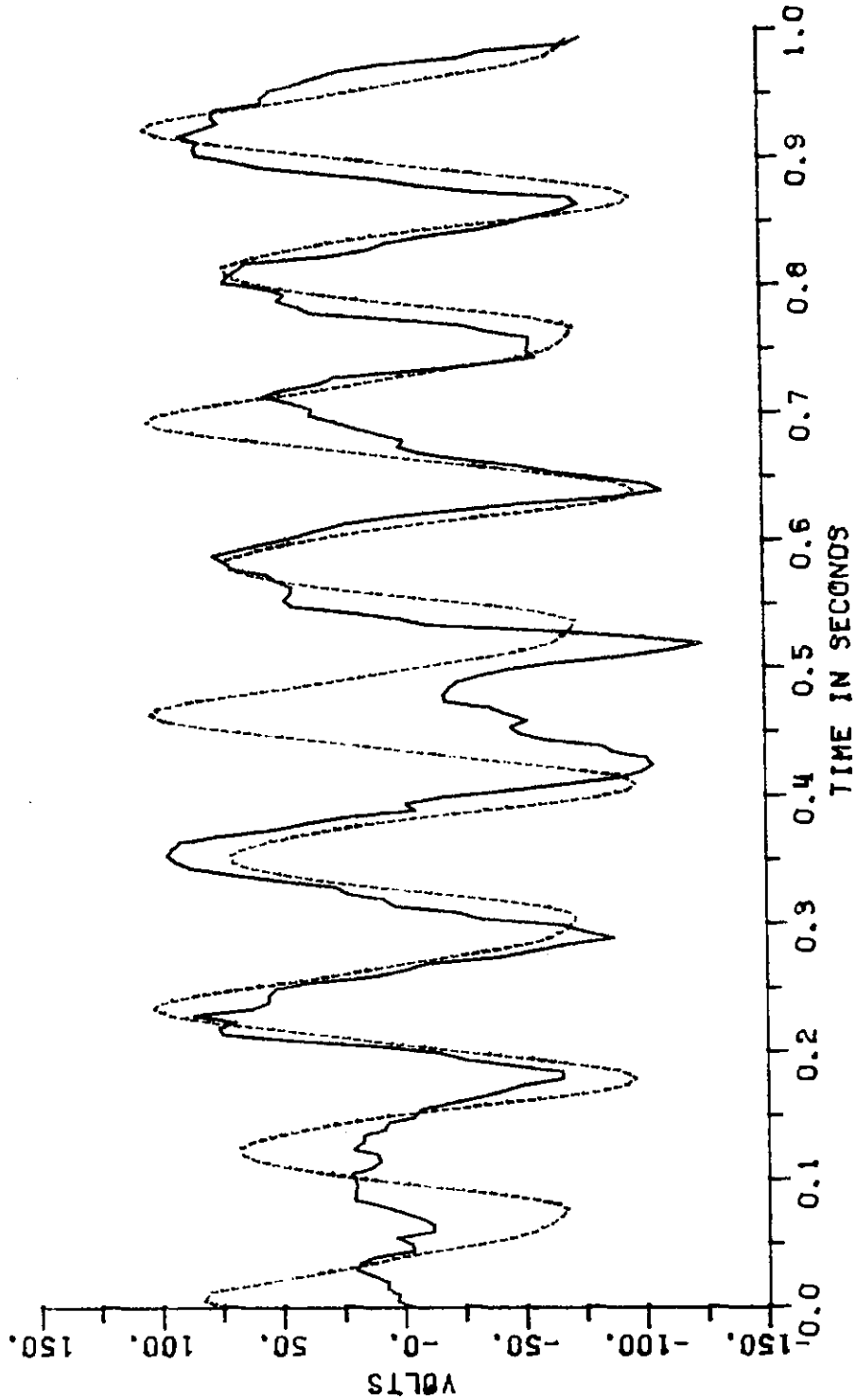

HEAVE VOLT TEST 1

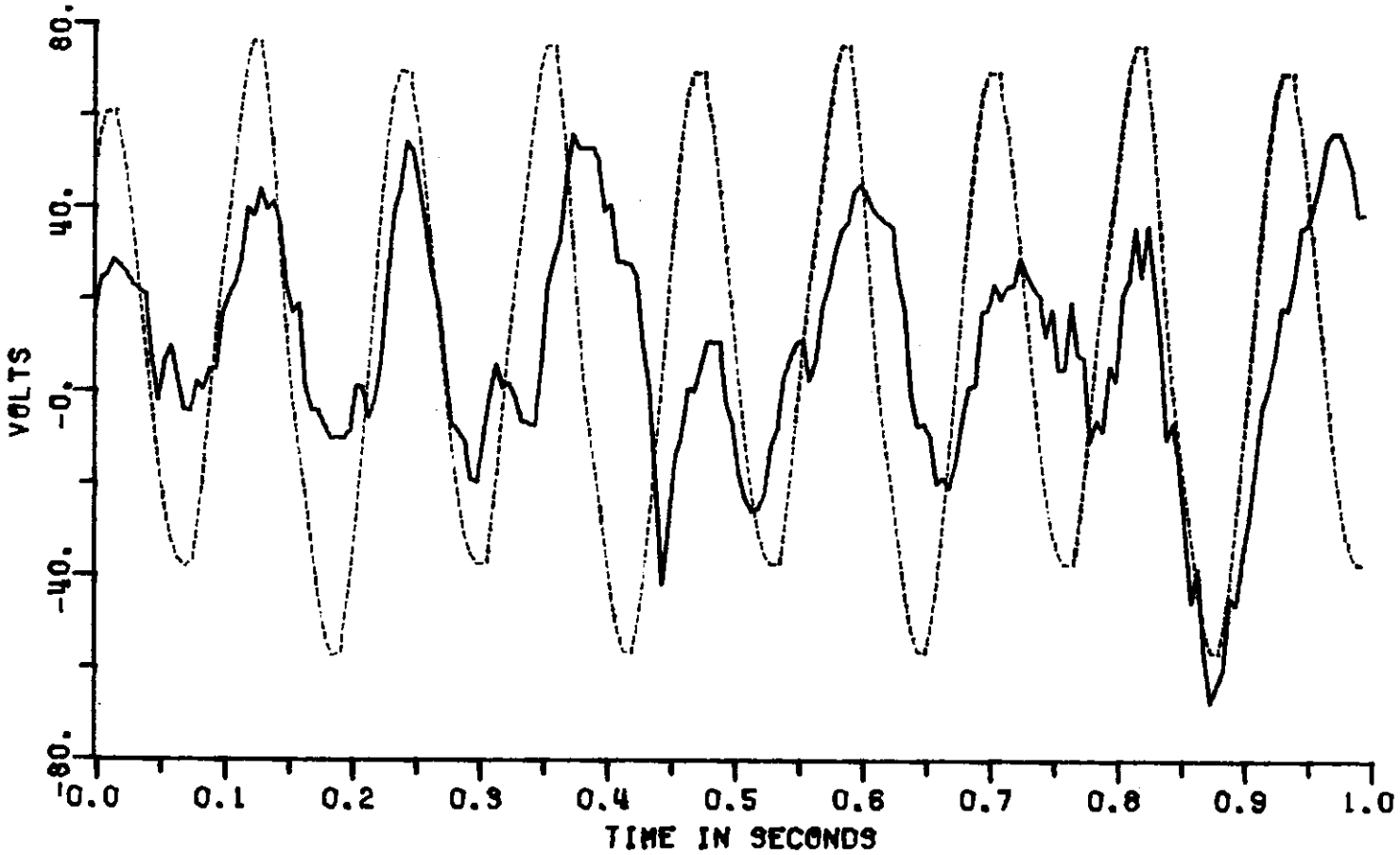

PITCH VOLT TEST 1

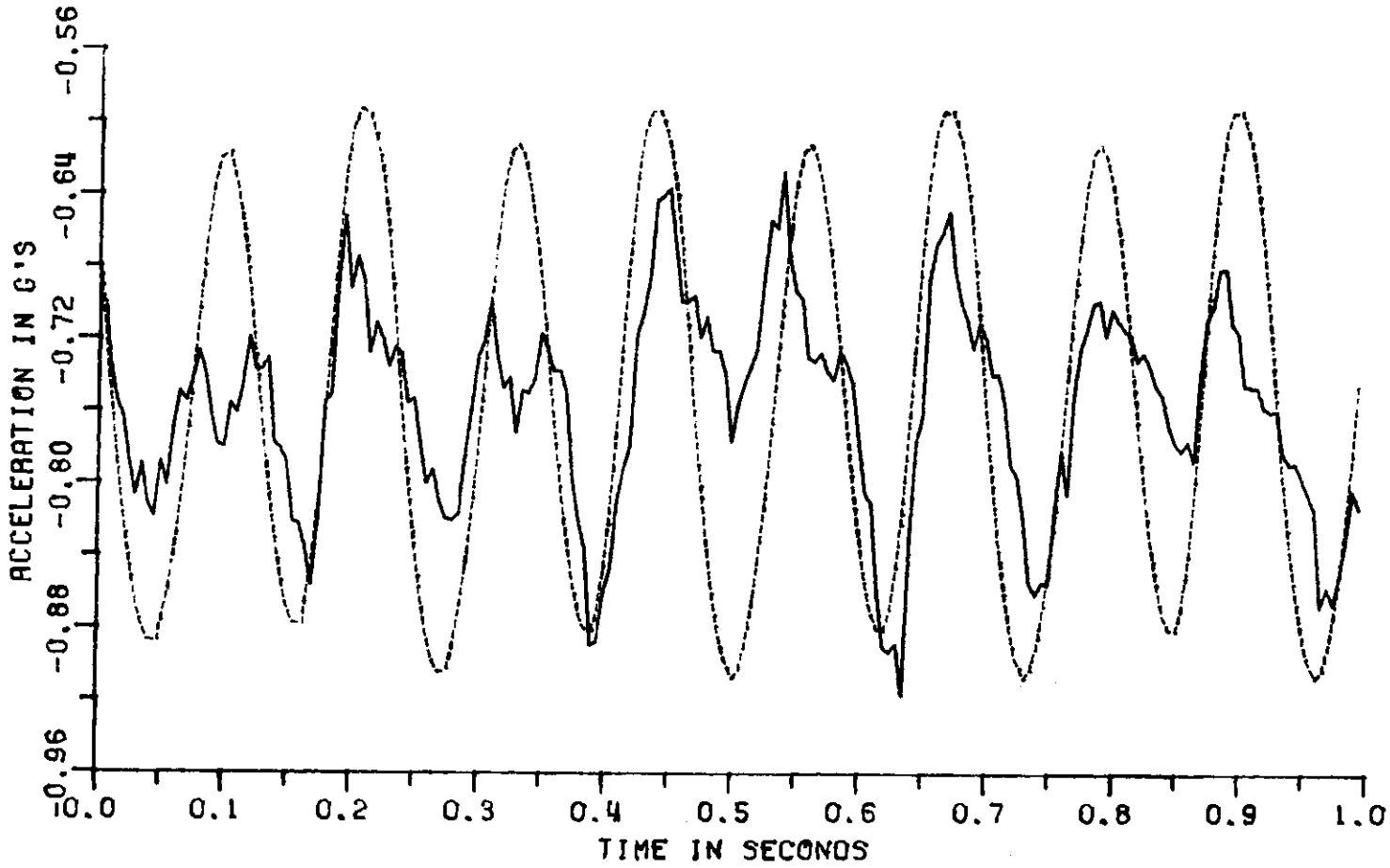

HEAVE ACC TEST 1

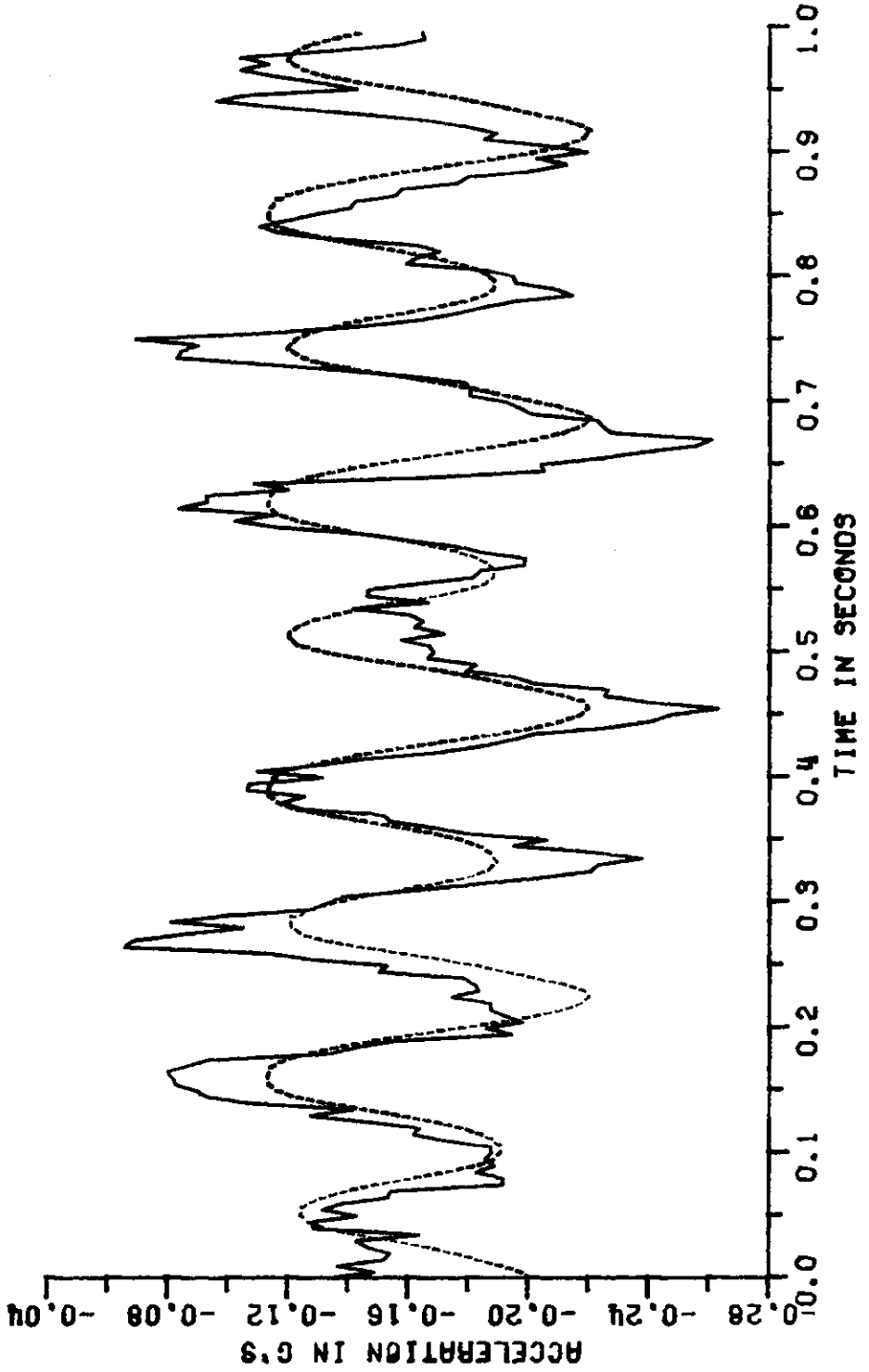

PITCH ACC TEST 1

APPENDIX J

Report of New Technology

After diligent review of the work performed under this contract, no innovation, discovery, improvement, or invention of a patentable nature was made. The unconventional vehicle configuration which is described herein originated from previous efforts. The main contribution of the present report is to obtain an improved understanding of the dynamic performance of the vehicle.

110 Copies

U.S. DEPARTMENT OF TRANSPORTATION
RESEARCH AND SPECIAL PROGRAMS ADMINISTRATION
TRANSPORTATION SYSTEMS CENTER
KENDALL SQUARE, CAMBRIDGE, MA. 02142

OFFICIAL BUSINESS
PENALTY FOR PRIVATE USE, $300

POSTAGE AND FEES PAID
U.S. DEPARTMENT OF TRANSPORTATION
513